Vehicle to Grid Implementation using Fuzzy Logic Controller

Mukesh Singh

Vehicle to Grid Implementation using Fuzzy Logic Controller

A

Thesis submitted

for the award of the degree of

DOCTOR OF PHILOSOPHY

By

Mukesh Singh

DEPARTMENT OF ELECTRONICS AND ELECTRICAL ENGINEERING

INDIAN INSTITUTE OF TECHNOLOGY GUWAHATI

GUWAHATI - 781 039, ASSAM, INDIA

November 2012

Certificate

This is to certify that the thesis entitled "**Vehicle to Grid Implementation using Fuzzy Logic Controller**", submitted by **Mukesh Singh** (09610202), a research scholar in the *Department of Electronics and Electrical Engineering, Indian Institute of Technology Guwahati*, for the award of the degree of **Doctor of Philosophy**, is a record of an original research work carried out by him under our supervision and guidance. The thesis has fulfilled all requirements as per the regulations of the institute and in our opinion has reached the standard needed for submission. The results embodied in this thesis have not been submitted to any other University or Institute for the award of any degree or diploma.

Dr. Indrani Kar
Assistant Professor
Dept. of Electronics and Electrical Engg.
Indian Institute of Technology Guwahati
Guwahati - 781 039, Assam, India.

Dr. Praveen Kumar
Assistant Professor
Dept. of Electronics and Electrical Engg.
Indian Institute of Technology Guwahati
Guwahati - 781 039, Assam, India.

Dedicated to

To

My Supervisors

Dr. Indrani Kar and *Dr. Praveen Kumar*

&

To

My dear parents,

my wife **Sanju**, my lovely sons **Shwet** and **Sitesh** and

my siblings **Alka, Priyanka** and **Rishu** for their love and support.

Acknowledgements

First and foremost, I feel it as a great privilege in expressing my deepest and most sincere gratitude to my supervisors Dr. Indrani Kar and Dr. Praveen Kumar, for their excellent guidance throughout my study. Their kindness, dedication, hard work and attention to detail have been a great inspiration to me. My heartfelt thanks to you mam and to you sir for the unlimited support and patience shown to me. I would particularly like to thank them for all their help in patiently and carefully correcting all my manuscripts. I have no doubts that finishing my degree in a proper and timely manner was impossible without their help, suggestions and advices.

I am also very thankful to my doctoral committee members Dr. H. B. Nemade, Prof. S. Majhi and Dr. Praveen Tripathy for sparing their precious time to evaluate the progress of my work. I express my heartfelt thanks to Dr. Praveen Tripathy for providing valuable suggestions on this thesis.

I would also like to thank the Head of the Department and the other faculty members for their kind help in carrying out this work. I am also grateful to all the members of the research and technical staff of the department without whose help I could not have completed this thesis. My special thanks to Sanjib Das sir for maintaining an excellent computing facility and various resources useful for the research work.

Thanks go out to all my friends at the Image and Signal Processing (ISP) Laboratory. They have always been around to provide useful suggestions, companionship and created a peaceful research environment. They all contributed directly or indirectly to this thesis, be it academic help, proofreading and volunteering to be a test subject.

I am extremely thankful to Ramesh Chandra Mishra sir for his kind support. My work and stay in this IITG would have been impossible without him. Thank you very much sir for your kind support and guidance.

I am also thankful to my seniors namely Rupaban sir, Sarada sir, Himanshu sir, Pati sir, Panda sir and Mithun sir.

I am extremely thankful to Kannan and Reena for the care shown and help in my research work.

I have no words to express my thanks to seven most important persons namely, Kuntal, Mridupawan, Deepak K T, Rajesh, Samdarshi, Samar and Sumit. My work in this remote place definitely would not be possible without their love and care that helped me to enjoy my new life in this IITG.

My special thanks to all power system group for their timely help in all respects. Special thanks also go to Ankit, Bhaskar, Ranjib, Sikandar, Umesh, Mridul, Rahul and Gaurav.

I thank all my fellow research students and B Tech students especially Rahul, Sidharth, Paloma, Sarthak, Narshimha, Mahesh, Dharmendra, Ashish, Naveen, Surya, Aishwarya, Surendra and Vivek for their cooperation. During these four years at IITG I have had several friends that have helped me in several ways, I would like to say a big thank you to all of them for their friendship and support.

Also my sincere thanks goes to Core II tea stall namely Mr. Lambu, Pranjal and Rajib. Without their tea, I think PhD at IITG would have been impossible.

I also thanks my colleague Nadgauda sir, Patil sir, Birangal sir, Chobe sir, Phatak sir, Patki sir, Sirwal sir for their kind suggestions and support from outside the IITG campus.

My relatives also played a great role in my PhD works and they are Arvind jee, Umanath uncle jee, Annu jee, Anshu jee, Abhijeet jee, Suman jee, Anil mama and Umesh Bhaiya. I am very grateful to them.

My deepest gratitude goes to my family for their continuous love and support throughout my studies. The opportunities that they have given me and their unlimited sacrifices are the reasons where I am and what I have accomplished so far. Special thank goes to Jawahar Kumar (JP) for his selfless support during my stay in IITG.

Finally, I believe this research experience will greatly benefit my career in the future.

Mukesh Singh

Abstract

This thesis proposes a Vehicle to Grid (V2G) system which coordinates among the Electric Vehicles (EVs) present at the Charging Station (CS) to charge their vehicles. A CS in this thesis is a place where EVs of a particular area will come together to charge their batteries in accordance to grid norms. A sufficiently large number of aggregated EVs in a CS could provide several important services to the grid such as voltage regulation, peak power shaving, spinning reserve and other ancillary services. However, allowing the EVs to charge and discharge without any control may lead to voltage variations at the distribution node. But, if the charging/discharging of the EVs are done in an intelligent fashion, they can act as distributed energy storage and can smoothen the load profile of the distribution network by providing peak shaving and valley filling.

In this thesis, different architectures of V2G system are modelled. Fuzzy Logic Controllers (FLC) are used to control the flow of power between the grid and the CS. Aggregator is designed to distribute the power among the batteries of EVs present at the CS during charging and discharging.

The presented work in this thesis mainly focus on the control architecture for using the EVs batteries as distributed energy storage systems. This enables in maintaining the node voltage within the prescribed limit by valley filling and peak shaving. The proposed architectures are tested on the modelled distribution network of Guwahati city, the state capital of Assam, India. Dynamic load profiles are used to check the effectiveness of the proposed architecture for flattening the load profile. Inclusion of renewable energy sources at the distribution node and its coordination with the developed V2G system has been analyzed.

The major contributions of this thesis are as follows:

- FLC based control mechanism for EVs present at the CS.
- Integration of renewable energy sources and its coordination with the CS is modelled.
- Multi-node CSs are modelled to coordinate EVs at the substation level.

Keywords: Charging Station, Distribution Substation, Electric Vehicle, Fuzzy Logic Controller, Renewable Energy Sources, Vehicle to grid.

Contents

List of Figures

List of Tables

List of Acronyms

AHR	Ampere Hours
ASEB	Assam State Electricity Board
ASLDC	Assam State Load Despatch Centre
BESS	Battery Energy Storage System
CEA	Central Electricity Authority
CSC	Charging Station Controller
CS	Charging Station
CSs	Charging Stations
DER	Distributed Energy Resource
DS	Distribution Substation
DG	Distributed Generation
DOD	Depth of Discharge
DSC	Distribution Substation Controller
EV	Electric Vehicle
EVs	Electric Vehicles
EEC	Electrical Equivalent Circuit
FLC	Fuzzy Logic Controller
G2V	Grid to Vehicle
HPWH	Heat Pump Water Heater
hrs	Hours
kWh	Kilo Watt Hour
kVA	Kilo Volt Ampere

kW	Kilo Watt
Li-Poly	Lithium Polymer Battery
LFC	Load Frequency Control
MCS	Multi Charging Station
MWh	Mega Watt Hour
MW	Mega Watt
NERLDC	North Eastern Load Dispatch Centre
PCC	Point of Common Coupling
PHEV	Plug-In Hybrid Electric Vehicles
PEV	Plug-in Electric Vehicle
SOC	State of Charge
V2G	Vehicle to Grid
W	Watt
Wh	Watt hour

List of Symbols

A	Pre-exponential factor of battery
AE_c	Available energy for Charging
AE_d	Available energy for Discharging
$\angle$	Angle
Ahr_j	Ampere Hour of the j^{th} battery
Ahr_{cr}	Current AHR of the battery
Ahr_{bi}	Current which flows between the battery and the grid
Ahr_{bj}	Current which flows between the battery and the grid
Ahr_{rating}	Rating of the battery in AHR
B	Pre-exponential factor of battery
C	Adjustable factor used in modelling the battery
C_{rate}	Charging/discharging rate
C_r	Charging rate (C_{rate})
C_{rate}^{lt}	Maximum charging/discharging rate limit
C	Effective capacitance
CS_1	Charging Station 1
CS_2	Charging Station 2
CS_3	Charging Station 3
CS_{11}	1^{st} charging station of subfeeder 1
CS_{12}	2^{nd} charging station of subfeeder 2
D	Adjustable factor used in modelling the battery
D_r	Discharging rate (C_{rate})

$D_{gridsprt}$	Duration of grid support
E	Voltage at the receiving end
E_1	Energy available/required by the CSs connected to subfeeder 1
E_2	Energy available/required by the CSs connected to subfeeder 2
E_3	Energy available/required by the CSs connected to subfeeder 3
E_i	Available energy of the i^{th} CS
E_{ij}	Available energy of the i^{th} subfeeder of j^{th} CS
Eb_i	Available energy of the i^{th} battery
Eb_{ij}	Available energy of the j^{th} battery of the i^{th} CS
E_{avail}^{com}	Energy available after commuting certain distance
E_{rated}	Rated energy of the EV's battery
E_{com}	Energy used while commuting
$Eb_i(avail)$	Energy availability i^{th} battery
$Eb_i(required)$	Energy required for the i^{th} battery
E_{avail}^{net}	Net available energy at the CSs
E_{11}	Energy available at CS_{11}
E_{12}	Energy available at CS_{12}
$E_{avail}^{CS_1}$	Total energy available at the CS_1
Eb_{ijk}	Available/required energy of the k^{th} battery of j^{th} CS of i^{th} subfeeder
I_c	Charging current
I_d	Discharging current
Ib_{ijk}	Battery current of k^{th} battery of j^{th} CS of i^{th} subfeeder
K	Factor which is either 0 or 1 depending on the (P_{status}) and the direction of power flow at PCC
K_{11}	K Factor for the 1^{st} CS of 1^{st} subfeeder 1
μ_v	Aggregated membership function
P	Power required by the grid or to be supplied to the MCS for charging their EVs
PE_c	Processed energy for charging scenario
PE_d	Processed energy for discharging scenario

Pb_i	Power required by the i^{th} battery of the CS
Pb_1	1^{st} battery of CS
Pb_n	1^{th} battery of CS
P_{EV}	Real power of EV
Pb_{ij}	Allocated power by the CS aggregator to j^{th} battery of i^{th} charging station
Pb_{11}	Allocated power to 1^{st} battery of 1^{st} charging station
Pb_{1n}	Allocated power to n^{th} battery of 1^{st} charging station
P_1	Power alloted by the MCS aggregator to 1^{st} charging station
P_2	Power alloted by the MCS aggregator to 2^{nd} charging station
P_3	Power alloted by the MCS aggregator to 3^{rd} charging station
P_i	Power required by the i^{th} CS
Pt_i	i^{th} CS's transformer power rating
P_{grid}	Power which is to be supplied/drawn to/from the CSs
$P_{surplus}$	Surplus power at the DS
$P_{surplus}^{grid}$	Power required/available for the grid support
P_{sf1}	Power allocated to subfeeder 1
P_{sf2}	Power allocated to subfeeder 2
P_{sf3}	Power allocated to subfeeder 3
P_{11}	Power supplied/drawn to/from CS_{11}
P_{12}	Power supplied/drawn to/from CS_{12}
P_{ij}^{net}	Net power of the i^{th} CS of n^{th} subfeeder as decided by the **CSC**
P_{11}^{net}	Net power exchanged at the CS_11 as decided by the CSC of CS_{11}
P_{22}^{net}	Net power exchanged at the CS_22 as decided by the CSC of CS_{22}
Pb_{111}	Power flow in 1^{st} battery of CS_{11} of subfeeder 1
Pb_{11n}	Power flow in n^{th} battery of CS_{11} of subfeeder 1
Pb_{ijk}	Power required by the k^{th} battery of j^{th} CS of i^{th} subfeeder
Q_{EV}	Reactive power of EV
Q	Current capacity of the battery in Ah

Q_l	Capacity Loss of the battery in Ah
Q_n	Rated capacity of the battery in Ah
Q_{ijk}	Current capacity of the k^{th} battery of j^{th} CS of i^{th} subfeeder
R	Gas constant (J/mol K)
R_1	Internal resistance of battery (Series)
R_2	Internal resistance of battery (Parallel)
S_{EV}	Apparent power supplied/taken from the EV battery
SOC_{cr}	Current state of charge (SOC) of the battery
SOC_{lt}	Maximum limit of SOC to discharge the battery
SOC_{rem}	Difference of the current SOC (SOC_{cr}) and SOC limit (SOC_{lt})
$SOC_{initial}$	SOC at the time of starting from home/office
$SOC_{postcom}$	SOC of the battery after commuting
SOC_{fc}	Final SOC of the battery
SOC_{fd}	Final SOC limit of the battery during discharging
T	Temperature (K)
t_c	Charging time
t_d	Discharging time
t_n	Simulation time for the charging
t_m	Simulation time for the charging
$u(t)$	Defuzzified overall control output
u_i	Output variable
V_0	Open circuit voltage
$V_{bc}(t_c)$	Battery charging voltage with respect to time
$V_{bd}(t_d)$	Battery discharging voltage with respect to time
V	Voltage at the sending end
V_j	Voltage of j^{th} battery
V_{11}	Voltage of node **1.1**
V_{ijk}	Voltage of the k^{th} battery of J^{th} node of i^{th} subfeeder

X	Reactance between the node and the EV terminal

Glossary

- **Aggregator:** Aggregator is a place where distribution of power is done among the batteries present at the CS and this is called CS aggregator. The distribution of power among different charging stations connected to a single node is termed as MCS aggregator. Subfeeder aggregator divides the power among CS present at different CSs of individual subfeeder.
- **Battery:** Battery refers to Electric Vehicle's battery.
- C_{rate}**:** An individual battery's preferred charging/discharging rate (C_{rate}) as set by the EV owner.
- **Charging Station (CS):** A charging station is a place, assumed to be near a distribution node (11kV/440V), where a large pool of EVs from that particular area will participate in grid support. CS can also be at parking lots or a basement of a commercial complex.
- **Controller:** All the controllers are Fuzzy Logic based.
- **Distribution Node:** Here distribution node means 11kV/440V system.
- **Electric Vehicles (EVs):** Electric Vehicles are the transport system whose primary source of energy is battery or in short they are battery operated cars whose energy rating varies from 8 kWh to 40 kWh.
- **Feeder:** It is the main 11kV line from which many subfeeder is branched.
- **Multi Charging Station (MCS):** Three charging station connected at a single distribution node to support the grid is called Multi Charging Station.

- **Substation:** Substation means 33kV distribution substation. This substation is a reduced network of typical Guwahati city distribution substation.

- **Subfeeder:** Subfeeder means 11 kV/440 V line spread across different area of the distribution network such as residential, office or commercial area.

1

Introduction

Contents

1.1 Introduction

Non-renewable energy sources are approaching extinction and therefore, countries are looking for new forms of energy that can replace them [1]. Electricity is the forerunner to replace fossil fuels like petrol and diesel. For example; the traditional vehicles which use petrol/diesel to generate power are being replaced by vehicles, which use electricity instead. Such vehicles are known as Electric vehicles (EVs) [2]. The penetration of EVs in the automobile market is increasing rapidly. This rise in demand will cause a lot of stress on the electric distribution system [3]. In India, despite a rise to the power generation, the power deficit rose to 7.5% of peak demand in May 2012 as against 6.5% last year [4]. The surge in the deficit has certainly increased the stress on the existing grid. It has been found that the rate of recurrence of voltage fluctuations has increased, which has led to damage several costly appliances over the period of time. Meanwhile, the share of EVs in the automobile sector can further increase the burden on the existing grid to a very high value which results in voltage imbalance and power outage.

The batteries of plug-in electric vehicles can be charged at home from a standard outlet or at a charging booth. These extra electrical loads will create an imbalance between the demand and supply, which in turn may lead to frequency and voltage instability. Indeed, a sudden discharge of energy from the EVs to the grid may cause a voltage swell at the concerned distribution node. Therefore, in order to maintain grid stability, the two way energy flow between the EVs and the grid need to be controlled properly. With the advent of large influx of EVs, new techniques for charging of EVs have to be framed which can handle the voltage fluctuations [5]. One possible solution to this problem is to use Vehicle to Grid (V2G) technique [6].

Vehicle to Grid (V2G) refers to a system in which the EVs communicates with the power grid to provide support by either delivering power to the grid or by charging its battery in controlled fashion [7]. V2G technology utilizes the stored energy in electric vehicles' batteries and supplies this energy to the grid whenever requested by the grid operators. Thus, like distributed energy resources, the V2G technique can reduce the stress on the overloaded distribution systems by meeting demand locally especially during peak hours.

Through a communication link, utility grid operators can communicate with the plugged-in vehicles (PEV). Utilities can buy energy from the car owners when it is needed and sell it back when the demand is low. Instead of the utility having to communicate with individual vehicles, an aggregator can be formed that would act as a commercial middleman between the utility and the multiple vehicles [8]. The aggregator will be responsible for taking real time decisions of charging or discharging the EVs depending on the prevailing grid conditions. Figure 1.1 shows the location of aggregator in V2G architecture.

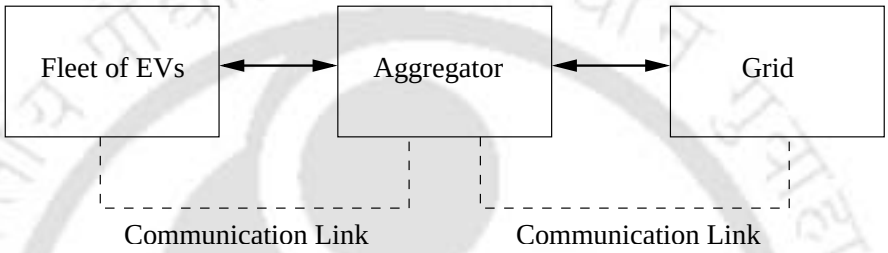

Figure 1.1: Aggregator in V2G system.

A block diagram of an EV which is connected to the grid and used as a V2G system is shown in Figure 1.2. Charging/discharging of EV will be done based on the grid conditions which will be accomplished by the controller present between the EV and the grid. The power electronics devices used for this purpose should have bidirectional converters. The control mechanism should consider the grid conditions such as voltage. If the node voltage is low, the controller will never allow to charge the batteries. Instead, EVs' batteries will discharge their excess energy to the grid. When the node voltage is high, the batteries will get charge.

The various services of the V2G for providing grid support are possible and is given in Figure 1.3. V2G based grid support are mainly divided into two parts: load leveling and ancillary services. Load leveling implies a method to balance the load and demand. It can be achieved with the help of regulation (to keep voltage and frequency stable) and spinning reserve (to meet sudden demands for power). The regulation can be divided in to two separate entity such as voltage and frequency regulation. These regulations can effectively be handled with the help of V2G system due to faster response as compared to traditional power generators.

Voltage regulation is aimed primarily to maintain voltage within certain limits. This is also

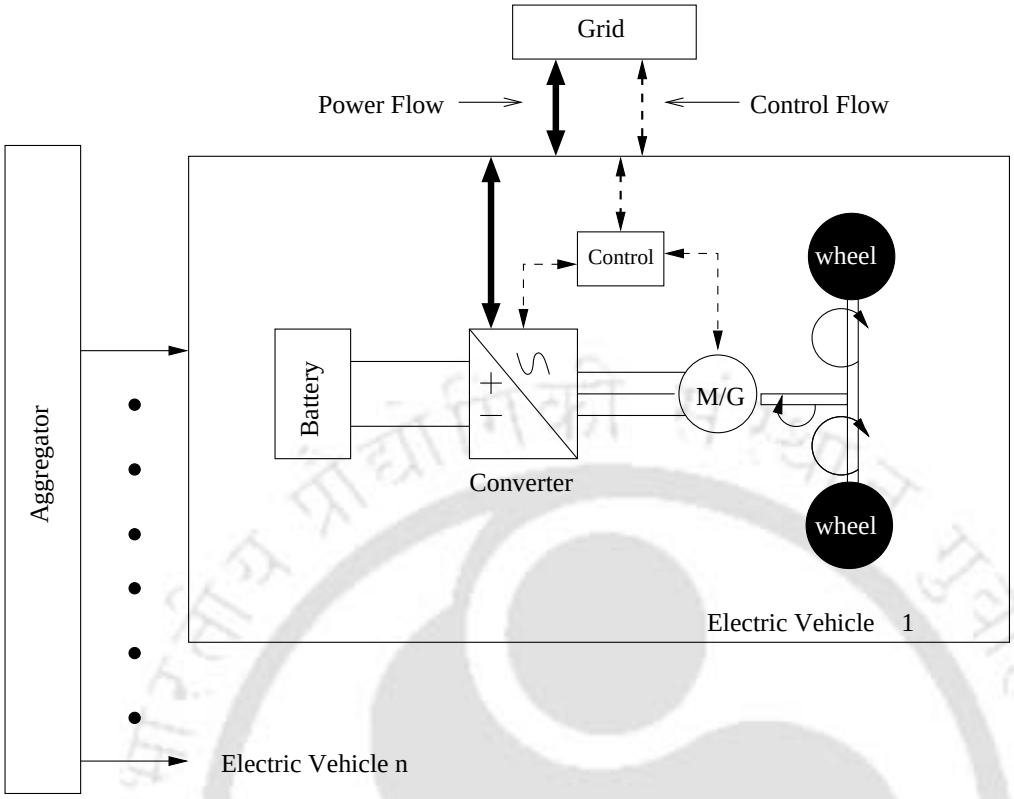

Figure 1.2: Electric Vehicles in V2G system.

concerned by minimising sudden variations in voltage. Voltage regulation is generally a local problem as this happens mostly due to reactive loads. Moreover, most devices (conductors, transformers, breakers, etc.) are limited by current rather than by real power. If they are carrying significant reactive power and reactive current, they have less capacity available to transport real power. Therefore, reactive compensation by the V2G at the distribution network will compensate the voltage imbalance since, reactive power management and voltage control are the same service.

Frequency regulation is used to fine tune the frequency of the grid by matching generation to load demand. Therefore, frequency regulation must be under direct real time control of the grid operator because it has to respond within a minute or less by increasing or decreasing the output of the generator. Some utility operators split regulation into two elements: one for the ability to increase power generation from a baseline level and the other to decrease from a baseline. These are commonly referred as “regulation up and “regulation down respectively.

For example, if load exceeds generation the frequency of the system drops and it indicates that regulation up is needed. If a large number of EVs penetrate and charging/discharging is controlled and monitored by the utility, frequency regulation can be achieved.

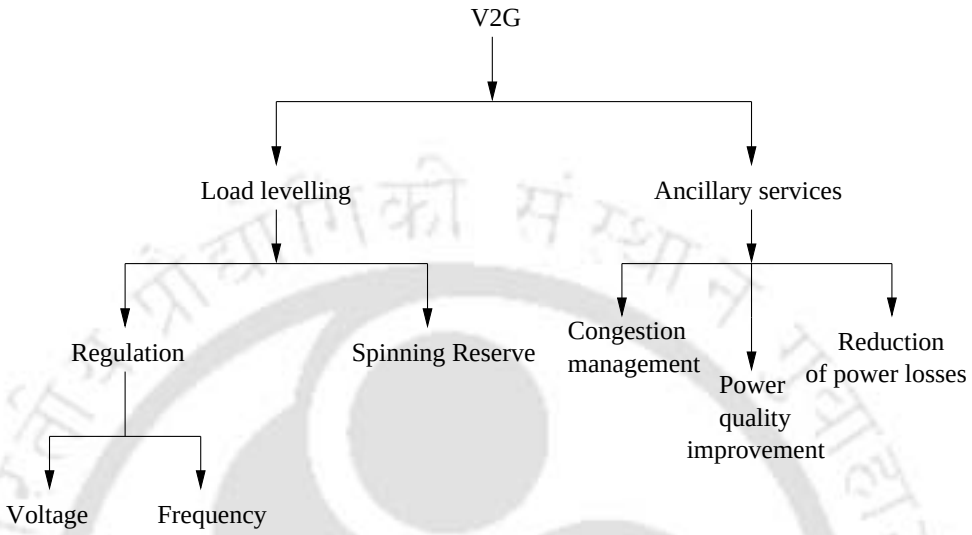

Figure 1.3: Different grid support provided by V2G.

Apart from power regulation, V2G system can be utilized for the ancillary services such as congestion management, power quality improvement and reduction of power losses. In the electric power system, ancillary services are very much necessary for maintaining grid reliability, balancing the supply & demand and the overall grid stability. The importance of ancillary services is taken into considerations when there is an outage or there is an issue of grid instability [9, 10]. The regular trend for providing ancillary services such as regulation is basically achieved by generators. They are operated differently which are just providing bulk power. For regulation, generators ramp up and down to match the needs of fluctuation in the grid [11].

However, the importance of V2G arises when the EVs' batteries can respond faster than generators (less than seconds) [12]. If a large pool of EVs is present, various ancillary services can be met with ease. Unlike large generators, EVs' batteries energy storage and power electronics are designed to provide large and frequent power fluctuations over short time period [13]. This makes the vehicles especially well engineered for regulation. Once a signal is

received from the aggregator, the vehicle can respond in less than a second to change its power output. A "regulation up" signal would cause the vehicle to provide power to the grid (V2G) and a "regulation down" signal would cause a decrease in the power output or even draw power from the grid (the regular battery charging mode). Brooks [14] successfully demonstrated use of a single battery electric vehicle to respond to a regulation signal. Many other ancillary services such as voltage sag, reactive power support, harmonics eliminations can be achieved with the V2G system.

V2G is going to be an extensive study on the technology as part of a national sustainable energy solution in various countries. V2G places smaller amounts of storage capacity at the demand point, directly serving the customer and eliminating the need for future expansion of a transmission and distribution grid that must meet the peak load demand [15]. This provides better service at affordable price and has the added benefits of being environmental friendly. The interconnection of EVs to the grid is sometimes referred to as distributed energy storage.

In future development, it is proposed that such use of EVs could buffer renewable power sources. Electricity produced from wind energy can be stored if excess energy produced during windy periods and can be provided it back to the grid during high load periods, thus effectively stabilizing the intermittency of wind power. Some researchers look at this application of vehicle-to-grid technology as an enabling factor for renewable energy to penetrate the baseline electric market [7]. In the next section, a detailed literature survey in the V2G area are explored.

1.2 Literature review

Very few work has been found in the literature where coordination among the EVs has been achieved to meet the ancillary services as well as on the control aspect of EVs and the grid. However, researchers have presented the utilization of EVs for grid support in terms of frequency regulation and as energy storage device which can help in peak shaving and valley filling and can thus flatten the load profile. The off line optimisation techniques have been used by many researchers to study the economic aspects of the V2G realization. Many researchers have developed the single EV's interaction with the grid to test the voltage and frequency

regulation.

Utilization of EVs for frequency control has been discussed by developing an optimal aggregator [16,17]. In these papers, authors have given emphasis on cost arising from the battery charging and the revenue obtained by providing the regulation. A similar work is found in [18], where optimal charging strategies for unidirectional Vehicle to Grid have been developed. Here authors have developed an algorithm for unidirectional regulation. A new theoretic model to understand the interactions among EVs and aggregators in a V2G market, where EVs participate in providing frequency regulation service to the grid has been developed in [19]. The authors have developed a smart pricing policy and designed a mechanism to achieve optimal frequency regulation performance in a distributed fashion. They have shown that the pricing model and designed mechanism work well and can benefit both EVs (in terms of obtaining additional income) and the grid (in terms of achieving the frequency regulation). Economic aspects of achievable power capacity from Plug-in Electric Vehicles (PEV) for V2G frequency regulation has been analysed in [20]. Here authors have developed the model to understand the market perspective of EVs when used for frequency regulations. In new method of frequency regulation, supplementary load frequency control by using both EVs and heat pump water heaters(HPWH) have been analysed [21]. In this paper, the authors have discussed about the battery energy storage system (BESS), which is one of the effective solutions to reduce the voltage and frequency fluctuation. However, due to high cost of the BESS, an application of controllable loads such as EVs and HPWH to the power system control is considered for reduction of the required capacity of the BESS. In another work, related to frequency regulation, a load frequency control by PHEVs, controllable loads and a co-generation unit have been discussed [22]. This paper presents a method for tracking a secondary frequency control signal by groups of PHEVs, controllable thermal household appliances and a decentralized combined-heat-and-power generation unit. EVs' batteries utilization as a storage device has been shown to be effective in suppressing fluctuations in power demand and providing frequency control in [16, 23]. Therefore, such systems can also provide local voltage support, thereby reducing the need for voltage regulation at distribution node [24, 25].

A different work is found in [26], where integration of V2G in a western Danish power system has been discussed; however, more importance has been given to energy storage rather than the V2G concept. Storage of energy in the EVs' batteries to meet peak load demands is discussed in [27, 28]. Here, authors have focused on the aggregated EVs' energy utilization for the transmission network. The impact of transport electrification on electrical networks has been studied in [29]. This paper has shown that for effective economic dispatch and to avoid large installations of fast-response generators, electrical networks integrating EVs must form a symbiotic relationship. This allows present residential peaks and fast acting loads to be met by EVs and in return, achieves well-defined load profiles. Impact of EVs on the distribution grid and its analysis using load flow techniques have been studied in [24]. This work, however, has not used any control techniques for charging/discharging of EVs energy from/to the grid. In another technique, Smart Load Management (SLM) approach for the coordination of multiple PEV chargers in distribution network is proposed [30]. Here authors have shown that by controlling the charging rate of the PEV, proper voltage profile on the distribution feeder can be achieved. Coordinated charging of PHEV to minimize distribution system losses has been analysed in [31]. In this work, the relationship between feeder losses, load factor, and load variance is explored in the context of coordinated PHEV charging and developed the optimal charging algorithm. Few researchers have developed the concept of storing the energy during off-peak hours and inject it back to the grid during peak hours thus achieving valley filling and peak shaving [32–34]. Here authors have discussed different strategy of V2G to support the grid and analysed the overall concept of V2G in terms of valley filling and peak shaving.

Economic assessment of the impact of PEVs on distribution networks has been studied in [35]. Here authors have proposed a detailed approach for evaluating the impact of different levels of PEV penetration on distribution network and discussed various investment and incremental energy losses. From the result of this work and depending on the charging strategies, investment costs can increase up to 15% of total actual distribution network investment costs, and energy losses can increase up to 40% in off-peak hours for a scenario with 60% of total vehicles being PEV. Load scheduling and dispatch for aggregators of PEVs has been discussed in [36]. In

this paper, scheduling and dispatch of electric power by aggregators of PHEV fleets, whose main objective is the maximization of energy trading profits has been developed. In a different approach, optimal scheduling for charging and discharging of EVs in V2G scenario is developed [37]. In this paper, scheduling optimization problem is discussed where charging powers of the EVs are optimized to minimize the total cost of all EVs which perform charging during the day. Through simulations, the authors have demonstrated that the locally optimal scheduling scheme can achieve a close performance compared to the globally optimal scheduling scheme. Coordinating V2G services for energy trading has been discussed in [38].

Few researchers have studied the economic aspects on ancillary services achieved by the V2G operation. Optimal bidding of EVs to meet ancillary services has been discussed in [18]. In this paper, an optimal bidding formulation for regulation and spinning reserves is developed which can be used by the aggregators. These algorithms maximise profits to the aggregator while increasing the benefits for the customers and utility. A new approach to analyse the economic impacts of V2G regulation reserves by simulating the restrictions arising from unpredictable mobility requests by vehicle users is studied in [39]. In this paper, two approach (static and dynamic) has been discussed to show the unpredictable mobility of EVs. Comparison of dynamic approach and static approach reveals that a significant difference in the power, a vehicle can offer for ancillary services and also provides good information regarding the size of vehicle pools. Modeling of V2G ancillary services by integrating probabilistic vehicle travel models and ancillary services pricing into a non-linear dynamic simulation of the driving and charging behavior of PHEVs has been studied in [40]. Results show that in order to integrate a V2G system into the existing market and power grid, the V2G system will require a high power home charging capability.

From the above discussions, it is analysed that the researchers have successfully studied and demonstrated the vehicle charging/discharging behavior to control the frequency and voltage of the grid as well as the economic aspects of V2G. However, the real time implementation of the individual EV and their coordination with other EVs present in the nearby area for grid support still needs deliberation. The detailed literature review is divided mainly into three

parts as shown in Figure 1.4. It is observed that researchers have focussed to solve the problem of regulation (voltage and frequency) through V2G as well as proved V2G to be one of the viable storage technology of the future. Various economic aspects such as distribution network investment based on different level of EVs penetration and the incremental energy losses are analysed. Now the need of real time coordination among EVs are required where EVs will be coordinated to achieve the desired power flow at the grid. This is important to validate the V2G concept in real scenario since EVs of different specification, energy level would come to charge/discharge. This complex scenario needs to be coordinated in real time to achieve the desired regulation.

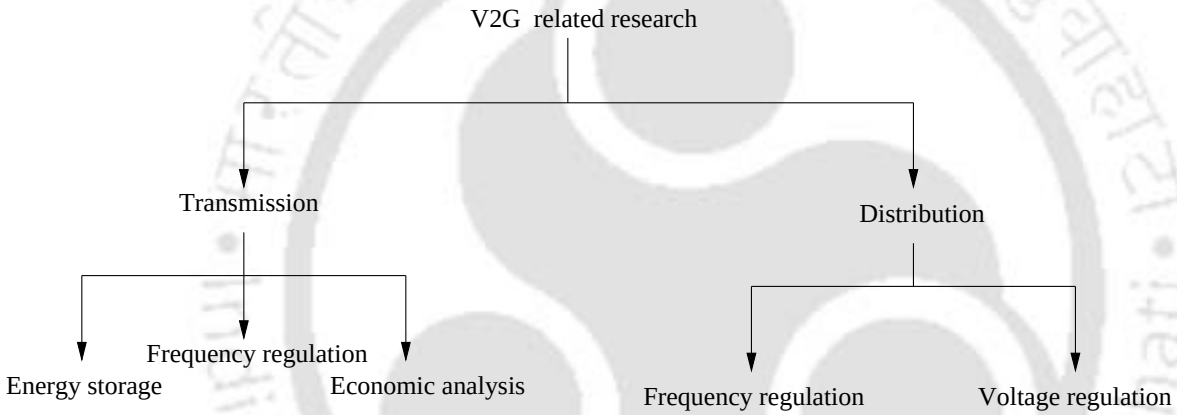

Figure 1.4: Outline of existing literature on V2G

1.3 Motivation

In the literature, many researchers have assumed aggregated energy of the EVs and mathematically analysed the economic aspect of the V2G in terms of frequency regulation, energy storage. They have made off line optimization techniques to study the behaviour of EVs in the V2G scenario by developing algorithm to control the charge/discharge rate. In few research papers, EVs and its impacts on the distribution and transmission network have been analysed with the load flow techniques. In these works, the authors have assumed different penetration level of EVs in a city and studied the impact on the grid in terms of voltage stability, peak shaving, and valley filling. In some literatures, single EV has been developed for V2G

scenario and connected to the home network for bidirectional power flow. Brooks et al [14] demonstrated that the regulation can be achieved with EVs connected to the grid. However, aggregating the EVs together at a common place and coordinating all the EVs to achieve the goal of grid support has not been studied. Also, it has been observed from the previous section that in the distribution system mainly two studies have been carried out and they are namely frequency regulation and voltage regulation. But these studies do not considered the real time coordination of PHEVs/PEVs/EVs at the distribution network.

In this thesis, mainly the voltage regulation at the distribution network has been achieved by coordinating the EVs. The distribution network has been taken for the analysis since EVs will be connected at the distribution network for charging. Generally EVs will be connected to the home network (110 V or 220V system) or at the common place to be called as charging station (11kV/440 V system). Therefore, the impact of charging can be easily analysed in the practical distribution network and can be studied in real time environment. Moreover, a microgrid can be formed at the distribution level where V2G system can support the grid in case of transmission grid failure.

For the successful implementation of the V2G, coordination of the EVs is very important. The coordination is achieved, if the EVs of nearby distribution node area accumulate at a particular place (charging stations) for charging during their idle time. The presence of EVs at the Charging Stations (CSs) is more likely because 90% of the time EVs will be idle [41]. Therefore, with large penetration of EVs, CSs will be one of the best viable options to charge the EV's battery and possible implementation of V2G scenario.

In this thesis, the main focus is given to coordinate the EVs present at the CSs. The decision regarding the magnitude of power flow between the CS and distribution node is decided by the suitable controller. In other words, power flow between the grid and the CS is controlled by designing a suitable controller which takes the information of the grid condition such as node voltage at the point of common coupling (PCC) and total energy information of EVs at the CS. Coordination of EVs present at the CS is shown in Figure 1.5. Power allocated by the controller for CS is distributed among EVs present at the CS by the aggregator. EVs present at

the CS are finally connected at a PCC(distribution node). By doing this, the energy will flow in a controlled fashion without any impact to the distribution grid. The proper distribution of power among the EVs present in a CS is a challenging goal, since the EVs present in the CS will have different battery's specification and different state of charge (SOC). In this figure, grid refers to the node of a distribution substation, where residential or commercial area exists and there is a possibility of large number of EVs present in this area.

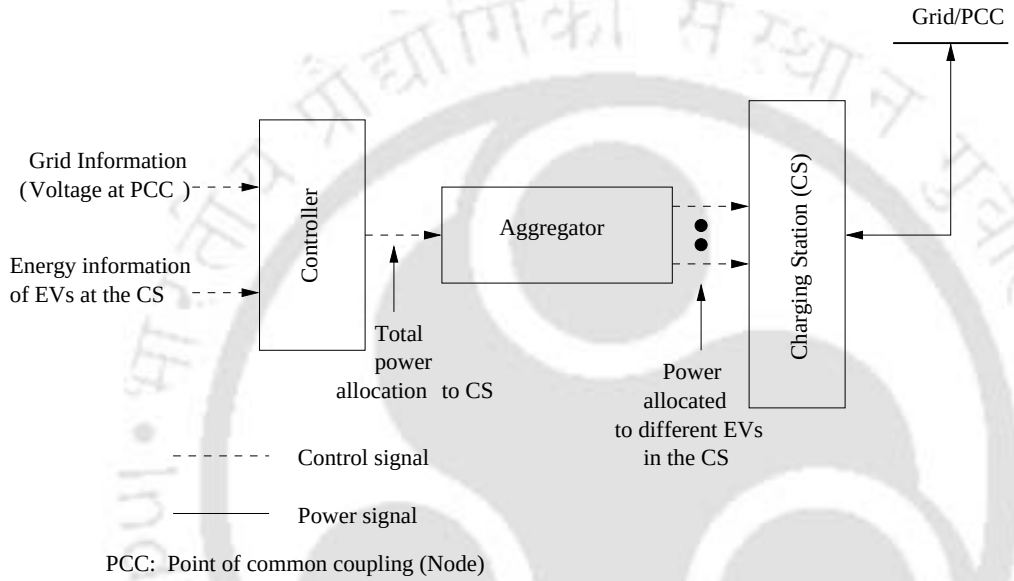

Figure 1.5: Coordination of EVs present at the CS.

1.4 Aim of the thesis

From the previous section, it is concluded that coordination of EVs in real time can be achieved through proper design of controller and aggregator. The net power which should flow between the CS and the grid is decided by the controller. Aggregator distributes the power among different EVs present at the CS.

The primary aim of this thesis is to present V2G architecture where EVs present at the CS coordinate among themselves to support the grid in terms of peak shaving, valley filling and thus maintain the node voltage within statutory limits. The coordination of renewable energy sources with the proposed V2G architecture has also been analysed.

The second objective is to develop different aggregators which will coordinate among the EVs. This is very important because the amount and direction of the power flow of individual EV's battery is decided at the aggregator level. Various algorithms have been developed to check the power flow between the EV's battery and the grid depending on the energy availability or requirement of the battery. The 'energy availability' implies excess energy available with EV to discharge to the grid and 'energy requirement' implies that the amount of energy required by the EVs to charge its battery.

A Fuzzy Logic Controller (FLC) has been designed to control the power flow between the node and the CS. FLC has been used due to its linguistic representation of rules without having to develop a mathematical model of the system.

The charging/discharging rate (C_{rate}) of the EV's battery is controlled to achieve the desired power flow between the grid and the battery. The owner's preferred C_{rate} limit is kept into consideration while charging or discharging of the EV's battery. Also, battery is not discharged beyond the state of charge (SOC) limit set by the vehicle's owner.

1.5 Contributions

The main contributions of this thesis are:

- A new methodology for V2G architecture has been developed at the CS and DS level.
- Multi charging station (MCS) for the EVs has been modeled and connected to a single distribution node.
- Peak shaving, valley filling, and voltage stability using the proposed V2G architecture are studied and analysed.

1.6 Thesis layout

Chapter 2 presents V2G implementation using FLC. Two levels of control have been modeled. First level of control is at the CS level and the second one is at the node level. Here node refers to 11kV/440 V node of a radial distribution system. The FLC takes decision based on

the node voltage and aggregated energy available at CS. Based on these inputs, FLC decides the amount of power flow between the CS and the node. The main work of this chapter is to control the flow of power between the aggregated EVs' batteries and the grid by keeping the node voltage within specified limit. Two scenarios are analysed and the proposed model is tested on a typical distribution grid model of Guwahati (the state capital of Assam, India). In the next chapter, detailed modeling of the CS is provided where individual battery is controlled to achieve the desired power flow.

In chapter 3, three different CSs are modelled. All these CSs are connected to a single distribution node of a test system. Here, group of CSs connected at single distribution node is termed as Multi Charging Station (MCS). The distribution of power among the CSs of the MCS has been achieved by designing a suitable aggregator. An another aggregator is modeled at the CS level which allocates the power among batteries present at the CS. The role of the individual battery its control of C_{rate} have been designed using new algorithms. These algorithms have been designed which can handle any charging/discharging efficiencies. Dynamic load has been considered to check the validity of the proposed V2G architecture. A real time scenario of the EVs movement at the MCS with intra-node driving has been considered. The dynamic load profile of the node is used to validate the FLC controller. It has been verified that the proposed V2G architecture can achieve the valley filling, peak shaving and it maintains the voltage profile of the node with the existing dynamic loading.

In chapter 4, the integration of renewable energy sources such as PV and wind energy in the distribution grid and their coordination with the developed V2G architecture has been presented. In this chapter, a single CS and its coordination with the renewable energy sources for real time scenario has been achieved. Dynamic load profiles of residential and commercial nodes have been used to test the proposed FLC controller.

In chapter 5, various CSs connected to different nodes of the distribution substation(DS) has been coordinated at the DS level to achieved the grid support. The detailed algorithms for coordination of the EVs among the CSs and the coordination of the CSs at the DS level have been developed. The main focus of this chapter is to coordinate the EVs present at the CSs of

multi node system and achieve the goal of V2G. In this chapter, batteries of EVs are modeled which can calculate the capacity loss and update the batteries' health and energy level at every instant of time.

Finally, the conclusions and future works are presented in chapter 6.

2

Implementation of Vehicle to Grid using Fuzzy Logic Controller

Contents

2.1 Introduction

Electric vehicle (EV) when communicates with the power system network to provide support by either delivering power to the grid or by charging their batteries in a controlled fashion is termed as Vehicle to Grid (V2G) [5]. V2G technology utilizes the stored energy in electric vehicles' batteries and supplies this energy to the grid whenever required by the grid operators. Thus, like a distributed energy resource, the V2G technique can reduce the stress on over-loaded distribution network by meeting demand locally, especially during peak hours.

During off peak hours, when the demand is low, the producers are reluctant to back down generation, resulting in increase in frequency of the system beyond healthy limits. Whereas, during peak hours, the producers are not able to meet the demand, thereby reducing the frequency and voltage, which results in power system outage. Hence, to maintain the overall system performance, there is a need to balance the off peak and peak demand. One of the method to balance the off-peak and peak demand is to find some method which will store the energy in the off-peak period and return to the grid during peak demand.

Hence, utilization of the traditional power plants at off peak by plugging in the Electric Vehicles (EVs) and storing the energy at off peak and return the power at peak will certainly balance the demand and supply gap. Being driven by a storage technology, EVs are bidirectional and can act as either a source or a load.

As discussed in the previous chapter, a very little work has been found on control aspect of EVs and the grid. Researchers have given more emphasis on the frequency regulation, energy storage and economic analysis by aggregating the EVs at the distribution level or at transmission level. Impact of EVs on the distribution grid and its analysis using load flow techniques has been studied in [24]. Here, authors have not used any controlled techniques for charging or discharging of EVs energy to the grid. In this chapter, control of energy flow between EVs and the grid has been demonstrated using Fuzzy Logic Controllers (FLC) mainly for voltage compensation by injecting real power. FLC has been used because it is the most suitable for this type of uncertain environments, which eliminates the need for complex

mathematical models of the systems. Thus, even with an involvement of a large number of EVs, a control technique for their charge and discharge rates can be easily designed.

In this chapter, two controllers have been designed based on fuzzy logic. The first controller, the 'Charging Station Controller', is at the charging station, while the second controller called the 'V2G controller' has been placed at the distribution node level as shown in Figure 2.1. The V2G controller has been placed on a particular 440V node of a 33kV substation. This substation is a part of the typical primary distribution system of Guwahati city, India. The main purpose of the V2G controller is to control the power flow between the concerned node and the charging station. A charging station is a place, assumed to be near a distribution node, where a large pool of EVs from that particular area will participate in grid support. The second controller, the Charging Station Controller, is placed at this charging station. This controller will decide on the individual participation of the EVs for charging or discharging. It has been seen that a co-ordinated charging or discharging of EVs enables V2G technology to meet voltage sag, power imbalance and other ancillary services like frequency regulation and transient mitigation. Peak power management and voltage stability have been explored in detail in this chapter.

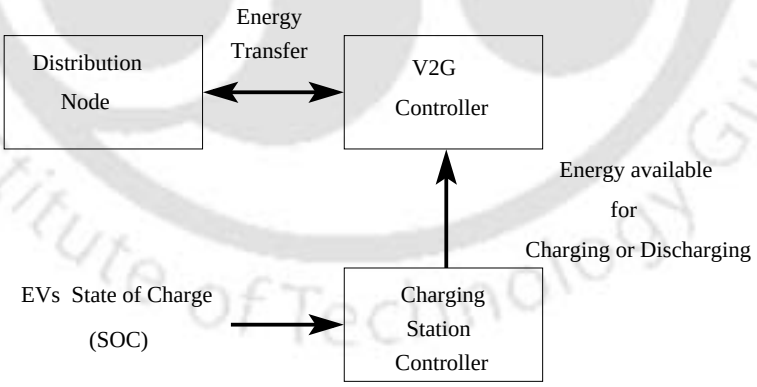

Figure 2.1: Controllers implemented in V2G infrastructure

This chapter is organized as follows.

Section 2.2 presents modeling of the distribution system of a 33 kV substation which comes under Guwahati city distribution system. Section 2.3 presents the V2G and its impact on the radial distribution network. Section 2.4 presents FLC used for the V2G system. Membership

functions for the charging station controller and V2G controller have been defined in this section. Two scenarios of EVs available at charging station is developed in Section 2.5. Analysis of charging and discharging of EVs using FLC and its positive impact on the voltage profile improvement and meeting peak demand are discussed in Section 2.6. Results and discussion are presented in Section 2.7. In this section, flattening of the load profile using the results discussed in previous section is also presented. Conclusion and future work is presented in Section 2.8.

2.2 Modeling of the V2G system

2.2.1 A typical distribution system

The typical distribution network considered in this thesis is the primary distribution system of Guwahati city, which is a part of the North Eastern Regional Grid of India. This network consists of 56 nodes where 36 nodes are of 11 kV and 20 nodes are of 33 kV [42]. In this work, a reduced 33 kV substation of the Guwahati distribution system has been modeled. A reduced system has been modeled to decrease the simulation time. The radial test feeder of 33 kV substation is shown in Figure 2.2. The main feeder has one transformer of 33/11kV, 5 MVA. There is 5 sub feeders of 11 kV and having transformers rating as 11 kV/440 V, 500 kVA. The total numbers of nodes are 20. Numbers (**2.1** to **6.3**) are sub feeders nodes. The charging station is connected to a 440 V node in the distribution system since a large number of EVs from that particular node area will accumulate at the charging station to charge or discharge their batteries.

The peak load hours of Guwahati city are between 1700 hrs and 2100 hrs. Off peak load hours are between 2100 hrs and 1700 hrs [43]. Peak hour load on the substation of a typical distribution system of Guwahati city is given in Table 2.1. Off peak hour load is approximated to be 60% of the peak hour load as per the data provided by the Assam State Electricity Board (ASEB) [43]. The impedance of the entire section is assumed to be constant with a resistance of 0.0027 p.u and reactance of 0.0023 p.u. The system is assumed to be a balanced three phase system.The base values used are 500 kVA and 0.44 kV and the feeder voltage is taken to be

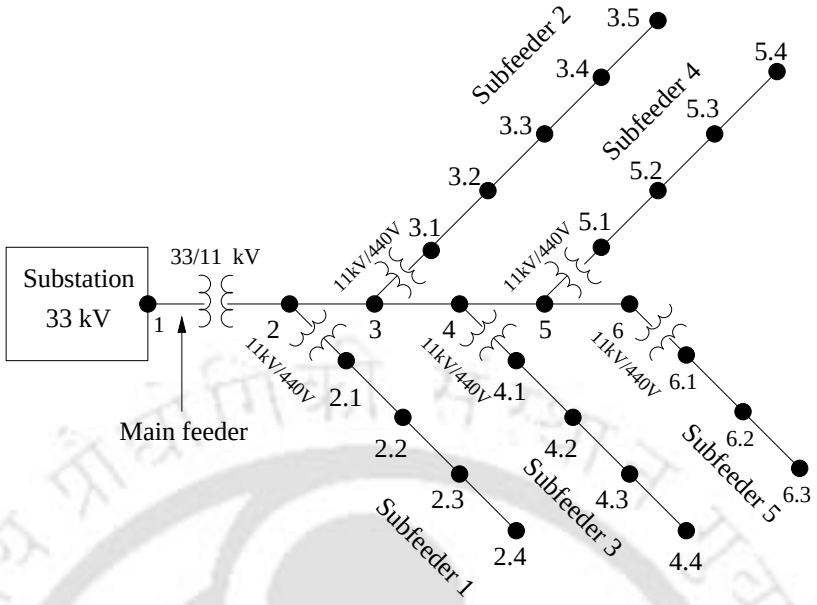

Figure 2.2: Radial test feeder of 33kV substation of Guwahati city.

1.0605 p.u.

2.2.2 EV's battery

The following assumptions have been made in modeling the EV's battery.

- Variation of the voltage with respect to SOC is not considered.
- Loss in the battery's capacity with respect to cycling is not considered.

Table 2.1: Existing load of substation

Nodes	P(p.u.)	Q(p.u.)	Nodes	P(p.u.)	Q(p.u.)
2.1	0.50	0.22	4.2	0.63	0.33
2.2	0.47	0.23	4.3	0.67	0.23
2.3	1.13	0.64	4.4	0.53	0.37
2.4	0.27	0.15	5.1	0.45	0.39
3.1	0.42	0.29	5.2	0.23	0.13
3.2	0.94	0.43	5.3	0.84	0.46
3.3	0.13	0.09	5.4	00	00
3.4	00	00	6.1	0.37	0.18
3.5	0.25	0.17	6.2	0.23	0.13
4.1	0.23	0.13	6.3	0.73	0.45

- Cyclic efficiency of the battery is not considered.
- Charging and discharging efficiency has not been considered.

The above mentioned assumptions are made in order to reduce the computation time. As a consequence of these assumptions, the battery is modeled as a source capable of delivering required power during discharging. In case of charging, the battery is modeled as a sink capable of absorbing power from the grid.

Due to this assumptions following parameters will not be studied

- Efficiency of the charging or discharging system is not studied since the battery capacity loss is one of the most important factor in evaluating the loss.
- Due to variation in voltage with respect to SOC, power drawn from/by the battery also changes which effect the total power exchange between the grid and the CS. However, due to this assumption power exchange between the grid and the CS remains constant through out the V2G operation.

2.2.3 EVs utilization for grid support

EV battery's energy can be utilized as a distributed energy storage and used for voltage sag reduction at a particular node. A schematic diagram of a battery and a bidirectional converter coupled with the distribution node via line reactance X is shown in Figure 2.3. In this figure, the battery represents a lumped parameter and can be understood to have the total available energy of the Charging Station (CS). With the bidirectional converter, this battery can behave both as a source or a sink i.e. the vehicles can collectively charge or discharge respectively.

The bidirectional converter, interfaced with the EV battery, is synchronized with the grid at point **a**. Power injection by the battery is the power at connection point **b**, which is at the grid side. Power delivered by the battery storage can be written as:

$$S_{EV} = VI^* \tag{2.1}$$

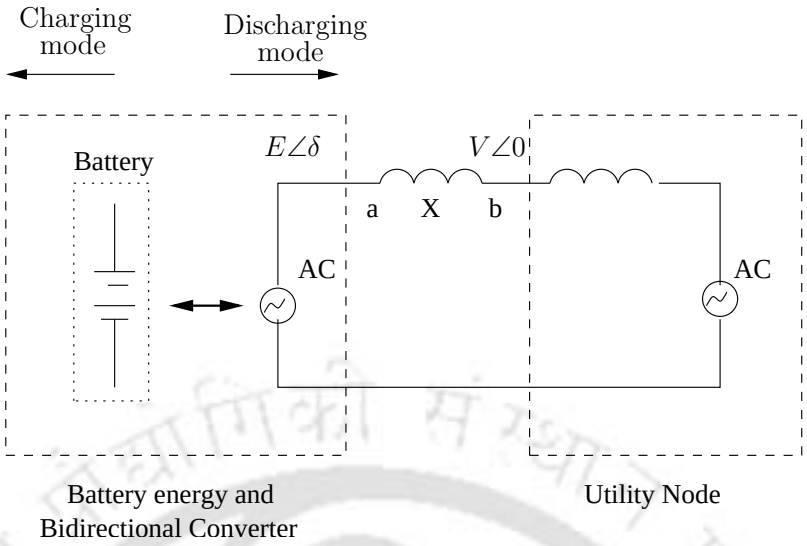

Figure 2.3: EVs' batteries used as a Distributed Energy Source

where,

$$I = \frac{E\angle\delta - V\angle 0}{jX} \tag{2.2}$$

In Eq (2.1) and Eq. (2.2), S_{EV} and I are the power and current supplied by the battery respectively. I^* is the complex quantity representation of I. During discharging, E and V are the voltages at the sending and receiving ends respectively. During charging of EVs' batteries E and V are the voltages at the receiving and sending end respectively. δ is the angle between E and V. X is the line reactance between the converter and the utility node. Substituting the value of I in Eq. (2.1) and separating the real and imaginary parts, power delivered by the battery to the grid is as follows:

$$S_{EV} = \frac{EV\sin(\delta)}{X} + j\frac{E\{E - V\cos(\delta)\}}{X} \tag{2.3}$$

From equation (2.3), real power P_{EV} and reactive power Q_{EV} are given below:

$$P_{EV} = \frac{EV\sin(\delta)}{X} \tag{2.4}$$

$$Q_{EV} = \frac{E\{E - V\cos(\delta)\}}{X} \tag{2.5}$$

If only reactive power injection by the EV is required, angle δ will be made zero. Substituting

$\delta = 0$ in equations (2.4) and (2.5), the active and reactive power at the sending end becomes as follows:

$$P_{EV} = 0 \tag{2.6}$$

$$Q_{EV} = \frac{E^2 - EV}{X} \tag{2.7}$$

Now if only real power injection by the EV is required, angle δ will be made equal to 90 degree. Substituting $\delta = 90$ degree in equations (2.4) and (2.5), the active and reactive power at the sending end becomes as follows:

$$Q_{EV} = \frac{E^2}{X} \tag{2.8}$$

Hence, EVs with the help of converters can support active as well as reactive power or a combination of both by selecting a desired value of angle δ. The converter will be controlled in such a way that the phase angle between E and V is always zero so as to inject only reactive power for low voltage correction. For large amounts of voltage correction, the angle has to be adjusted in order to inject real as well as reactive power at the concerned node. Since the aim of this work is to present the concept of grid support by injecting only real power, a power factor of 0.9 is assumed for all cases of charging and discharging systems.

Thus, the EVs at the charging station will be discharging during peak hours to improve voltage level of the grid and charging during the off-peak hours of the day. During the charging phase, the EVs' batteries will consume power from the grid system while the power consumption will become zero when the battery system is fully charged.

2.3 V2G and its impact on the radial distribution network

A typical radial distribution system is shown in Figure 2.4, where $S_0 = P_0 + jQ_0$, $S_{i-1} = P_{i-1} + jQ_{i-1}$, $S_i = P_i + jQ_i$, $S_{i+1} = P_{i+1} + jQ_{i+1}$ and $S_n = P_n + jQ_n$ are the total apparent power flowing in the respective branch. The apparent power is a combination of both real and reactive power. $S_{Li-1} = P_{Li-1} + jQ_{Li-1}$, $S_{Li} = P_{Li} + jQ_{Li}$ and $S_{Li+1} = P_{Li+1} + jQ_{Li+1}$ are

the loads at respective node. V_i is the voltage of bus i, P_i and Q_i are the real and reactive power flows in line i. P_{Li} and Q_{Li} are the loads at bus i. The batteries of the EVs, behaving as a distributed energy resource (DER), are connected at bus i via a charging station. This charging station injects real power P_{EV} and reactive power Q_{EV}. The equation for voltage at $(i+1)^{th}$ bus can be obtained as [44],

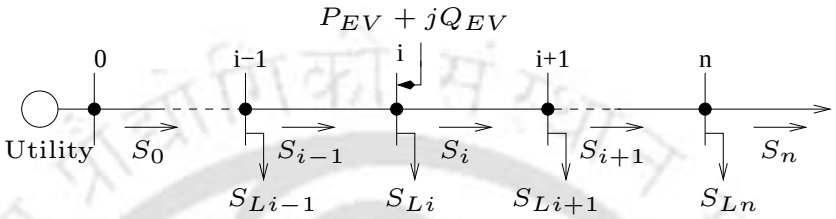

Figure 2.4: A Radial System.

$$V_{i+1}^2 = V_i^2 - 2(P_i r_i + Q_i x_i) + (\frac{P_i^2 + Q_i^2}{V_i^2})(r_i^2 + x_i^2) \tag{2.9}$$

where r_i and x_i are the resistance and reactance of the i^{th} line respectively. V_i is the voltage of the i^{th} node. From Figure 2.4, active power and reactive power at $(i+1)^{th}$ node can be calculated with the help of forward branch equation [45].

$$\begin{aligned} P_{i+1} &= P_i - P_{Li+1} - P_{lossi} \\ Q_{i+1} &= Q_i - Q_{Li+1} - Q_{lossi} \end{aligned} \tag{2.10}$$

In above equations, P_i and Q_i includes the P_{EV} and Q_{EV} which are the active and reactive power supplied by the charging station.

The real and reactive power losses for line i are

$$P_{lossi} = P_{i+1} + P_{Li+1} - P_i \tag{2.11}$$

$$Q_{lossi} = Q_{i+1} + Q_{Li+1} - Q_i \tag{2.12}$$

As P_{EV} and Q_{EV} which are the active and reactive power supplied by the charging station is included in the P_i and Q_i of Eq. (2.11) and Eq. (2.12), the real and reactive power loss will reduce.

The real and reactive power loss can also be written as follows.

$$P_{Lossi} = (\frac{P_i^2 + Q_i^2}{V_i^2})r_i \tag{2.13}$$

$$Q_{Lossi} = (\frac{P_i^2 + Q_i^2}{V_i^2})x_i \tag{2.14}$$

For example, let P_{Li+1} is 150 kW, P_{i+1} is 350 kW and P_i without inclusion of P_{EV} is say 450 kW. Then the P_{Lossi} is 50 kW. If there is P_{EV} of 40 kW which is included in Eq. (2.11), P_{Lossi} will be 10 kW. Therefore, it can be proved that the real power loss can be reduced with the injection of power by the EVs batteries.

Voltage rise caused by injection of EV's energy to the i^{th} node is approximated by the following equation [46].

$$\Delta V_{EV} = \frac{P_{EV}r_i + Q_{EV}x_i}{V_i} \tag{2.15}$$

As explained in the above example, power loss will reduce due to injection of real power into the grid. However, injection of real and reactive power if not controlled, node voltage will rise which can be observed in Eq. 2.15.

From Eq. (2.11), Eq. (2.12) and Eq. (2.15), it is found that the power injection by EVs' battery reduces power losses and improves node voltage of the network. This is due to the fact that power flow in the transmission and distribution systems is reduced, as EV battery generates power locally to fulfill demand. This reduction in power losses is one of the main features of V2G . Other benefits of V2G are peak demand management, voltage stability and reactive support. The main work of this chapter is to utilize the V2G for voltage support and peak demand management using Fuzzy Logic Controller (FLC).

2.3.1 Need for coordination of EVs batteries at the CS

It is observed in the previous section that by selecting the proper value of angle δ, real and reactive power can be injected to the node. The real and reactive power losses get reduced due to injection of power from the battery to the i^{th} node. It implies that the control of power flow

between the battery and the grid needs to be control. In the case of a single battery, the power flow can be easily control by changing the proper value of angle δ. However, if a large number of EVs are present in a CS, proper coordination among the EVs is a must to achieve the desired power flow. Moreover, EVs which will arrive at the CS, may have different energy ratings and initial state of charge (SOC). Therefore, a suitable algorithm has to be developed so that it can handle different types of EVs' batteries. Also, the proper control techniques have to be used which can control the charging/discharging rate of EV's battery. Injection of large power to the node may lead to voltage rise and over-drawal of large power to charge the battery may lead to voltage collapse. Hence, a proper control techniques needs to be developed which takes a grid condition such as voltage of the distribution node in to account while charging/discharging. In this chapter, the proper control techniques has been developed to control the power flow between EVs and the grid.

2.3.2 Assumption

Following assumptions have been made in this work:

- V2G implementation using FLC has been designed at a system level. Due to large dynamics involved in the distribution system, converters connected to charge and discharge the EVs' batteries have not been modeled.
- Efficiencies of the batteries, charging system and converters have not been considered since the aim of this work is to coordinate the EVs at the CS to provide the grid support.
- Generally, the batteries of EVs ranges from 8 kWh to 40 kWh depending on the type of EVs [47]. In this chapter, three types of EVs are assumed to be present at the charging station with a battery energy of 10 kWh, 16 kWh and 20 kWh respectively. Assumed energy ratings are the standard battery ratings which have been used in the EVs.
- Total number of EVs are assumed to be 100 at the charging station. This assumption is based on the maximum power transfer capability at the desired node (point of common coupling).

2.4 V2G infrastructure based on a Fuzzy Logic Controller

As discussed in subsection 2.3.1, uncontrolled charging/discharging of EVs can disturb the voltage profile of the node at which the CS is connected. Therefore, there is a need of coordinating the EVs at the CS to control the flow of power between the CS and the node. In this chapter, charging and discharging rates of batteries have been controlled using a Fuzzy Logic Controller (FLC). For example, the input parameters to the charging station controller are taken as the current SOC of each vehicle and the voltage profile at the node on which the charging station is connected. For a low SOC and high node voltage, EV will charge while for a high SOC and low node voltage, EV will discharge. However, there may also be cases where both the SOC and node voltages are high or both are low. For such situations, low charging or discharging rate needs to be employed. Thus, the FLC has been fine tuned to take care of such situations as well, so as to keep the node voltage fluctuations within the specified norms.

2.4.1 Fundamentals of Fuzzy Logic Controller

Unlike binary logic, Fuzzy Logic is a many-valued logic where the fuzzy logic variables may have truth values ranging in different degrees between 0 and 1, known as their membership grade. Fuzzy Logic can deal with the uncertainties in the system through a simple IF-THEN rule based approach, thereby eliminating the need for a mathematical model of the system. This is especially useful in complex systems for which a complete mathematical model representation may not be possible. However, the fuzzy logic based system complexity increases rapidly with more number of inputs and outputs.

As shown in Figure 2.5, a FLC consists of four principal components: a fuzzification interface, a rule base, inference logic and a defuzzification interface. The fuzzification interface converts the binary logic inputs into fuzzy variables, while the defuzzification interface converts the fuzzy variables into binary logic outputs. This conversion is achieved by means of a membership function. The rule base is a collection of IF-THEN rules that describe the control strategy. The output from each rule in the rule base is deduced by the inference logic to arrive

at a value for each output membership function [48]. The "fuzzy centroid" of the composite area of the output membership function is then computed in order to obtain a binary output value [49, 50]. In this chpater, Mamdani type FLC [51] has been designed for the controllers. The detail explanations of the FLC is mentioned in Appendix A.

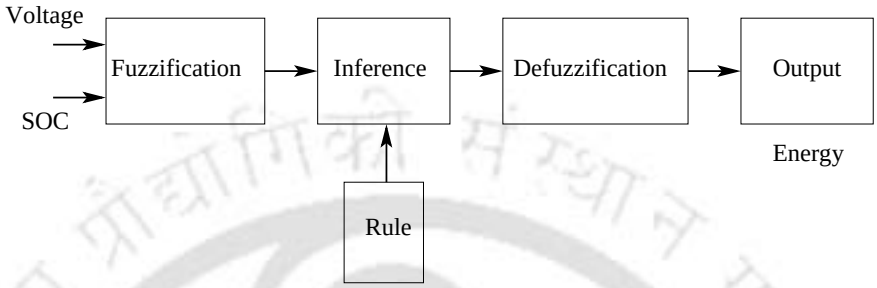

Figure 2.5: Fuzzy Controller

2.4.2 Design of Fuzzy Controllers for V2G

The control scheme has been designed at two levels. The first one is at the CS level, while the second is at the distribution node level. The CS level controller, named as Charging Station Controller (CSC), will decide on the individual participation of the EVs for charging or discharging. The input parameters to the CSC would be the individual vehicle battery's SOC and the current node voltage. Thus, depending on battery's SOC and the present grid conditions, CSC will decide the amount of energy available at the CS for grid support. For a positive energy output, the net energy flow is from CS to the grid, while for a negative energy output, the net energy flows from the grid to the CS.

Availability of energy will be based on number of EVs at the charging station, their battery rating and their present SOC. The charging station will have **n** number of controllers, which will depend upon the number of EVs in that node area. Designing a large number of controllers will increase the computation time. Hence, in this chapter, three levels of SOC with different energy rating of the batteries are considered. Therefore, only three FLC have been designed at charging station and the structure is shown in Figure 2.6. First Controller has 30 % SOC, second one is 60 % SOC and third one is 90% SOC. These divisions are based on the three

levels of the SOC of vehicles reaching the charging station.

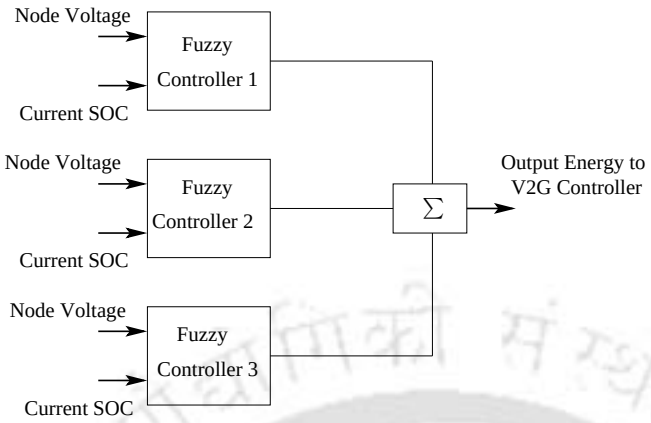

Figure 2.6: Charging Station Controller

The second controller used at the distribution node level, known as the V2G controller, is placed after the CSC. Depending on the energy output information from the CSC, the V2G controller decides the amount of power flow to and from the node on which the charging station has been connected. As shown in Figure 2.7, the energy output from the CSC is fed to a summing block. The present energy value at the node serves as the second input to this summing block. The net energy output from this summing block thus takes into account both the batteries' energy and the current grid energy. This net energy output is in turn given as an input to the V2G controller, while the other input parameter to the V2G controller is the current node voltage. The V2G controller now outputs the power to be given or taken from the node. This output power is taken negative for the case where the charging station is acting as an energy source i.e. the energy output from the CSC is positive. Whereas a positive output power indicates that the charging station is acting as a load i.e. when the energy output from the CSC is negative. The notations used is shown in Table 2.2. This sign convention has been taken so as to provide a negative feedback of the grid energy at the summing block.

The output of the V2G controller, as shown in Figure 2.7 (PQ point), is connected to sub feeder node **6.3** of Figure 2.2 for controlling the power flow between EVs and the grid. This PQ node is the ultimate node of interest for voltage support and peak load management. FLC output of V2G controller is the set point for the real power controller.

Table 2.2: Controllers notations

CSC		V2G	
Operation Mode	Output Energy	Operation Mode	Output Power
Charging	Positive	Source	Negative
Discharging	Negative	Load	Positive

For example, let us suppose that total available energy at the CS is 300 kWh and the node voltage is 0.91 p.u. The CSC controller decides that only 250 kWh of negative energy can be given to the grid. Now 250 kWh of energy as decided by the CSC will be one of the input to the V2G controller. This input energy information will be updated every instant of time with the amount of power supplied to the grid with the help of integrator. This updated energy information of the CS and the current node voltage will be the input to the V2G controller. Now V2G controller decides the amount of power which can be supplied to the node. Let this power be 50 kW, which should flow between the node and the CS, to maintain the node voltage within specified limit as well to support the grid in terms of peak shaving. It implies that 50 kW can be supplied to the grid for 5 hrs.

The advantage of using a two-level control strategy here is that the current energy supplied by the charging station to the distribution node or energy required to charge the EVs is directly fed back to V2G controller. For a situation with a single level of control i.e. with only the CSC present, the grid energy feedback would have to be given to all 'n' CSCs, where 'n' is the total number of vehicles at the charging station. The merit of the distributed control architecture implemented in this work is that in case of some fault in the centralized control system, operation of other controllers will also be affected, whereas with distributed control, if a controller fails, only a certain section of the grid is affected.

2.4.3 Fuzzy membership functions for V2G and CS controller

The fuzzification is largely determined by the choice of the shape of the membership functions. The most common shape of membership functions is triangular, however trapezoidal and bell curves are also used in many application. The type of shape is generally less important

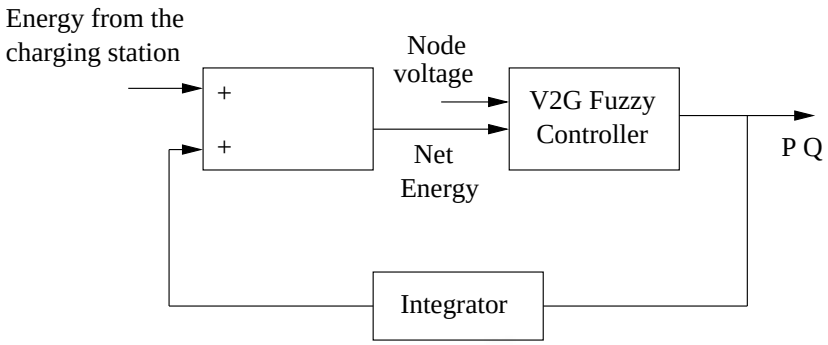

Figure 2.7: V2G Controller

as compared to the number of curves and their placement. In order to facilitate computations, triangular membership functions are utilized in this study for both the input and output membership functions. The Mamdani type inference (also known as the maxmin inference method), utilizes the minimum function for the implication of the rules. Defuzzification is performed using the center of gravity method where the center of the area encompassed by all the rules, and is mathematically described by

$$u(t) = \frac{\sum_{i=1}^{n} u_i \mu_v(u_i)}{\sum_{i=1}^{n} \mu_v(u_i)} \tag{2.16}$$

where $u(t)$ refers to the defuzzified overall control output, u_i refers to the output variable and μ_v represents the aggregated membership function.

- The input voltage is fuzzified into corresponding fuzzy signals with five linguistic variables; very low (VL), low (L), medium (M), high (H) and very high (VH).
- The input energy is fuzzified into ten fuzzy regions representing the linguistic variables; very negative high (VNH), negative high (NH), negative medium (NM), negative low (NL), very negative low (VNL), very positive low (VPL), positive low (PL), positive medium (PM), positive high (PH) and very positive high (VPH).
- The output is fuzzified into 12 fuzzy regions represented by linguistic variables;

very negative high (VNH), negative high (NH), very negative medium (VNM), negative medium (NM), negative low (NL), very negative low (VNL), very positive low (VPL), positive low (PL), positive medium (PM), very positive medium (VPM), positive high (PH), very positive high (VPH).

Similar membership functions can be defined for the charging station controller where voltage and SOC are the two inputs and the output is the corresponding energy. The membership functions for V2G controllers are shown in Figure 2.8, Figure 2.9 and Figure 2.10. The rule base for V2G controller is given in Table 2.3, where 'E' refers to energy and 'V' refers to voltage.

Table 2.3: Rules for V2G Controller

$E \downarrow \backslash V \rightarrow$	VL	L	M	H	VH
VNH	VPL	PL	PM	VPM	PH
NH	VPL	PL	VPM	PH	VPH
NM	VPL	PL	PM	VPM	PH
NL	VPL	PL	PM	PH	VPH
VNL	VPL	PL	VNL	NL	NM
VPL	VNL	VNL	NL	PL	VPL
PL	VNL	NL	NM	NM	VNM
PM	NH	VNH	NM	NL	VNL
PH	VNH	NH	NM	NL	VNL
VPH	VNH	NH	VNM	NL	VNL

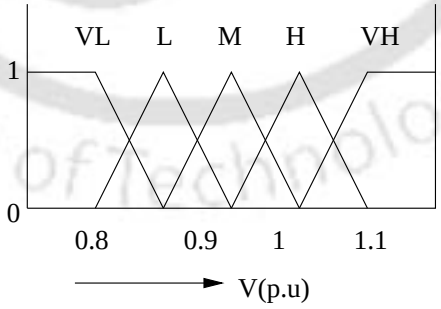

Figure 2.8: Fuzzy Membership Function (Voltage)

Similarly, the fuzzy membership functions for the CSC are shown in Figure 2.11. Membership functions for voltage and energy are similar to V2G controller. The rule base for charging station is given in Table 2.4.

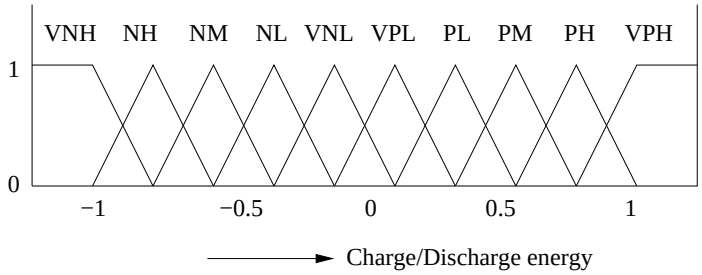

Figure 2.9: Fuzzy Membership Function (Energy)

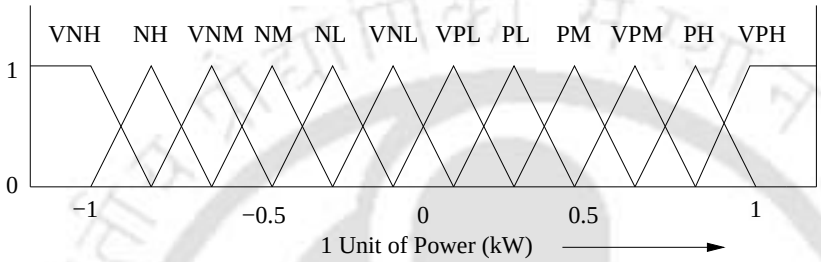

Figure 2.10: Fuzzy Membership Function- load/source of EV battery

Fuzzification and defuzzification example by taking practical case has been demonstrated in Appendix A.

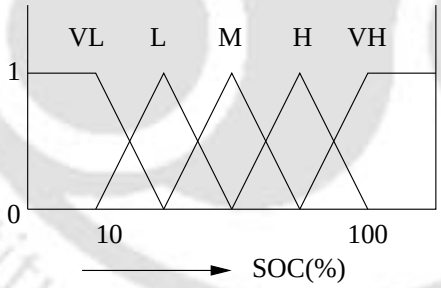

Figure 2.11: Fuzzy Membership Function (SOC)

Table 2.4: Rules for Charging Station Controller

$V \downarrow \backslash SOC \rightarrow$	VL	L	M	H	VH
VL	VPL	PL	PM	PH	VPH
L	VPL	PL	PM	PH	PH
M	VNL	VPL	PL	PM	PM
H	VNH	NH	NM	NL	VNL
VH	VNH	NH	NM	NL	VNL

Table 2.5: Total energy available for grid support (Scenario I).

SOC	Energy (kWh)	No. of EVs	SOC required for discharging (%)	Available energy for the grid support (kWh)
30	10	25	-20	-50
60	16	25	10	40
90	20	50	40	400
Total energy for discharging				390

2.5 Possible scenarios of EVs at charging station

Primary job of the EVs are commutation and hence a minimum SOC value should always be maintained to meet any emergency needs. A minimum SOC of 50% has been assumed to meet any emergency needs. Two scenarios are developed for calculating the energy available for grid support as well as energy required for charging the EVs. In the first scenario, it is assumed that 390 kWh of energy is available which is shown in Table 2.5. In the second scenario, 192 kWh of energy is available which is given in Table 2.6. These two scenarios together serve as a base case for the study of grid support by EVs. Available energy of the battery can be found from following equation.

$$Energy_{available} = (\frac{SOC - 50}{100})Energy_{rated} \tag{2.17}$$

where $Energy_{available}$ is the available energy for the grid support in kWh, $Energy_{rated}$ is the rated energy of the battery in kWh.

For example, if the current SOC of the battery is 60%, a minimum SOC is kept to be 50% and energy rating of the battery is 16 kWh then for the available energy for 25 EVs of similar rating will be 40 kWh (Table 2.5). Similarly, if EVs arrive at the CS with 30% SOC and having energy rating of 10 kWh with 50% minimum SOC limit, the total available energy for 25 EVs of similar rating will be -50 kWh. The negative energy implies that instead of excess energy, batteries need 50 kWh to charge.

Similar assumption is made for developing the scenarios for charging of EVs as well such

Table 2.6: Total energy available for grid support (Scenario II).

SOC	Energy (kWh)	No. of EVs	SOC required for discharging (%)	Available energy for the grid support (kWh)
20	10	20	-30	-60
40	16	30	-10	-48
80	20	50	30	300
Total energy for discharging				192

as initial SOC and energy rating of the batteries. It can be seen from Table 2.7 that charging scenario I requires 435 kWh of energy and from Table 2.8, it is clear that charging scenario II requires 648 kWh of energy to charge the EVs. The energy required for charging can be found from the following equations:

$$Energy_{required} = (\frac{100 - SOC}{100})Energy_{rated} \tag{2.18}$$

where $Energy_{required}$ is the required energy from the grid to charge the battery in kWh and $Energy_{rated}$ is the rated energy of the battery in kWh.

For example, battery with current SOC of 30%, needs to charge upto 100%. If the energy rating of the battery is 10 kWh, then the energy required to charge during off-peak hours for 25 EVs of similar rating will be 175 kWh.

Following equations can also be used for calculating the total energy required for charging and total energy of EVs available during discharging:

$$E_{charging} = NRS_{req} \tag{2.19}$$

$$E_{discharging} = NRS_{av} \tag{2.20}$$

where $E_{charging}$ is the total energy required during charging, $E_{discharging}$ is the total energy available for grid support, N is the total number of EVs, R is the kWh rating of battery, S_{req} is the required amount of charging in SOC and S_{av} is the SOC required for discharging to the grid. Eq. (2.19) and Eq. (2.20) are used for calculating the total energy of EVs during charging

Table 2.7: Total energy required during charging (Scenario I)

SOC	Energy (kWh)	No. of EVs	SOC required for charging (%)	Energy required for charging (kWh)
30	10	25	70	175
60	16	25	40	160
90	20	50	10	100
Total energy for charging				435

Table 2.8: Total energy required during charging (Scenario II)

SOC	Energy (kWh)	No. of EVs	SOC required for charging (%)	Energy required for charging (kWh)
20	10	20	80	160
40	16	30	60	288
80	20	50	20	200
Total energy for charging				648

and discharging.

2.6 Analysis of charging and discharging

In this section, V2G capabilities for voltage stability and peak demand management have been explored. The simulations have been performed for both cases i.e. charging as well discharging of the EVs. For each of these cases, the two scenarios developed in the previous section have been simulated for a dynamic behavior of the grid. Charging and discharging of EVs for the two scenarios are presented separately. In this analysis, grid support is provided by injecting active power with a constant power factor of 0.9. Reactive support has not been considered in this work. Analysis of the V2G controller is carried out for node **6.3** of Figure 2.2 for all test cases.

2.6.1 Discharging of EVs' energy to the grid

Based on the number of EVs and their SOCs, total available energy for the first scenario is 390 kWh, which is shown in Table 2.5. As explained earlier, the V2G controller can control the flow of power to the distribution node based on the information regarding the available energy at the charging station and the present node voltage. The simulation results of voltage and power discharge to the node are presented in this part. Finally the results are compared with discharging system of EVs at 0.85 p.f.

During peak hours, the node voltage before discharging of EVs' energy to the grid is found to be 0.93 p.u. and it is shown in Figure 2.12. However, the node voltage improved to 0.98 p.u. after discharging of EVs energy to the grid as shown in Figure 2.13. It is observed that the voltage level has settled at 0.05 second. From the simulation results, it has been found that net power discharged to the node is 104 kW and is shown in Figure 2.14. It is seen that power injection by EV's battery improves the node voltage of the network. Net energy supplied by

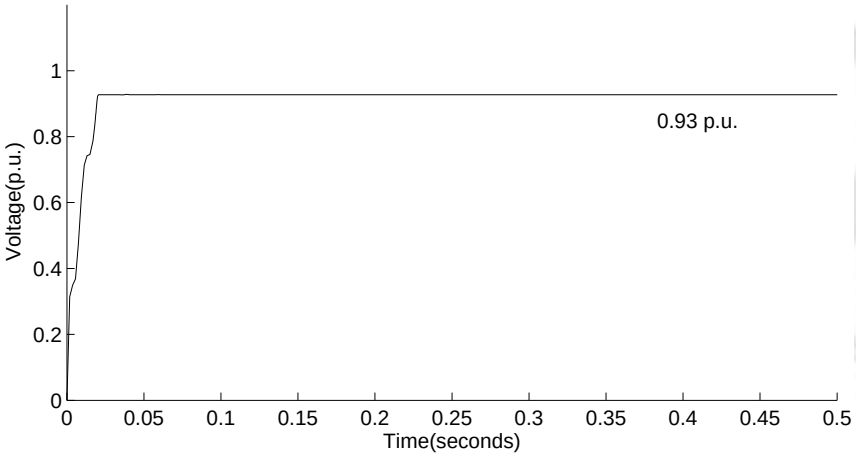

Figure 2.12: Peak hours voltage before discharging of EVs' energy to the grid

the charging station and the individual charging station controllers with their SOC are shown in Figure 2.15.

Another simulation has been carried out by making the power factor of the discharging system to be 0.85. The voltage profile at 0.85 p.f has been shown in Figure 2.16. It is seen that voltage has been reduced to 0.956 p.u. as compared to 0.98 p.u. in the previous case.

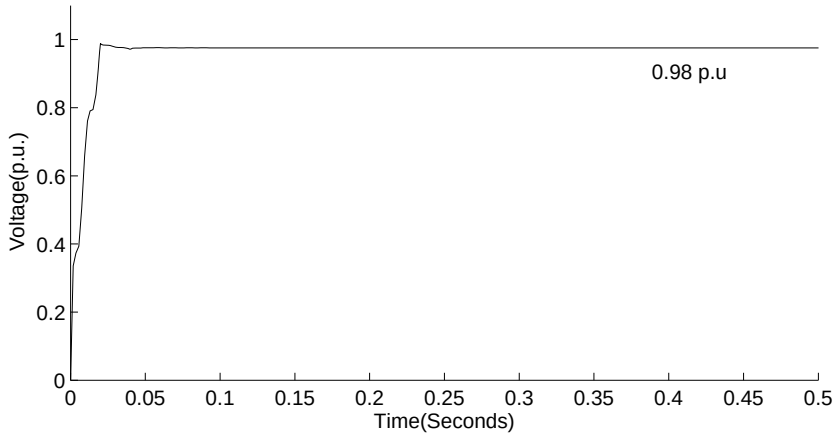

Figure 2.13: Peak hours voltage after discharging of EVs' energy to the grid (Scenario I)

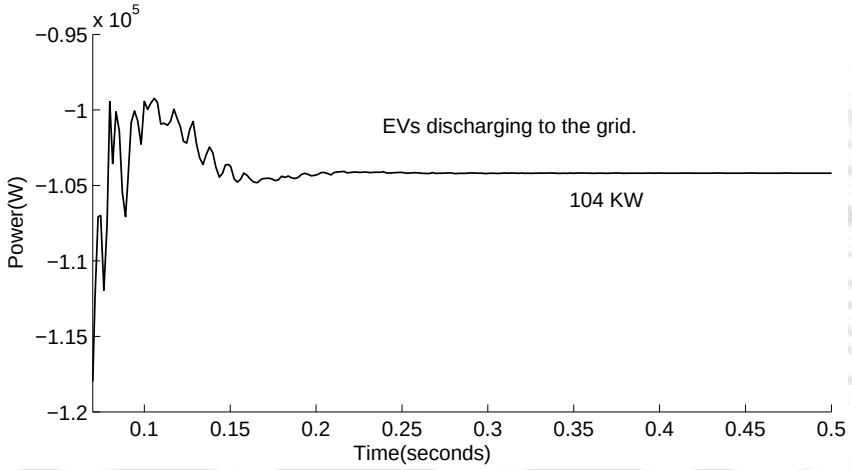

Figure 2.14: Power supplied by EVs charging station (Scenario I)

This implies that discharge of energy from the EVs with low power factor results in a poorer grid support. This happens because a lower power factor will limit the amount of real power output for a given apparent power rating, as the net apparent power output (VA) from the EVs cannot exceed the given apparent power rating. This can be verified from Figure 2.17, where the power discharge has been reduced to 98.5 kW as compared to 104 kW in the previous case. In further simulations, a p.f of 0.9 will be used for all scenarios and test cases.

In scenario II, energy from the EVs available for grid support is 192 kWh as given in Table 2.6. It can be seen from the simulation results, given in Figure 2.18, that the net power

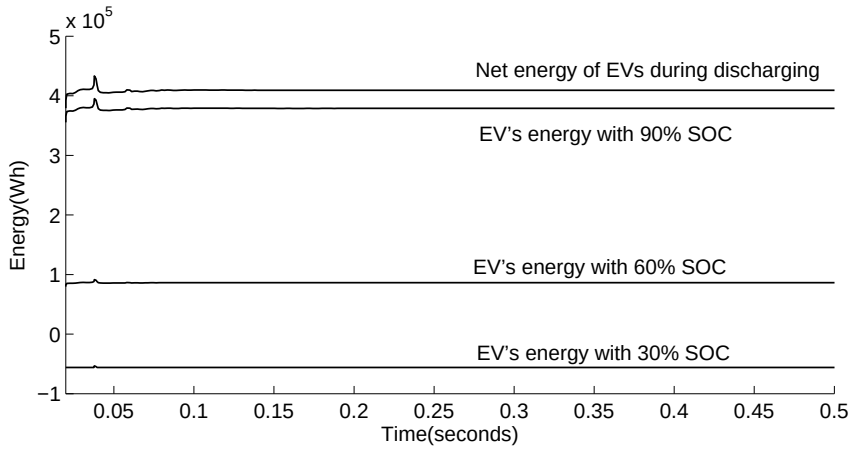

Figure 2.15: Energy from individual charging station Controllers (Scenario I)

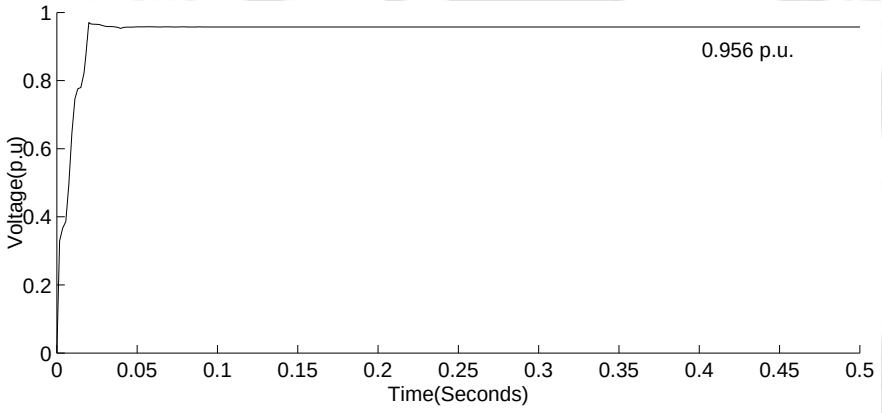

Figure 2.16: Voltage at node 6.3 of subfeeder 5 at a p.f of 0.85

discharged to the node is 70 kW. Figure 2.19 shows that the final voltage is 0.95 p.u. This implies that for a low value of energy available from the EVs (192 kWh), very little improvement is found in the voltage profile. This improvement in voltage is compared with the original node voltage of 0.93 p.u before discharge, as in Figure 2.12. Hence, we observe that for such situation the FLC is tuned so as not to allow any further decrease of the node voltage when grid conditions are poor.

After the discharge of energy from the EVs, it was found that the SOC levels have also changed. SOC levels of EVs' battery before and after discharging are shown in Figure 2.20. It can be observed from the figure that the charging station always ensures that the SOC of the batteries are maintained at least at 50% level during grid support operation.

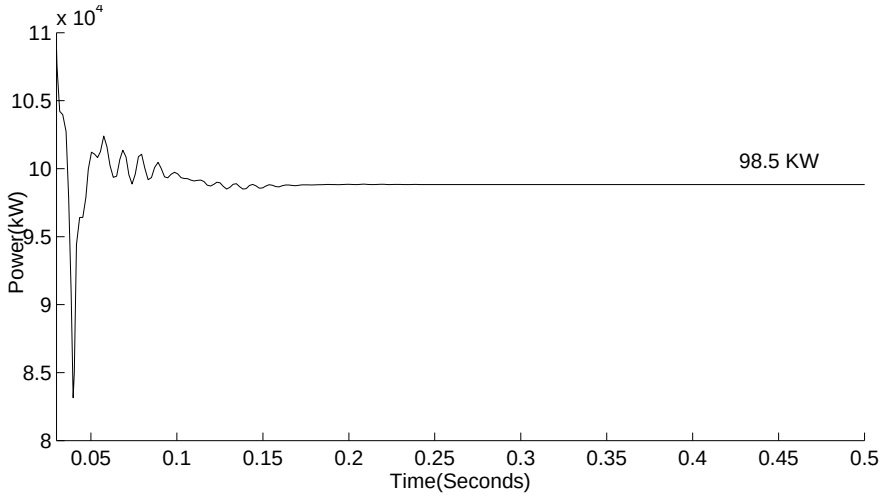

Figure 2.17: Power discharge during off peak hours at a p.f of 0.85

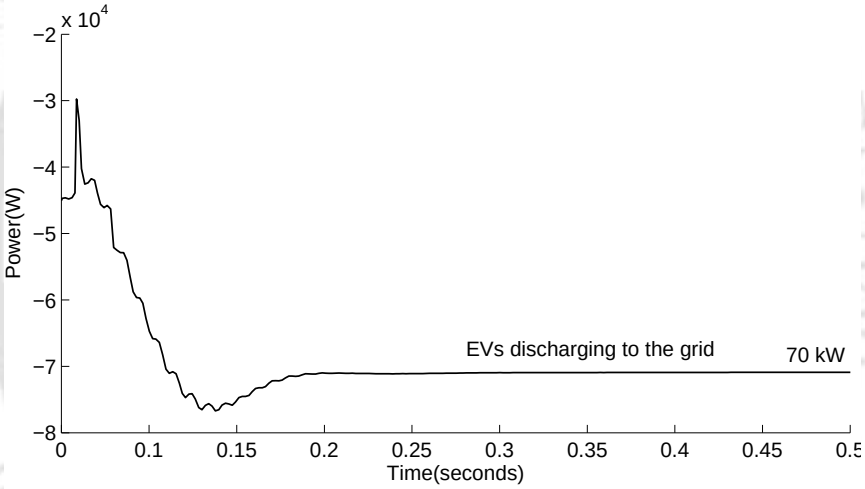

Figure 2.18: Power supplied by EVs charging station (Scenario II)

Let take an example to illustrate the SOC level of the battery. It has been observed that 50% should always be there even during grid support. Therefore, the battery with low SOC (SOC less than SOC limit) will charge first to reach the SOC limit. However, the batteries with higher SOC will discharge. The net discharge to the grid will be the algebraic summation of charge as well as discharge. This can be seen in Table 2.5 where net energy available for discharging to the grid is 390 kWh. This net energy includes the charging energy of the first type of battery which is -50 kWh. As observed from Figure 2.15, that 104 kW of power is being discharged to the grid. It implies that 390 kWh can support the grid for 3.75 hrs. Therefore,

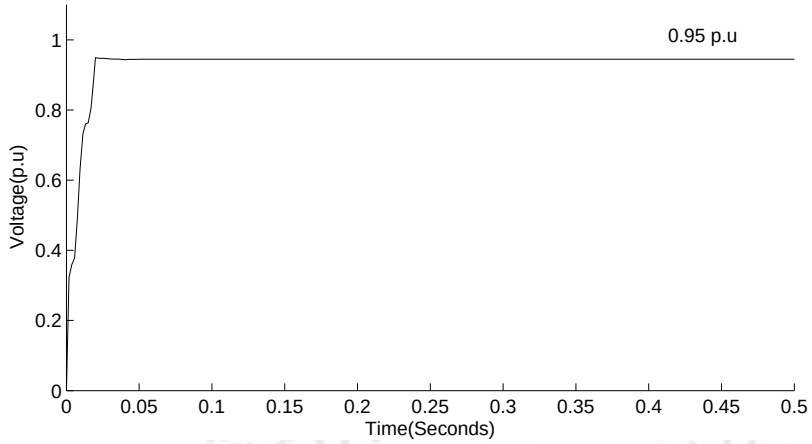

Figure 2.19: Voltage at node 6.3 of subfeeder 5 (scenario II)

the batteries with low SOC will charge to reach SOC limit of 50% even during peak hours and the batteries with higher SOC will discharge to the grid. After 3.75 hrs, it has been observed from the figure that batteries with 30% SOC charge to reach 50% and the batteries with 60% and 90% will reach to 50% after discharging to the grid.

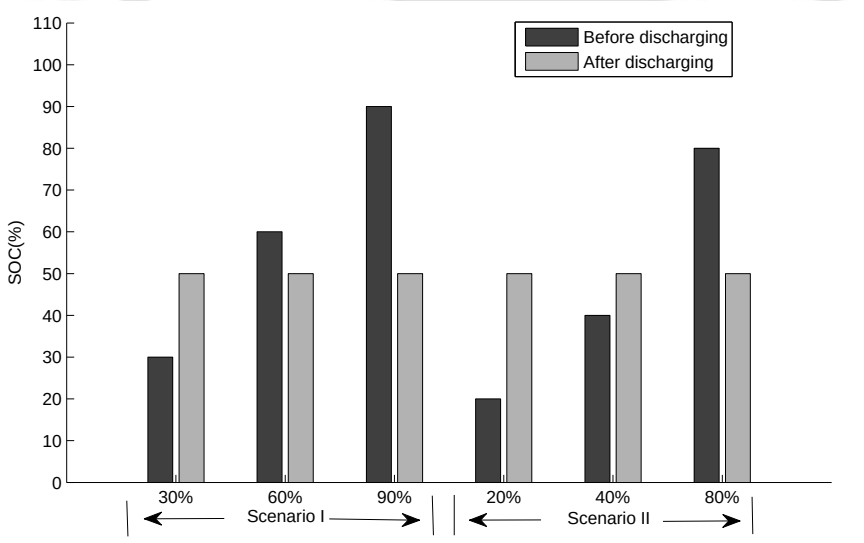

Figure 2.20: SOC after discharging of EVs' energy to the grid.

2.6.2 Charging of EVs from the grid

In Section 2.5, EVs' energy required for charging is developed for two scenarios. Scenario I given in Table 2.7 is used during peak hours and scenario II given in Table 2.8 is used during

off peak hours. During peak hours, distribution grid is heavily loaded and thus, the controllers will not allow all EVs to charge to their full capacity during these periods.

Charging of EVs' batteries is analyzed for scenario I, as given in Table 2.7. In this scenario, 435 kWh of energy is required to charge the EVs. In this case, the charging station controller will not allow all EVs to charge at the same time. The controller will restrict the flow of power based on node voltage. It has been shown in Figure 2.21 that node voltage during charging is 0.91 p.u. Figure 2.22 shows that a total of 60 kW is drawn from the grid to charge the EVs. The settling time is found to be 0.15 sec. The controller has limited the power flow to the EVs so that voltage should not fall below the standard norms.

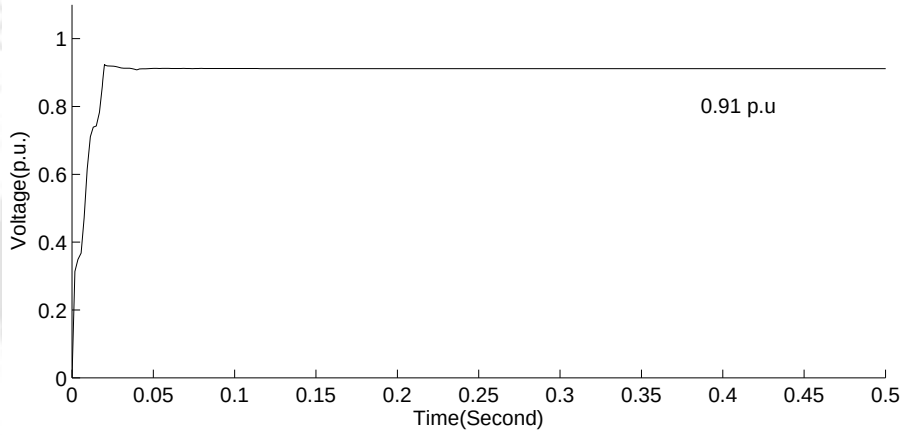

Figure 2.21: Voltage during charging(Scenario I)

The second scenario as given in Table 2.8 has been simulated for charging of EVs during off peak hours. In this case, a total of 648 kWh of energy is required to charge the EVs. Generally, a high node voltage is observed during these periods because the grid is lightly loaded and hence, the controller allows more EVs to charge. Voltage levels before and after the charging of EVs have been shown in Figure 2.23. Initially, voltage at the node was 1.02 p.u. and due to charging of EVs, voltage has reduced to 0.96 p.u. This reduction in voltage is due to heavy power drawn by EVs during charging. In Figure 2.24, it is seen that a power of 170 kW is being drawn. This implies that the controller has allowed more EVs to charge during off peak hours as it has sensed the high node voltage during these periods.

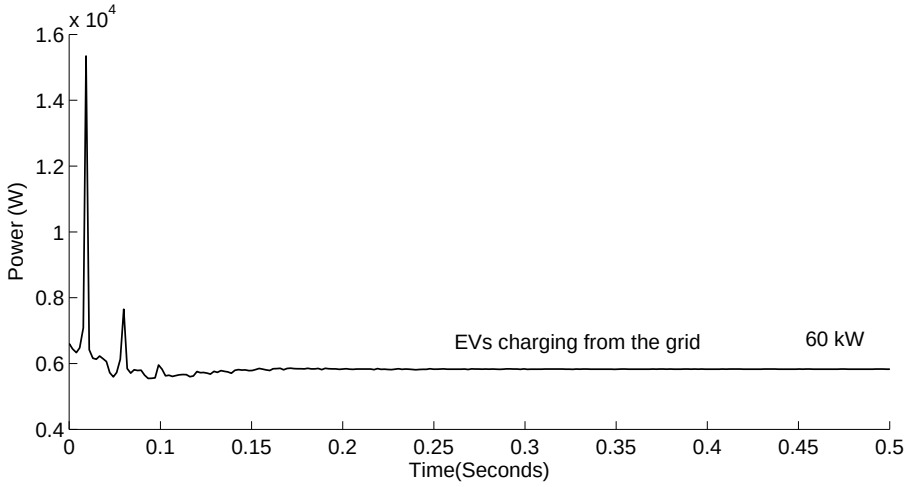

Figure 2.22: EVs charging from the grid (Scenario I)

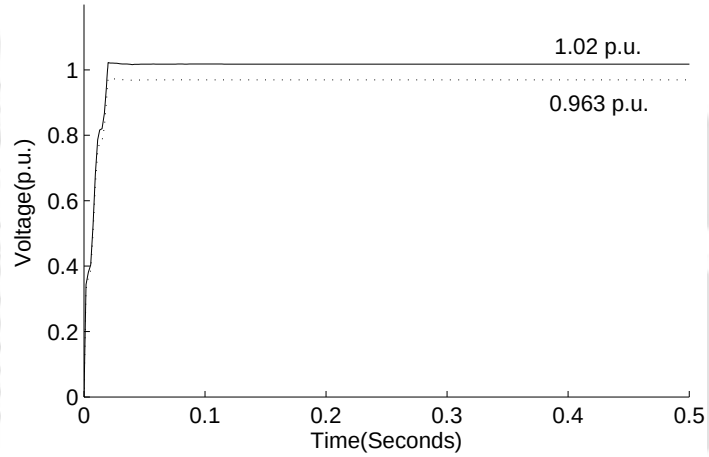

Figure 2.23: Voltage during charging (scenario II)

After charging of the EVs, it was found that the SOC levels have changed. SOC of EVs' batteries before and after charging are shown in Figure 2.25. EVs have attained 100% SOC in both the scenarios after completion of the simulation.

This can be better explained, by taking a example for charging the EVs batteries for Scenario I (Table 2.7). In this table, it has been found that 435 kWh of energy is required by the CS to charge their batteries and from Figure 2.18, it is seen that 60 kW of power has been drawn by the CS. It implies that during off-peak hours, the batteries will charge for 7.25 hrs. Once the batteries completely charged, the SOC of the batteries will be 100%. Therefore, it can be

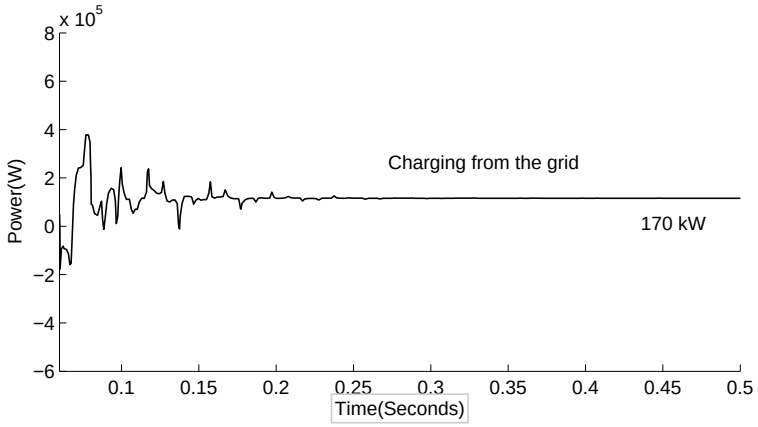

Figure 2.24: EV's charging from the grid (Scenario II)

concluded that the EVs batteries will charge for longer duration so that it can support the grid in most of the off-peak hours.

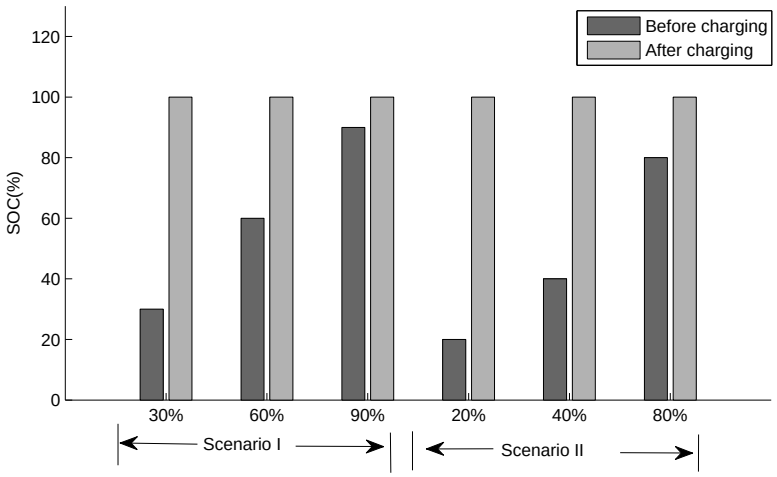

Figure 2.25: SOC of EVs' battery after charging

2.7 Discussion of results

In the previous section, analysis of V2G using FLC has been presented for charging and discharging of EVs. In this section, results obtained from the previous section are illustrated for meeting the peak demand. Charging and discharging behavior of the EVs during peak and off peak period is analyzed with the help of two scenarios developed in Section 2.5. In the

last part of this section, flattening of load profile is demonstrated with the help of simulation results.

2.7.1 Discharging energy to the grid

Guwahati city alone has 58 MW of peak power deficit [52]. The 33kV substation of Guwahati city used in this work has a peak deficit of 3 MW. This substation has 20 nodes and each node has a power deficit of 150 kW. For meeting the peak demand, scenario I developed in Section 2.5 is used. For discharging of EVs's energy, 390 kWh of energy is available, as given in Table 2.5. The duration for which the power is available for supporting the grid can be calculated by the following equations:

$$S_{grid} = \sqrt{P_{grid}^2 + Q_{grid}^2} \tag{2.21}$$

$$T = \frac{E_{av}}{S_{grid}} \tag{2.22}$$

where, S_{grid} is the total power taken from the battery, Q_{grid} is the reactive power of the discharging system, T is the time in hours, E_{av} is the energy of the batteries available in kWh and P_{grid} is the real power given to the grid.

Peak demand management using EVs' energy for various possibilities is shown in Figure 2.26. In this figure, peak deficit of 150 kW can be managed using EVs energy in several ways. If power injection is more than the deficit, the voltage will rise at that particular node whereas selecting the lowest power injection, which is 97.5 kW, will make the deficit 52.5 kW for 4 hrs. As mentioned earlier, the FLC has been designed so as to decide the power injection based on the nodal voltage and energy available from the EVs.

Analysis of the first scenario can be validated from Figure 2.14, where power discharge to the node during peak hours is 104 kW. The controller has sensed the node voltage and based on the availability of EVs' energy at the charging station, it has allowed only 104 kW of power to be discharged. Using Eq. (2.21) and Eq. (2.22), the time required to discharge 390 kWh of energy to the grid at 0.9 p.f is 3.375 hrs. Meeting the peak demand with the help of controller is shown in Figure 2.26.

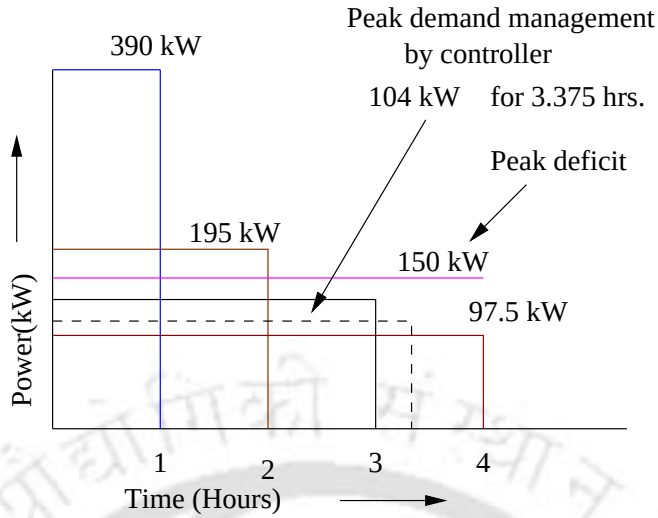

Figure 2.26: Peak demand management using available energy of EV's battery (scenario I)

Discharging of EVs for scenario II, as shown in Table 2.6, has also been demonstrated. In this scenario, 192 kWh of EVs'energy was available for meeting the peak demand. Figure 2.27 shows various possibilities to inject the EVs' power at the node to minimize the peak demand deficit of 150 kW. Analysis of the second scenario can be validated with the controller output shown in Figure 2.18, where power discharge to the node is found to be 70 kW. This implies, the controller will allow 70 kW of power (at 0.9 p.f) to discharge for 2.47 hrs and it will also maintain the voltage profile of the node during these periods. The voltage of node **6.3** for the second scenario is shown in Figure 2.19. Hence, it is concluded that discharging of EVs energy to the grid using FLC can improve the voltage profile and also meet the peak demand without over loading the distribution grid.

2.7.2 Charging of EVs from the grid

Charging of EVs for the two scenarios developed in Section 2.5 has also been demonstrated. In the first scenario, as given in Table 2.7, a total of 435 kWh of energy is required. The charging scenario I is simulated during peak hours to observe the effect on node voltage. Different possibilities of charging the EVs' batteries with 435 kWh energy are shown in Figure 2.28. It is found that EVs will take 72.5 kW power to charge in 6 hrs. The time duration for drawing

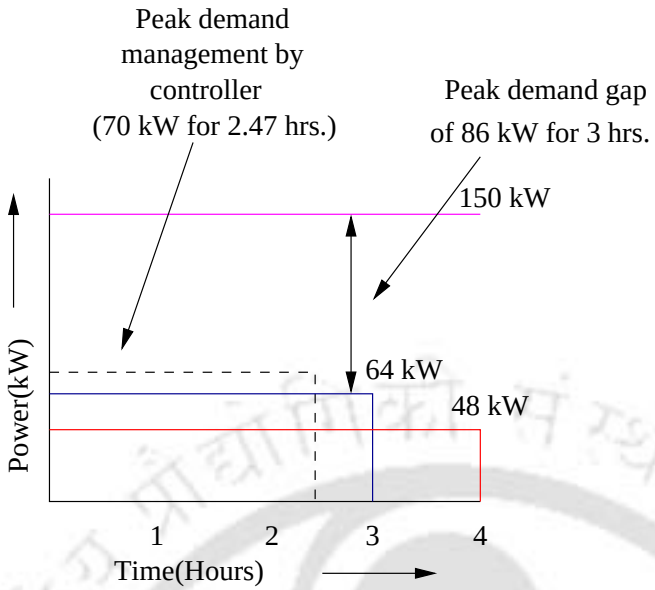

Figure 2.27: Peak demand management using available energy of EV's battery (scenario II)

total power for charging the EVs' batteries can be calculated by the following equation.

$$T = \frac{E_{req}}{P_{grid}} \tag{2.23}$$

where T is the time taken to charge the EVs' batteries. E_{req} is the total energy required for charging, P_{grid} is the active power drawn from the grid to charge the battery. From Figure 2.22, we observe that 60 kW of power was drawn for charging the EVs during peak hours. Like earlier situations, a p.f of 0.9 has been assumed for charging. From Eq. (2.23), the time required to charge the EVs is calculated to be 7.25 hrs. Hence, the controller allows EVs to charge for a limited amount of power (60 kW) so that the grid voltage does not fall below the specified limit.

Similarly, for the second scenario as given in Table 2.8, charging of EVs was allowed during off peak hours where 648 kWh of energy was required for charging. Different possibilities of charging schemes for the second scenario are shown in Figure 2.29. Selection of the appropriate charging scheme from these different possibilities is done based on the results obtained from Figure 2.24, where power drawn by the charging station is found to be 170 kW. Using Eq. (2.23), the time required to charge the EVs with 648 kWh is 3.81 hrs. This implies that during the off

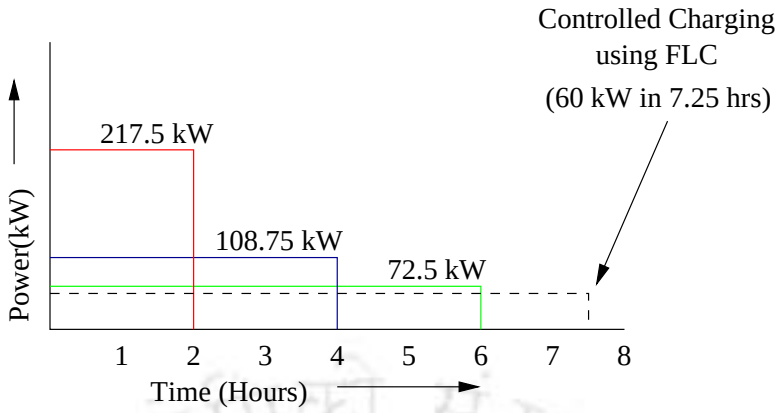

Figure 2.28: Charging schemes of EVs for scenario I

peak hours, node voltage is high and the controller has allowed charging of EVs within a very short span of time.

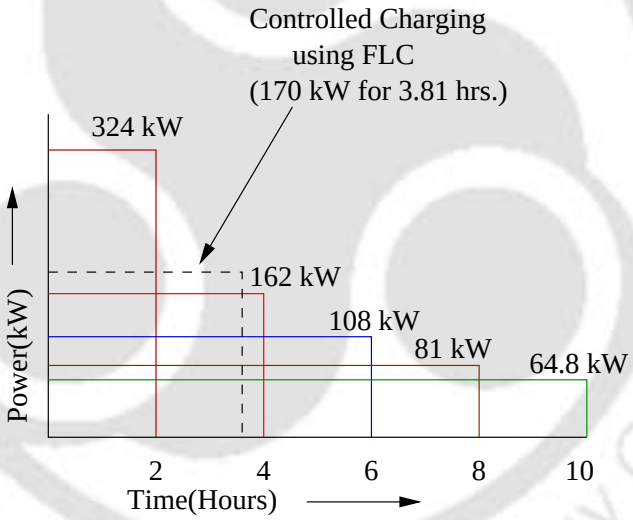

Figure 2.29: Charging schemes of EVs for scenario II

2.7.3 Flattening of load profile

Analyses of the results obtained in part A and B of this section reveal that the charging and discharging of EVs can be easily controlled using FLC. Load profile can be flattened with the charging of EVs during off peak hours and discharging during peak hours. The voltage stability of the distribution system is improved. As the demand is met locally, losses in the distribution system will reduce. Using the results obtained in the previous section, flattening

of load profile at node **6.3** is shown in Figure 2.30 . It can be seen that, as a result of this V2G operation, there is a reduction in the peak demand deficit and a rise in the off peak load. In the figure, load leveling has been shown for the peak and off-peak hours, only for the simulated time. However, this operation can be extended for 24 hrs if the EV penetration in that area is large. The charging and discharging of EVs for such a scenario can be done in slots at the charging station.

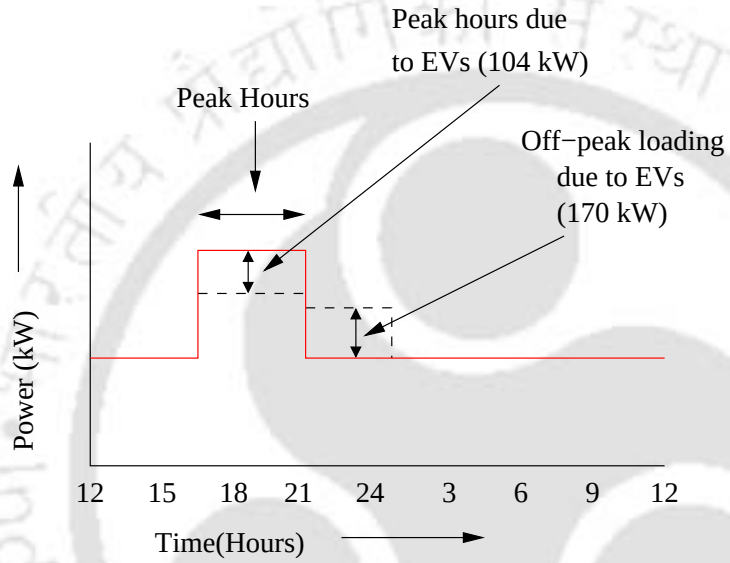

Figure 2.30: Flattening of load profile at node 6.3 during discharging and charging of EVs (Scenario I)

2.8 Summary

In this chapter, the V2G concept has been explored through simulation of a typical distribution system of Guwahati city. The concept of a charging station has been introduced where all EVs from a particular area will charge or discharge their energy to the grid from the same location. V2G controller and a charging station controller have been designed using fuzzy logic. These controllers have been used to control the flow of energy between EVs and the grid. FLC has been implemented to achieve V2G operation and the impact of this V2G operation, in terms of voltage stability and peak demand management, has been analyzed for two different scenarios. Simulation results reveal that charging and discharging of EVs can be

easily controlled using an FLC. Power leveling and peak saving can be achieved by charging of EVs during off peak hours and discharging the EVs energy during peak hours.

In the next chapter, coordination of EVs at the charging station to achieve the desired power flow is presented. The coordination of individual EVs are achieved by designing a suitable aggregators at the CS level and at the node level.

3

Multi Charging Station for dynamic load management

Contents

3.1 Introduction

In the previous chapter, concept of CS has been introduced to achieve voltage support as well as peak shaving and valley filling using Fuzzy controllers. Aggregated EVs energy is assumed at the CS to show the control aspects of power flow between the CS and the grid. Two FLCs have been developed to control the flow of power

- Between the node and CS.
- Between the CS and EVs' batteries.

However, the control strategy of charging/discharging of individual battery present in the CS has not been considered in the previous chapter. This chapter is devoted to the discussion of coordination among each EV present at the CS to achieve the desired power flow between the CS and the grid. Furthermore, the coordination of CSs connected at a single distribution node is also achieved to support the grid in terms of valley filling and peak shaving.

In this chapter, three CSs are modelled and connected to a test node of a radial subfeeder of a substation. A group of CSs connected to a single distribution node is termed as Multi Charging Station (MCS). Each CS consists of charging bays to accommodate the EVs to charge their batteries. All the EVs batteries will charge in accordance to grid norms. Here grid norms implies node voltage and it should be within specified limits (0.95 p.u to 1.05 p.u) as per the Central Electricity Authority(CEA). The purpose of designing the MCS is due to the mobility of most of the EVs at different places such as residential area, office area and market area. If all these areas share a common distribution node, the grid can be supported throughout a day. Moreover, in a realistic situation EVs may traverse between the CSs or can be in transit/idle. The EVs not present in these areas is understood to be in transit or in idle.

The reason of having a four area based system is to provide continuous support to the test node using the EVs. Since, the EVs would traverse within these four areas, the number of EVs at any instant of time will nearly be the same. All the CSs may have unequal numbers of EVs in different time slots but the total number of EVs at the MCS will always be equal in any time slot. Thus having MCS at one node covering these regions would ensure grid support in

terms of voltage, peak shaving and valley filling at any instant of time. By considering a real situation, one can model the MCS to support the grid throughout a day.

In this chapter, the concept of a multi charging station (MCS) together with its control architecture has been presented. A simulation based analysis of the proposed concept is done to test the CSs capability to handle different scenarios. Different scenarios include sudden arrival and departure of EVs at the CSs. Novelty of the proposed system is that, while maintaining the voltage profile of the node, it takes into account an individual battery's preferred charging/discharging rate (C_{rate}) as set by the EV owner. Moreover, the system does not discharge the batteries beyond the specified SOC limit set by the owner. The block diagram of MCS connected to the distribution grid is shown in Figure 3.1.

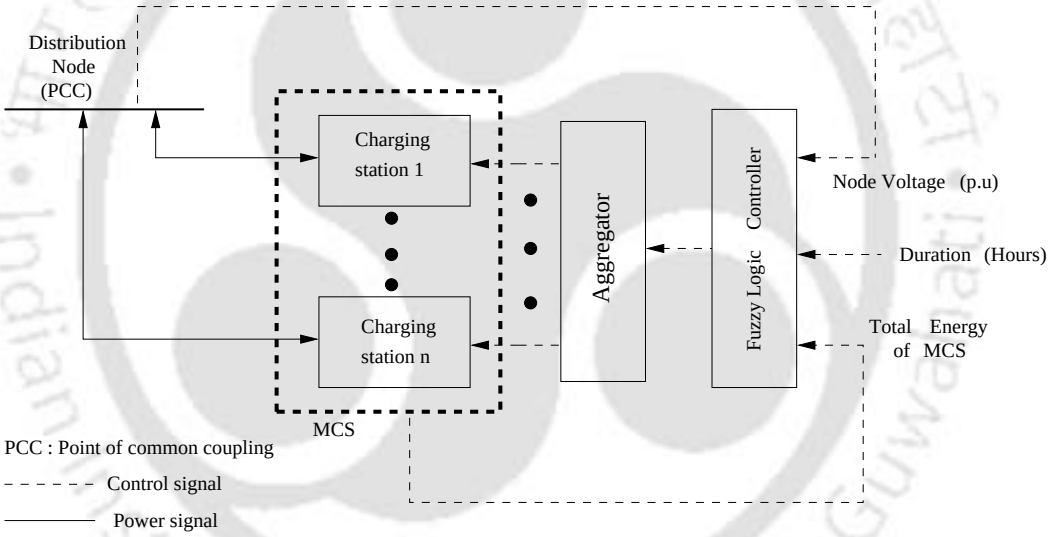

Figure 3.1: MCS connected to the distribution grid.

At the heart of the architecture, a fuzzy controller is located at the distribution node. This controller decides the direction and the magnitude of power transfer between the grid and the MCS using three inputs. The first input is the available energy of the EVs' batteries. The second input is the duration for grid support and the third input is the voltage of the distribution node at which the CSs are connected. The output of the FLC is the power required from the CSs which may be negative or positive. Negative power implies that energy is transferred to the grid from the batteries while positive power implies that energy is drawn from the grid to charge

the batteries. The entire model of the MCS is implemented on a typical distribution system of Guwahati city (the state capital of Assam, India).

- MCS has been designed at system level.
- Converters connected to charge and discharge the EVs have not been modelled since, the aim of this work is to show the V2G implementation at system level.

The chapter is organised as follows: Section 3.2 discusses the modelling of the MCS, distribution grid and the battery. Section 3.3 presents the design methodology adopted for the MCS, algorithm and development of possible scenarios. The results and their analyses are presented in Section 3.4. Finally, conclusions are presented in Section 3.5.

3.2 Modelling of the system

Usually, the position of the EV changes as per the owner's change of stay throughout 24 hrs duration. If the EVs are charged or discharged at different CSs at different times, an existing load profile of the particular node can get flattened for maximum period of time. In this section, the MCS and the EV's battery is modelled. The existing load curve of the node (point of common coupling) and a typical radial distribution feeder are presented along with the practical data. The proposed model will be tested on the typical radial distribution feeder of Guwahati city.

3.2.1 Multi charging station

MCS, which is considered in this work, comprises of three different CSs connected at a distribution node or PCC as shown in Figure 3.2. Each CS consists of 150 charging bays i.e., a maximum of 150 EVs can be charged at a particular CS. Figure 3.2 shows the conceptual block diagram of the MCS connected to a distribution node. The FLC at the test node level collects the information about the current node voltage in p.u., total energy of the MCS in kWh and the duration in hours (period of charging/discharging the batteries). On the basis of

these three inputs, the FLC decides the magnitude and direction of power flow(P). The total power P as decided by the FLC is divided among the CSs (as P_1, P_2 and P_3)

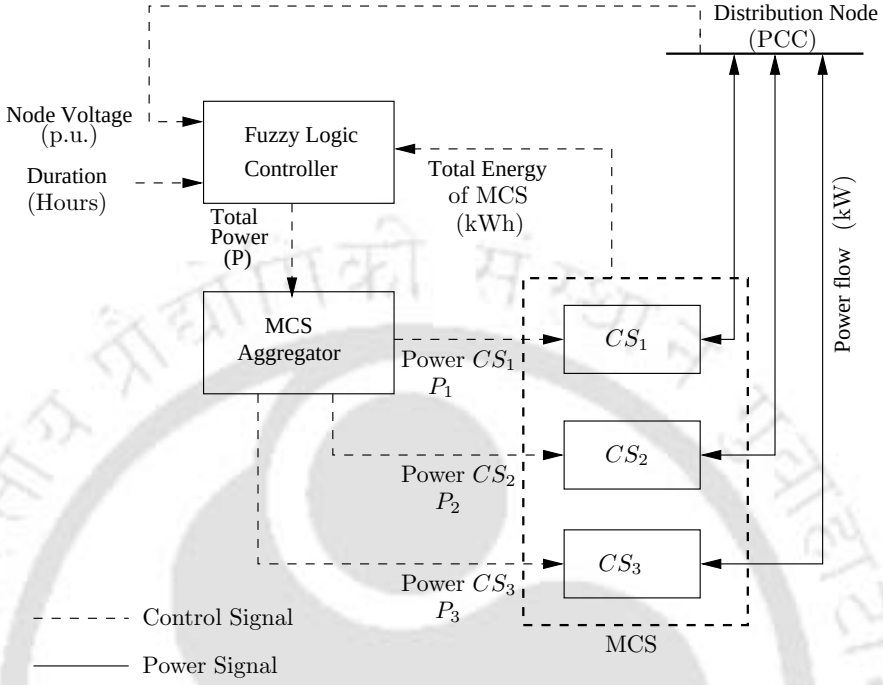

Figure 3.2: Block diagram representation of MCS.

Further, the power P_1 is divided (by the aggregator at the CS_1) among the batteries of CS_1 as Pb_{11} (1^{st} battery of CS_1) to Pb_{1n} (n^{th} battery of CS_1) as shown in Figure 3.3. These are the actual powers which flow between the batteries and the grid. Now to obtain this power of Pb_{11} from the battery, a new C_{rate} has to be obtained and is named as *current* C_{rate}. This is calculated on the basis of the SOC, SOC limit, AHR and the power requirement by the battery(Pb_{11}). The *current* C_{rate} is the final charging/discharging rate at which the power will flow between the grid and the battery. The detailed algorithm of the individual battery control along with the flow chart have been presented in Section 3.3.

3.2.2 Battery

The model of the battery is taken from the simpower of the matlab simulink library [53]. Since, this chapter aims to develop the V2G implementation at the system level, EV's battery efficiency and its degradation have not been considered. C_{rate} of the batteries are controlled

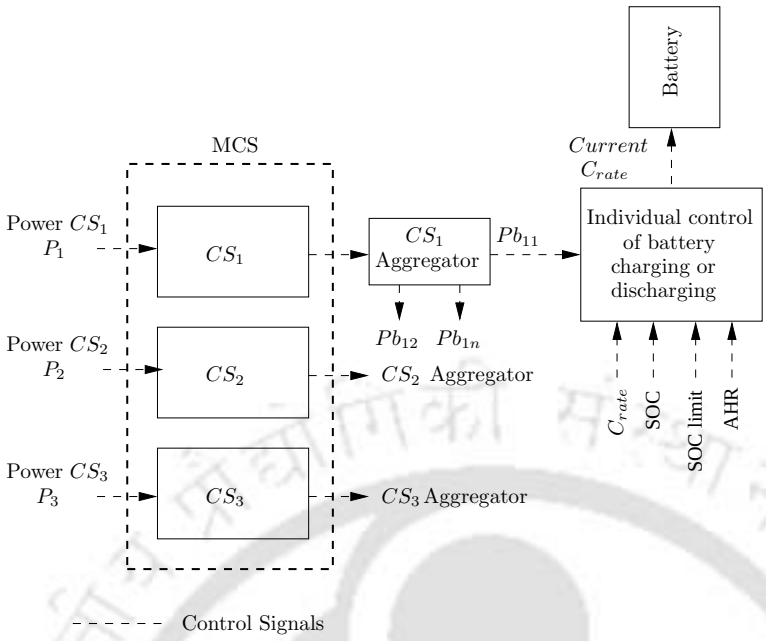

Figure 3.3: Block diagram representation of a CS and the individual battery control.

during charging/discharging. Batteries are not discharged beyond SOC limit and they are not charged/discharged beyond the C_{rate} limit as fixed by the EVs owners. The batteries are charged when the node voltage is high and the batteries are discharged when the voltage of the node is low taking into account their SOC. C_{rate} is decided on the basis of power requirement and the available battery energy. A limit to the C_{rate} is also taken in to consideration as set by the EV's owner.

The following assumptions have been made regarding the EV's battery:

- Loss in the battery's capacity with respect to cycling is not considered.
- Cyclic efficiency of the battery is not considered.

However, the charging/discharging efficiency of the system has been assumed to be 90% to validate the model for any efficiency.

3.2.3 Distribution network

A reduced network of a distribution substation in the Guwahati city, India has been modelled. The reduced system is a 33 kV feeder which consists of three sub feeders with 12 nodes in

total. The main feeder has one transformer of 33/11 kV, 5 MVA rating. The sub feeders are of 11 kV and have transformer ratings of 11 kV/440 V, 500 kVA. Numbers 1.1 to 3.4 in Figure 3.4 are the sub feeder nodes. Peak hours load on the substation of a typical distribution system of

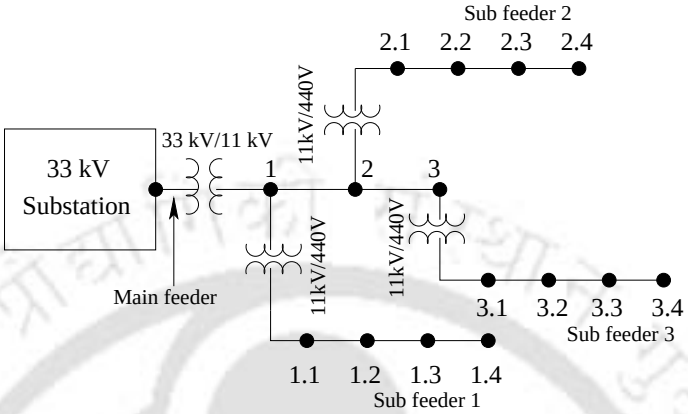

Figure 3.4: Radial distribution system of a substation of Guwahati city.

Guwahati city is given in Table 3.1. In this table, P and Q are the active and reactive power respectively. The last node of a radial sub feeder is more susceptible to voltage instability as compared to other nodes [54], [44]. Therefore, MCS is connected to the last node of the radial sub feeder (**Node 3.4**). Off peak hour load is approximated to be 60% of the peak hour load as per the data provided by the Assam State Electricity Board (ASEB) [43]. The impedance of the entire section is assumed to be constant with a resistance of 0.0027 p.u and reactance of 0.0023 p.u. The system is assumed to be a balanced three phase system. The base values used are 500 kVA and 0.44 kV and the feeder voltage is assumed to be 1.0605 p.u.

Table 3.1: Existing load of substation

Nodes	P(p.u.)	Q(p.u.)	**Nodes**	P(p.u.)	Q(p.u.)
1.1	0.39	0.13	**2.3**	0.43	0.21
1.2	0.51	0.31	**2.4**	0.00	0.00
1.3	1.01	0.61	**3.1**	0.33	0.18
1.4	1.21	0.75	**3.2**	0.65	0.32
2.1	0.34	0.19	**3.3**	0.71	0.35
2.2	0.81	0.33	**3.4**	0.61	0.31

Having discussed the general model of the system, the next section deals with the problem formulation.

3.3 Design of MCS for dynamic load management

The changes in distribution node voltage are generally caused due to variation of load on the system. Low voltage causes loss of revenue, inefficient lighting and possible burning out of some motors. High voltage causes lamps to burn out permanently and may cause failure of other appliances. Therefore, a good distribution system should ensure that the voltage variations at consumers' terminals are within permissible limits. The statutory limit of voltage variations as per Indian Electricity Grid Code is approximately +/- 10% of the rated value at the consumer terminals [55]. Thus, if the declared voltage is 440 V, then the highest voltage at the consumer end should not exceed 484 V while the lowest permissible voltage at the consumer's side should not be less than 396 V.

With the penetration of a large number of EVs, maintaining the grid voltage will be a challenging task. Due to the movement of the EVs from one place to another, their load on the grid will be unpredictable. The grid connected CSs will be one of the most suitable methods to balance the EVs load on the distribution network. The proposed MCS will maintain the node voltage within statutory limit and will also operate the grid in stable region by controlling the flow of power between the grid and the batteries. This section discusses the individual battery control and its algorithm, the algorithm for power division among the CSs and also among the batteries. Finally, the FLC is presented which controls the flow of power.

3.3.1 Individual battery control and its algorithm for charging and discharging

Charging and discharging of an EV's battery can be controlled by changing the C_{rate}. The required c_{rate} of the individual batteries can be calculated as follows.

$$C_{rate} = \frac{Pb_{ij}}{V_j Ahr_j} \tag{3.1}$$

where, Pb_{ij} is the power required/available to charge/discharge the j^{th} battery of i^{th} CS. V_j and Ahr_j are the voltage and current Ampere Hour (AHR) of the j^{th} battery of i^{th} CS. However, the C_{rate} calculated in Eq. (3.1) should not exceed the preferred rate of the vehicle's owner and

this is taken into account in the proposed model as shown in the flow chart in Figure 3.5.

Current Ampere Hour is calculated as:

$$Ahr_j = Ahr_{rating}(SOC_{rem}/100) \tag{3.2}$$

where, Ahr_{rating} is the rated AHR of the battery. In the case of discharging, SOC_{rem} is the difference of the current SOC (SOC_{cr}) and SOC limit (SOC_{lt}) and it is calculated as below.

$$SOC_{rem} = SOC_{cr} - SOC_{lt} \tag{3.3}$$

In the case of charging, SOC_{rem} is calculated as below.

$$SOC_{rem} = 100 - SOC_{cr} \tag{3.4}$$

Using Eq. (3.1) and Eq. (3.2), the current of the battery is calculated based on the required C_{rate} and Ahr_j of the battery and is given below.

$$Ahr_{bj} = Ahr_j C_{rate} \tag{3.5}$$

where, Ahr_{bj} is the current which flows between the battery and the grid. Ahr_{bj} is positive, if power is flowing to the battery during charging and negative if power is flowing to the grid from the battery during discharging.

The detail flow chart for charging and discharging of a battery is shown in Figure 3.5. In this figure, C_{rate}^{limit} is the preferred maximum C_{rate} set by the vehicle's owner. V_{bat} is the voltage of the battery. All the other symbols have same description as mentioned in Eq. (3.1) to Eq. (3.5).

For example, if AHR_{rating}, V_{bat}, SOC_{cr} and SOC_{lt} of a battery (1^{st} battery of CS_1) is 32 AHR, 250 V, 90 and 25 respectively then SOC_{rem} can be found from Eq. (3.3) to be 65 and Ahr_j can be found from Eq. (3.2) to be 20.8 AHR. If Pb_{11}= 1.16 kW, which is the power required for discharging to the grid by the EV's battery as decided by Eq. (3.12) during peak hours, C_{rate} at 90% of SOC can be calculated using Eq. (3.1) as 0.223.

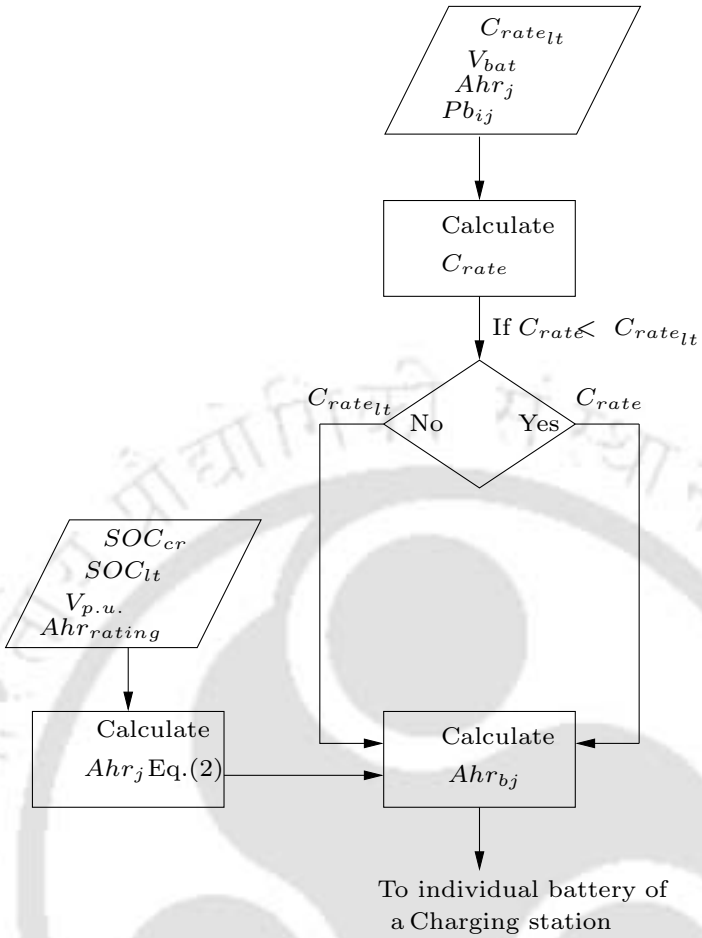

Figure 3.5: Flow chart for controlling the flow of power in individual battery.

3.3.2 Distribution of power among CSs and batteries

The division of power among the CSs is based on the capacity of the CS to handle the power. This is restricted by the power rating of the device. Power can not be injected into the grid beyond the rating of the transformer. Different rating of the transformers implies different power handling capacity of CSs. If transformers' rating for the three CSs are assumed to be 150 kVA, 100 kVA and 150 kVA, then the maximum power that can be injected or drawn by the MCS will be 400 kVA. Therefore, the FLC will be set to deliver a maximum of 400 kVA of power to/from the MCS. Power required by each CS can be calculated on the basis of the transformer ratings as follows.

The distribution of power among the CSs can be achieved based on the transformer ratings

of the CSs or the energy available/ required by the CSs. Power can not be injected into the grid or drawn by the CS beyond the rating of the CS's transformer and it is calculated using the following equations.

$$P_i = (\frac{Pt_i}{\sum_{i=1}^{n} Pt_i} P)\eta \tag{3.6}$$

where, P_i is the power available/required by the i^{th} CS, Pt_i is the i^{th} transformer power rating in kVA, P is the power injected/drawn from the grid which is decided by the FLC and η is the efficiency of the charging/discharging system. Power division based on the transformer rating is effective if the CS has energy in accordance with the rating of the transformer.

The division of power among the CSs can be made on the basis of transformer's rating. However, there can also be a situation in which one of the CS has the highest available energy with a lower transformer rating. In this chapter, each CS has different energies at different time slots and hence, the division of the power is made according to Eq. (3.7) and Eq. (3.8). In the case of charging and discharging, the distribution of power among the CSs are as follows.

$$P_i = (\frac{E_i}{E} P)\eta \qquad (Charging) \tag{3.7}$$

$$P_i = (\frac{E_i}{E} P)\frac{1}{\eta} \qquad (Discharging) \tag{3.8}$$

where P is the power which should be drawn/supplied from/to the node, P_i is the net power exchanged at the i^{th} CS, E_i is the available/required batteries energy of the i^{th} CS and E is the total energy available/required by the MCS. η is the charging/discharging efficiency of the system.

Available/required energy E_i can be calculated as follows.

$$E_i = \sum_{j=1}^{m} Eb_{ij} \tag{3.9}$$

where Eb_{ij} is the energy available/required by the j^{th} battery of the i^{th} CS and is calculated

as follows:

$$Eb_{ij} = \frac{SOC_{rem}}{100} V_{bat} Ahr_{rating} \tag{3.10}$$

where SOC_{rem} is same as of Eq. (3.3) or Eq. (3.4) depending on whether Eb_{ij} is the energy available in the battery during discharging or energy required by the battery during charging. Total energy of the MCS can be calculated as follows.

$$E = \sum_{i=1}^{n} E_i \tag{3.11}$$

Similarly, P_i can be redistributed to each battery of the i^{th} CS and this is as follows.

$$Pb_{ij} = \frac{Eb_{ij}}{\sum_{j=1}^{m} Eb_{ij}} P_i \tag{3.12}$$

In Eq. (3.12), Pb_{ij} is the power available/required by the j^{th} battery of i^{th} CS and P_i is same as defined in Eq. (3.7). Power division among the batteries is based on the available/required energy of the battery.

For example, suppose the power required to be discharged to the grid is found to be 246 kW as decided by the FLC. If energy available at CS_1, CS_2 and CS_3 are found to be 255 kWh, 700 kWh and 200 kWh respectively. By using Eq. (3.7), P_1 can be calculated to be 54.31 kW. Similarly, if available energy of each battery is known, the power to be discharged to the grid by an individual battery can be calculated using Eq. (3.12).

3.3.3 Fuzzy logic based V2G controller

Mamdani type FLC [49, 51] has been designed in this work. Defuzzification is performed using the centre of gravity method [50, 56]. FLC designed for the MCS have three inputs and one output.

The output membership function indicates positive power or negative power.

- 'Positive power' implies that CSs require power to charge their batteries.
- 'Negative power' implies that CS is supplying power to the grid.

The membership functions of the controller are as follows:

- The first input, i.e., voltage is fuzzified into corresponding fuzzy signals with three linguistic variables; low (L), medium (M) and high (H).
- The second input, i.e., total available energy and third input, i.e., duration for the grid support are fuzzified with three linguistic variables similar to the first input.
- The output is fuzzified into six fuzzy regions represented by linguistic variables; negative high (NH), negative medium (NM), negative low (NL), positive low (PL), positive medium (PM) and positive high (PH).

The rule base for V2G controller is given in Table 3.3. The membership functions for three inputs, i.e. voltage (Vp.u.), Energy (E) and Duration (D) are shown in the Figure 3.6. The membership for the output power is also shown in the same figure.

For example, if node voltage is 0.95 p.u, energy availability is high and the duration is high (say 5 hrs during peak hours), then FLC will decide the power flow to be negative. It infers that the batteries have to discharge their stored energy for peak shaving and voltage support. In another case, though very exceptional, where say all the batteries arrive below the SOC limit and the voltage is very low (say 0.92 p.u). The controller will not allow the batteries to charge. Take another scenario, where the node voltage is (0.98 p.u), and all the batteries arrive at lower SOC than SOC limit. In this case, the batteries will charge but with a very low C_{rate} because the controller will limit the power drawn by the batteries. Some critical cases are summarized in Table 3.2, when all the EVs arrived have either SOC $< SOC_{lt}$ or SOC $> SOC_{lt}$.

3.3.4 Assumptions and background

In this work, the total numbers of EVs are assumed to be 200, out of which 150 are assumed to be at the CS and 50 in transit/idle. For ease of representation, all the EVs at the CSs have been divided into five groups namely A,B,C,D and E, each consisting of 40 EVs. This division is based on energy rating, SOC initial (SOC at the time of EVs arriving at the CS), SOC limit (the vehicle owner's preferred minimum state of charge), Ampere Hour (AHR) and C_{rate}^{limit} of

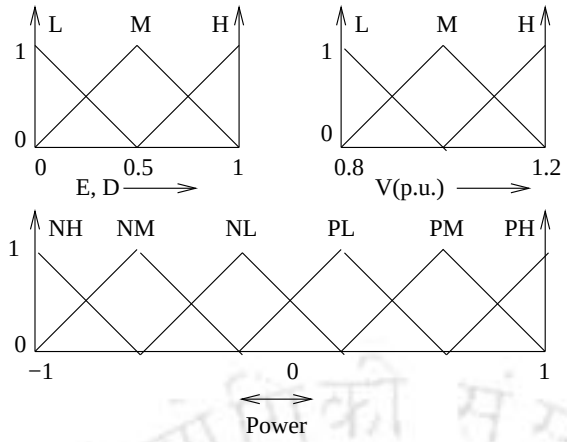

Figure 3.6: Membership functions for three inputs and one output of the V2G Controller.

Table 3.2: Some critical cases for the V2G Controller

Node voltage	Batteries' SOC	Controller action	Remarks
0.92	SOC $<SOC_{lt}$	Not allow to charge	Charging power P is zero
0.98	SOC $<SOC_{lt}$	Allow to charge but with slow rate	Charging power P is very low
1.02	SOC $>SOC_{lt}$	Allow to discharge but with slow rate	Discharging power P is very low
1.08	SOC $>SOC_{lt}$	Not allow to discharge	Discharging power P is zero

the batteries as shown in Table 3.4. Initial SOC of the batteries can be categorised into three groups namely Low (below 40%), Medium (40% to70%) and High (70 % and above). Few EVs are assumed to have arrived at lower SOC than specified SOC limit. This assumption is valid because in real scenario, EV's battery may arrive below specified SOC limit. Such batteries will always charge first even during peak hours. For example, 10 kWh batteries (40 % SOC) will always charge first to reach the SOC limit (45%). The Li-Ion batteries have been used in the proposed work. Generally, the nominal voltage of the EVs' batteries ranges from 96V to 300 V [57]. In this work, the nominal voltage of the batteries is assumed to be 250V.

It is assumed that the EVs have only three possible destinations and all the EVs are doing intra-node driving. These are namely residential, commercial and office areas as given in

Table 3.3: Rule base for V2G controller

Input			Output
Voltage	**Energy**	**Duration**	**Power**
L	L	L	NH
L	L	M	NM
L	L	H	NL
L	M	L	NH
L	M	M	NM
L	M	H	NL
L	H	L	NH
L	H	M	NM
L	H	H	NL
M	L	L	PL
M	L	M	PL
M	L	H	PL
M	M	L	NH
M	M	M	NM
M	M	H	NL
M	H	L	NH
M	H	M	NM
M	H	H	NL
H	L	L	PH
H	L	M	PM
H	L	H	PL
H	M	L	PH
H	M	M	PM
H	M	H	PL
H	H	L	PH
H	H	M	PM
H	H	H	PL

Table 3.4: Specifications of the EVs' battery

Type of battery	Energy (KWH)	SOC initial (%)	SOC limit (%)	AHR	C_{rate}^{limit}
A	8	70	25	32	3
B	10	40	45	40	2.5
C	16	50	30	64	3
D	20	85	40	80	4
E	24	30	20	96	4

Table 3.5. Some of the EVs which are not present in CS of these areas are assumed to be in transit/idle. The reason of having a four area based system is to provide continuous support to the test node using the EVs. Since, the EVs would traverse within these four areas, the number of EVs at any instant of time will nearly be same. The transition diagram is shown in Figure 3.7. As shown in Table 3.5, all the CSs have unequal numbers of EVs in different time slots but the total number of EVs at the MCS will always be 150. Thus having MCS at one node, covering these regions, would ensure grid support in terms of voltage, peak shaving and valley filling at any time. In Table 3.5, 'To' indicates that EVs will depart to CS/Transit in next time slot. 'From' indicates that EVs have arrived from CS/Transit from previous time slot. For example, 'To-T' (0900 hrs-1700 hrs in CS_1) implies that EVs will depart to Transit, 'From-C'(1700 hrs-2200 hrs in CS_3) implies that EVs have arrived from the CS of commercial area. First and third time slots indicate off peak hours and the second time slot indicates peak hours [43]. 10% of SOC is assumed to be consumed when an EV moves from one CS in previous time slot to the other CS in next time slot. It means that EVs with 45% SOC in peak hours(1700 hrs-2200 hrs) at CS_1 will have 35% SOC in off-peak hours(2200hrs-0900 hrs) when it arrives at CS_3. EVs coming from 'Transit' have same SOC initial as mentioned in Table 3.4.

3.4 Results and discussions

In this section, two case studies of the proposed MCS and their corresponding results have been demonstrated. The simulation results are presented for the following case studies. The

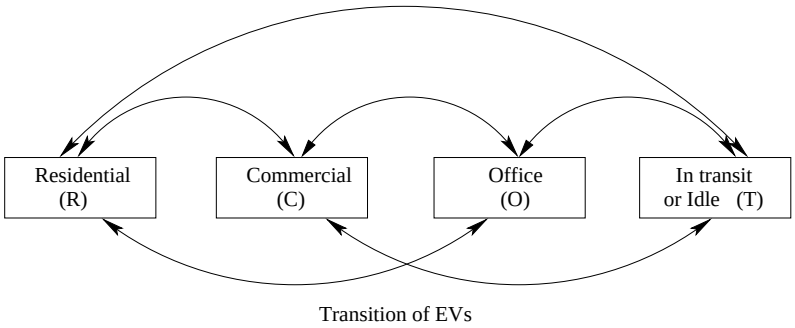

Figure 3.7: Transition of EVs between possible destination.

power factor of the entire system is assumed to be unity. The case studies are as follows.

Case I: This case study consists of three parts because simulation is carried out for three different time slots as mentioned in Table 3.5. Sudden departure of certain high SOC EVs during peak hours and arrival of low SOC EVs during off peak hours is also studied along with the controller output. Each node of the test system including the test node (**3.4**) has a steady state load as mentioned in Table 3.1.

Case II: Similar to case I, but the simulation is carried out for variable load on test node(**3.4**). Load curve for 24 hours on a particular day is obtained from the substation and is used as a dynamic load at the test node. The behavior of the CS is analysed for flattening the load profile and mitigating the voltage imbalance.

3.4.1 Case I

Initially, the simulation is carried out for three time slots. It is followed by the analyses of sudden departure and arrival of certain EVs at the CS. In every analysis, simulation result of the power flow is shown for 1 second to demonstrate the dynamics of the controller. Charging/discharging efficiency of the system is assumed to be 100%. However, for the shake of comparison, Case I(a) and Case I(b) are also simulated by taking the efficiency to be 90% and the results are compared. C_{rate} of the batteries for different time slots and for each CS has been mentioned in Appendix C.

Table 3.5: Time wise distribution of EVs between CSs

Time slot	EVs in Residential area (R): CS_1	EVs in Commercial area (C): CS_2	EVs in Office area (O): CS_3	EVs in Transit or Idle (T)
0900 hrs-1700 hrs	10 To-T=10	40 To-T=20 To-O=20	100 To-C=60 To-R=20 To-T=20	50 To-R=20 To-C=30
1700 hrs-2200 hrs	40 From-O=20 From-T=20 To-R=20 To-T=10 To-O=10	90 From-T=30 From-O=60 To-R=70 To-T=20	20 From-C=20 To-T=10 To-C=10	50 From-R=10 From-C=20 From-O=20 To-T=10 To-R=40
2200 hrs-0900 hrs	130 From-C=70 From-R=20 From-T=40 To-O=80 To-C=30 To-T=20	10 From-O=10 To-R=10	10 From-R=10 To-C=10	50 From-T=10 From-O=10 From-C=20 From-R=10 To-T=30 To-O=20

3.4.1.1 Case I(a): 0900 hrs-1700hrs (off-peak hours)

The third input i.e. 'duration' of the FLC in this case is 8 hrs. Based on the grid health (in this case, node voltage) and the total energy required by the MCS, the controller decides that 126.50 kW of power has to be drawn from the grid to charge the batteries as shown in Figure 3.8. Positive power indicates that the power is drawn by the CS to charge the batteries. The division of the power between the CSs is based on the energy required by each CSs. It is found that CS_1, CS_2 and CS_3 require 8.43 kW, 33.7 kW and 84.3 kW of power respectively. Total energy required by the MCS for the entire duration is 1086 kWh and is shown along with the required energy of the individual CS in Figure 3.9. As the energy reduces over a period of time, the power remains same due to increase in C_{rate} of the batteries. The status of the batteries, i.e., initial and final SOC, is shown in Figure 3.10.

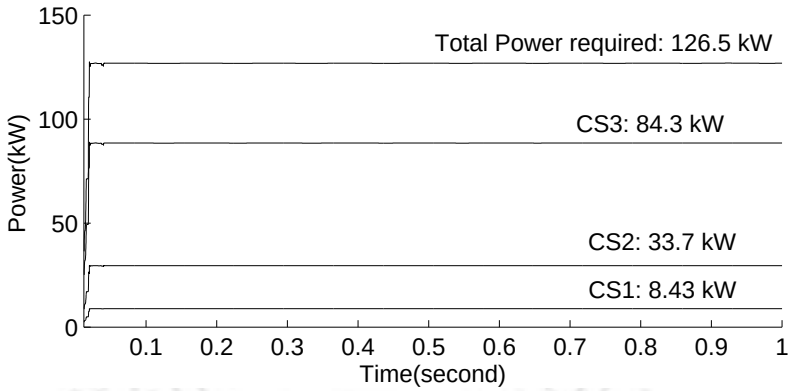

Figure 3.8: Case I(a): (Off-peak hours: 0900 hrs-1700 hrs):- Power supplied by the grid to the CSs.

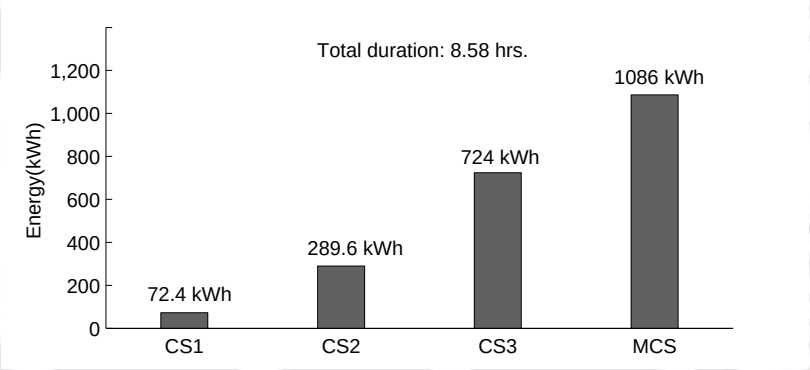

Figure 3.9: Case I(a): (Off-peak hours: 0900 hrs-1700 hrs):- Energy required by CSs for charging the EVs' batteries.

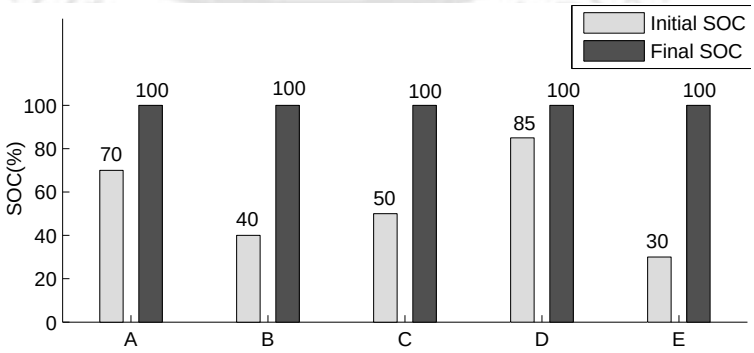

Figure 3.10: Case I(a): (Off-peak hours: 0900 hrs-1700 hrs):- Initial SOC and final SOC of the batteries.

The control architecture works even after taking the charging efficiency of the system to be 90%. The total power drawn from the grid to charge the batteries is 126.5 kW at η=0.9 (Eq. (3.7), which is similar to the power drawn at η=1 (Figure 3.8). However, charging power received at the MCS is 113.85 kW. The power received by the MCS at η=1 and η=0.9 have been shown in the Figure 3.11 along with the charging power received by the individual CS at η=0.9. Since, the power drawn by the node is equal in both the cases, node voltage do not change and hence no effect on the control scheme. However, the duration of charging will increase with the change in the efficiency from 8.58 hrs(η=1) to 9.53 hrs(η=0.9).

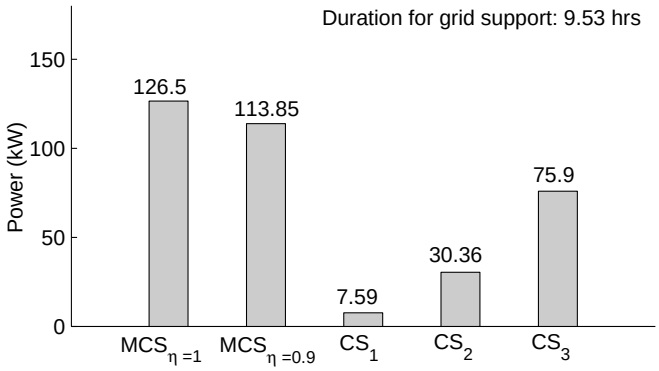

Figure 3.11: Case I(a): (Off-peak hours: 0900 hrs-1700 hrs):- Power received at the MCS for charging their batteries at η=1 and η=0.9.

3.4.1.2 Case I(b): 1700 hrs-2200hrs (peak hours)

The peak period is between 1700 hrs and 2200 hrs and therefore, FLC takes 5 hrs duration as one of the input. During peak hours, the voltage of the node is generally below 0.95 p.u [43] and therefore, the batteries with higher SOC (>SOC limit) will start discharging and will stop when the SOC limit is reached. Total power delivered by the MCS is 246 kW and is shown in Figure 3.12. This power is negative, which implies that the power is flowing from the CS to the grid as per the convention explained in Section 3.3. Total energy drawn by the grid is 1099 kWh and the duration for which the grid is supported is 4.47 hrs as shown in Figure 3.13. Initial and final SOC of the EVs batteries which have arrived from CSs and Transit have been

shown in Figure 3.14. It is observed that EVs which come from CSs have initial SOC of 90% while EVs coming from Transit have initial SOC similar to that as mentioned in Table 3.4. It is important to note that EVs have not been discharged beyond the SOC limit.

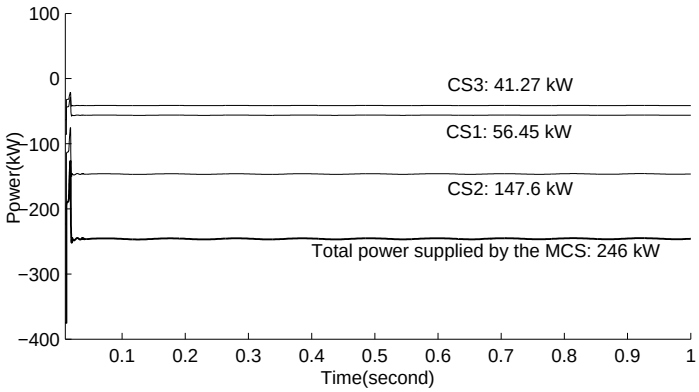

Figure 3.12: Case I(b): (Peak hours: 1700 hrs-2200 hrs):- Power supplied to the grid by the CSs.

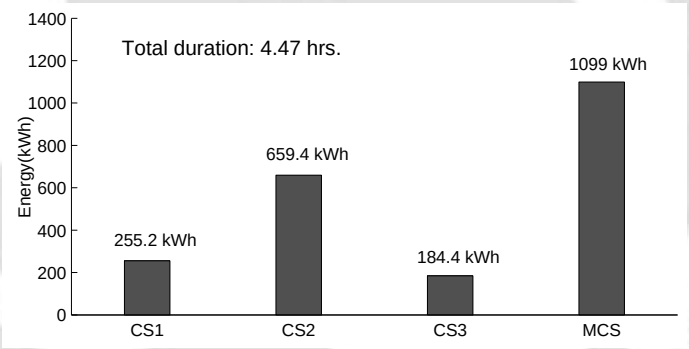

Figure 3.13: Case I(b): (Peak hours: 1700 hrs-2200 hrs):- Energy available at CSs for discharging to the grid.

Now, after including the discharging efficiency to be 90%, the net power discharged to the grid is 246 kW and it is equal to the power discharged at η=1 (Figure 3.12). However, the power drawn by the MCS is 273.33 kW (Eq. (3.8)) and is shown in Figure 3.15. Since, the power injection to the node is equal in both the cases of η, node voltage do not change and hence no effect on the control scheme. The only visible difference is in the duration for the grid support which will reduce from 4.47 hrs(η=1) to 4.02 hrs(η=0.9). This implies that with a change in η, the net power injection to the grid remains same, but the power discharged by the MCS has increased and is shown in Figure 3.15.

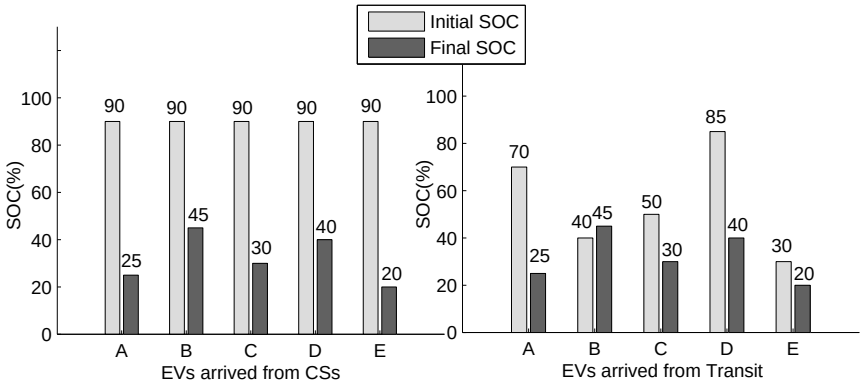

Figure 3.14: Case I(b): (Peak hours: 1700 hrs-2200 hrs):- Initial SOC and final SOC of the batteries.

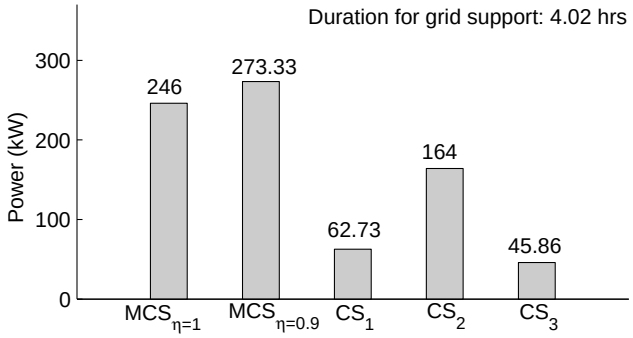

Figure 3.15: Case I(b): (Peak hours: 1700 hrs-2200 hrs):- Power supplied to the grid by the MCS at η=1 and η=0.9.

3.4.1.3 Case I(c): 2200 hrs-0900hrs (off peak hours)

During off peak hours, the node voltage is generally high (1.05 p.u to 1.1 p.u). The duration of the off-peak period is more than the peak period and therefore, the length of charging can be extended for maintaining the node voltage within specified limit (0.95 p.u. to 1.05 p.u.) for longer period. Also, durability of the batteries increases with slower rate of charging/discharging. A total of 157 kW of power is required by the CSs to charge their batteries as shown in Figure 3.16. Total energy required by the MCS is 1646 kWh and is shown in Figure 3.17. For complete charging of the EVs batteries, the time required is 10.48 hrs. This is a valid result which shows that the voltage has been maintained near unity for a longer duration. During off peak hours, batteries of all the CSs have been charged up to 100% of SOC as shown in Figure 3.18.

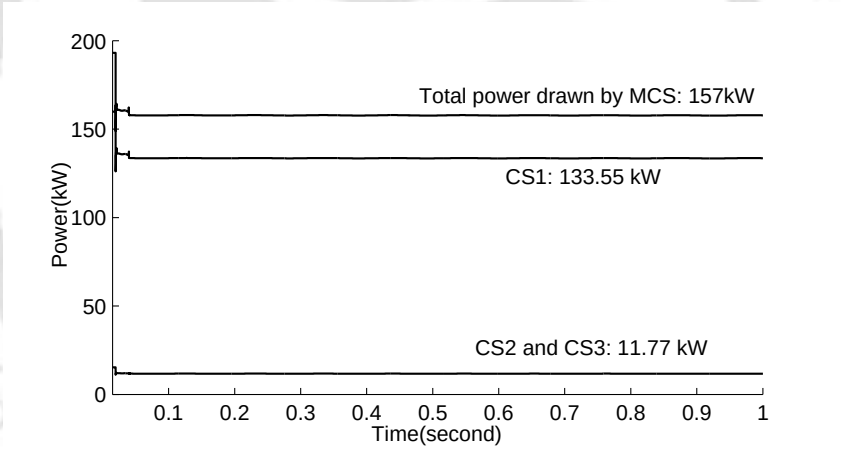

Figure 3.16: Case I(c): (Off-peak hours: 2200 hrs-0900 hrs):- Power supplied by the grid to the CSs.

Voltage of the sub feeder node has been shown in Table 3.6 with and without MCS for the three different time slots. It is observed that MCS connected at the test node have higher voltage support as compared to the adjacent nodes. However, because of the MCS, all the other nodes'(3.1, 3.2 and 3.3) voltage have been improved and they are near to the specified limit.

3.4.1.4 Case I(d): High SOC EVs leave CS_2 during peak hours

In this case, 30 EVs of CS_2 during peak hours have suddenly departed after 2 hrs. This results in drop of energy level by 244.58 kWh at CS_2 as shown in Figure 3.19. As a result,

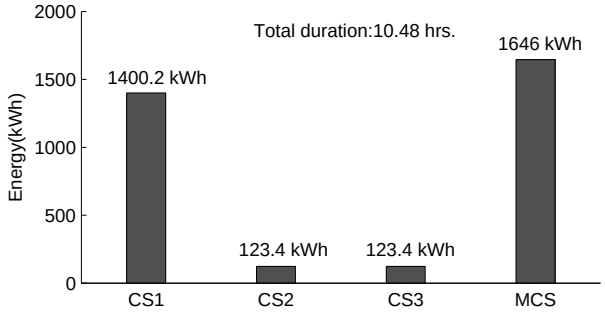

Figure 3.17: Case I(c): (Off-peak hours: 2200 hrs-0900 hrs):- Energy required by CSs for charging the EVs batteries.

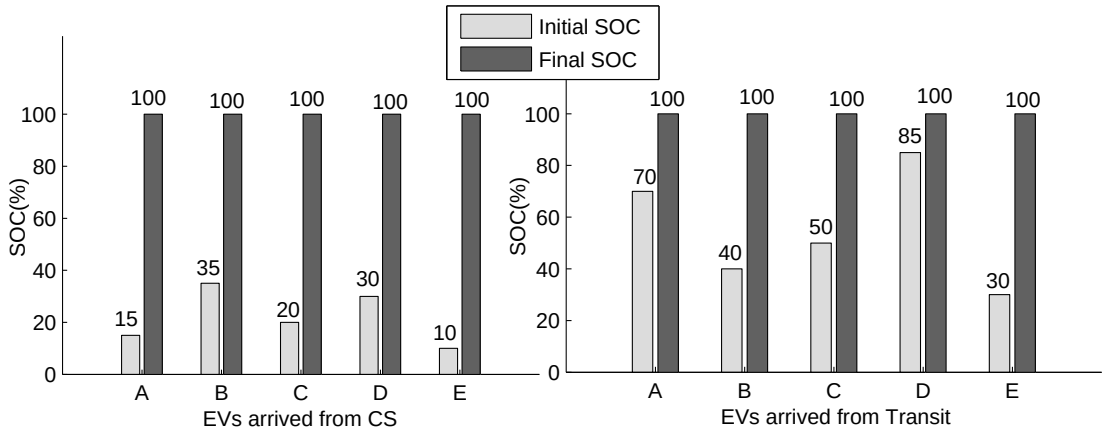

Figure 3.18: Case I(c): (Off-peak hours: 2200 hrs-0900 hrs):- Initial SOC and final SOC of the batteries.

Table 3.6: Voltage(p.u) of the sub feeder nodes

Sub feeder 3 Nodes	Case I(a)		Case I(b)		Case I (c)	
	Without MCS	With MCS	Without MCS	With MCS	Without MCS	With MCS
3.1	1.08	1.05	0.99	1.01	1.09	1.06
3.2	1.05	1.03	0.97	0.98	1.08	1.05
3.3	1.05	1.02	0.94	0.97	1.08	1.04
3.4	1.06	1.01	0.92	0.99	1.07	1.02

the controller adjusts the power distribution with the remaining batteries' energy. This can be calculated as follows.

$$E_{rem} = E_{avail} - E_{exit} \tag{3.13}$$

where, E_{rem} is the remaining available energy at the MCS after sudden departure of certain EVs, E_{avail} is the total energy available at the MCS before departure of these EVs and E_{exit} is the total available energy of the departed EVs at the time of exit. It is observed in Figure 3.20 that the controller has maintained a lower power level of 160.72 kW as compared to 246 kW (case I(b)) so that the voltage does not fall below a specified limit. The duration of the grid support has also been reduced to 4.24 hrs in comparison to 4.47 hrs (case I (b)). Voltage of test node without MCS support, with MCS support and after the departure of high SOC EVs from CS_2 have been shown in Figure 3.21.

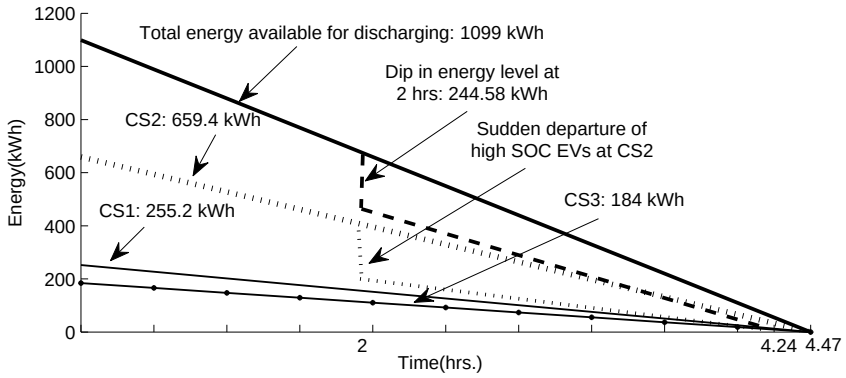

Figure 3.19: Case I(d): (High SOC EVs leave CS_2 during peak hours: 1700 hrs-2200 hrs):- Energy available before and after sudden departure of high SOC EVs.

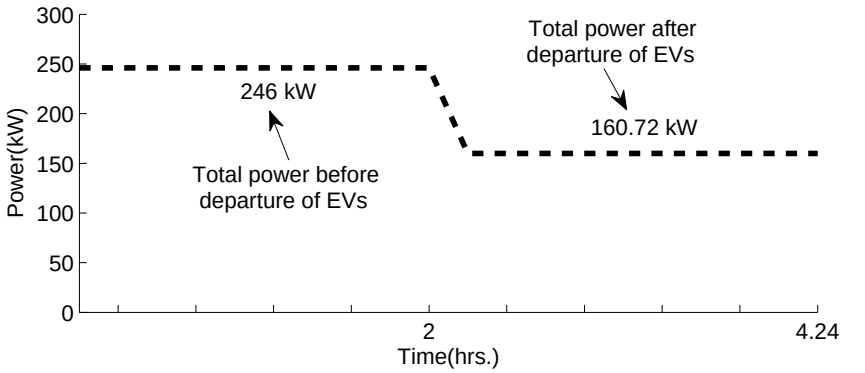

Figure 3.20: Case I(d): (High SOC EVs leave CS_2 during peak hours: 1700 hrs-2200 hrs):- Total power before and after departure of high SOC batteries from CS_2 after 2 hrs.

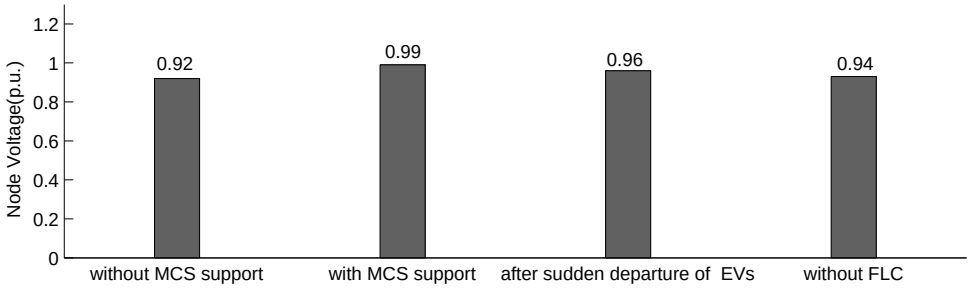

Figure 3.21: Case I(d): (High SOC EVs leave CS_2 during peak hours: 1700 hrs-2200 hrs):- Voltage of Node 3.4, before CS support, with CS support and after departure of high SOC from CS_2.

3.4.1.5 Case I(e): Low SOC EVs arrive at CS_1 during off-peak hours

With sudden arrival of few EVs with low SOC batteries at the CSs during off peak hours, the node voltage may fall. This is due to increase in load as the new EVs will also charge their batteries. Figure 3.22 shows that the required energy to charge the EVs is increased due to sudden arrival of low SOC EVs after 4 hrs and the duration for charging has been increased from 8.58 hrs to 8.95 hrs. Now, the FLC will adjust the power flow to maintain the voltage within specified limit. Total energy required after the sudden arrival of EVs during off peak hours is given below.

$$E_{total} = E_{req} + E_{arrival} \tag{3.14}$$

where, E_{total} is the total energy required to charge the EVs' batteries at the MCS after sudden arrival of certain EVs, E_{req} is the total energy required by the MCS before arrival of the EVs and $E_{arrival}$ is the total required energy to charge the EVs battery which have suddenly arrived at the CS. The power required by the CSs to charge the EV's batteries before and after the arrival of EVs has been shown in Figure 3.23. It is seen that the power drawn by the MCS after arrival of new EVs at CS_1, is increased to 182.63 kW compared to 126.5 kW(case I(a)). The power requirement has been increased but not in the ratio of arrival of low SOC EVs' batteries. This is due to the controller action, which maintains the voltage of the node by allowing the EVs to charge the batteries with lower C_{rate}. Voltage of the test node during off-peak hours without MCS support, with MCS support, after the arrival of low SOC EVs are shown in Figure 3.24. Voltage of the node without FLC is found to be 0.94 p.u. after sudden arrival of low SOC EVs. Similar results can be shown during peak hours and off- peak hours with various combinations of sudden arrival and departure of the EVs.

3.4.2 Case II: Validation of MCS by implementing the actual load curve of Node 3.4

In this part, load curve of a particular node has been implemented as a dynamic load to observe the behavior of the proposed MCS. Figure 3.25 shows the load curve of test node (**3.4**) of 33 kV substation model. The output of the proposed FLC has been shown in Figure 3.26,

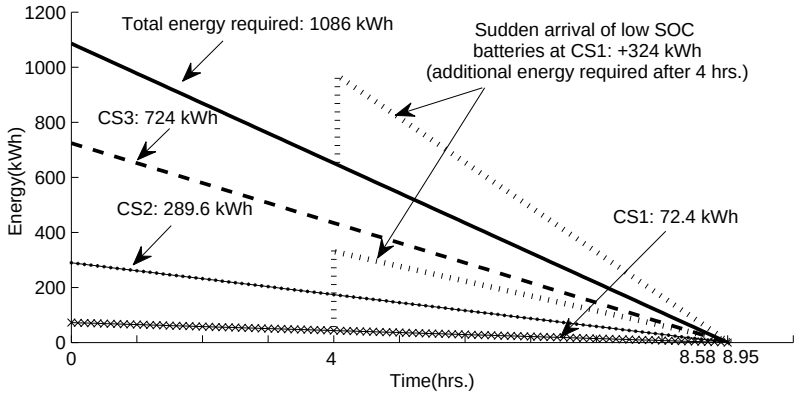

Figure 3.22: Case I(e): (Low SOC EVs arrive CS_1 during off-peak hours: 0900 hrs-1700 hrs):- Energy available before and after sudden arrival of low SOC EVs after 4 hrs.

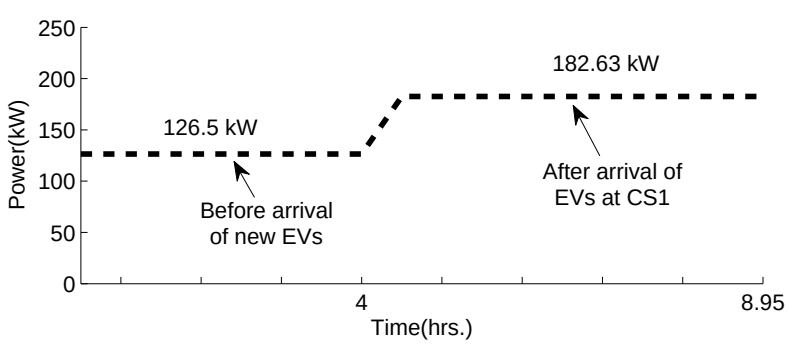

Figure 3.23: Case I(e): (Low SOC EVs arrive at CS_1 during off-peak hours: 0900 hrs-1700 hrs):- Total power before and after arrival of low SOC batteries at CS_1 after 4 hrs.

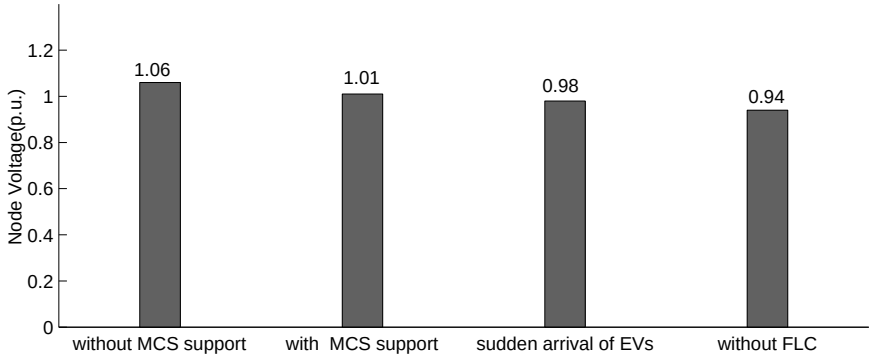

Figure 3.24: Case I(e): (Low SOC EVs arrive CS_1 during off-peak hours: 0900 hrs-1700 hrs):- Voltage of Node 3.4, before CS support, with CS support and after arrival of low SOC EVs at CS_1.

for 24 hrs duration. Positive power indicates charging of the EVs' batteries and negative power indicates discharging of EVs' batteries to the grid. Voltage of the test node with and without implementation of the MCS have been shown in Figure 3.27. It is observed that V2G implementation has improved the voltage profile of the node as well as helped in peak shaving & valley filling. FLC controls the voltage of the node by controlling the flow of power between the node and the MCS. The same EVs configuration defined in Table 3.5 has been used for three different time slots with dynamic loading and all the parts are shown together to show the combined effect. As the load changes, the controller adjusts the power requirement of the CSs by changing the flow of power between the grid and the batteries.

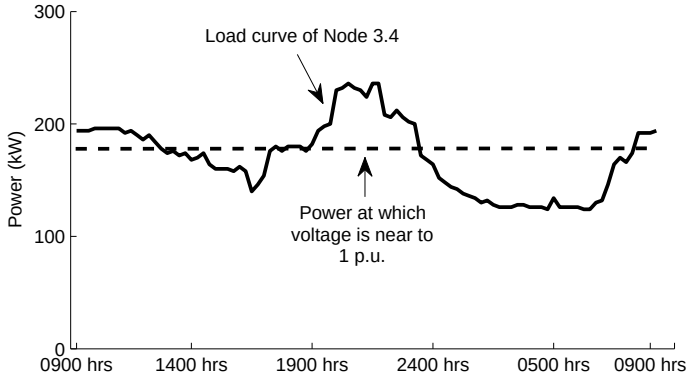

Figure 3.25: Case II: Load curve of Node 3.4 without MCS.

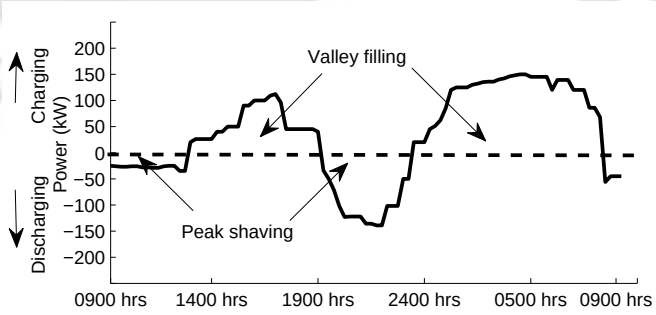

Figure 3.26: Case II: V2G controller decision of power flow between grid and battery. (positive : charging, negative: discharging).

Energy available/required by the MCS due to dynamic load on the test node is shown in Figure 3.28. In this figure, negative energy implies that energy is available at the MCS and power is drawn by the grid. Similarly, positive energy implies that energy is required by the

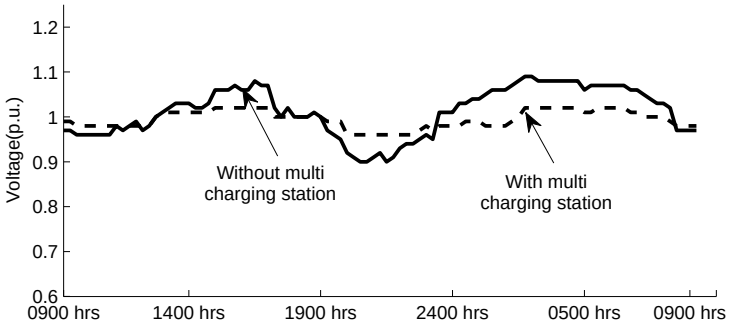

Figure 3.27: Case II: Test node (3.4) voltage with and without MCS.

MCS to charge the EVs batteries and MCS draws the power from the grid. The SOC of the batteries for first time slot at CS_1 is shown in Figure 3.29. From this figure, it can be observed that the battery type A arrives with an initial SOC of 70% at 0900 hours. According to Figure 3.25, the grid is under stress and needs energy. Since the battery type A has healthy SOC, it discharges energy to the grid from 0900 hours to 1300 hours. At the end of this interval the SOC of the battery becomes 44%. From 1300 hours to 1700 hours, the grid is no more under stress (Figure 3.25) and the battery can charge itself. At 1700 hours the SOC of the battery reaches 72%. This strategy shows that the starting SOC (the SOC when the vehicle arrives at the CS at 0900 hours) is almost same as the end SOC (when the vehicle leaves the CS at 1700 hours). However, in between when the vehicle was idle, it interacted with the grid and provided grid support. This holds true for battery types C, D and E as well. In case of battery type B, the initial SOC is low but by the time EV leave the CS, its SOCs have reached a healthy level. As shown in Figure 3.29, EVs are not discharged up to SOC limit due to low requirement of power by the grid. Also, the EVs are not charged up to 100% SOC due to less energy drawn from the grid.

From the results of Case I and Case II, it is observed that the proposed MCS can handle the flow of power between the grid and the batteries without affecting the stability of the grid. In both the cases, the voltage is found within acceptable norms of the grid. SOC of the batteries have been maintained as per the SOC limit set by the vehicles owner.

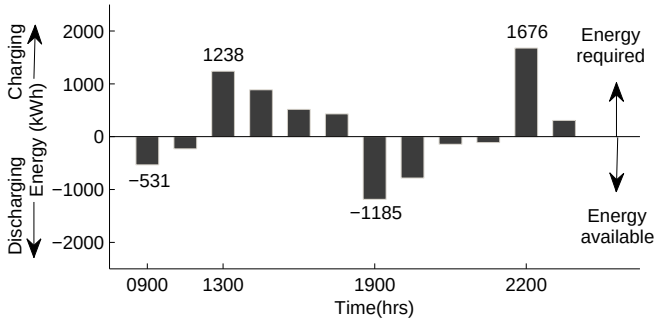

Figure 3.28: Case II: Energy available/required at the MCS due to dynamic load at the test node.

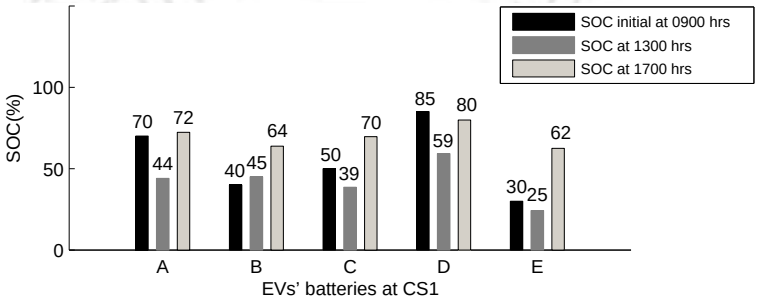

Figure 3.29: Case II: SOC of the batteries at CS_1 at the MCS due to dynamic load at the test node.

3.5 Summary

In this chapter, MCS for the EVs has been modelled at the system level. The purpose of designing the MCS is to coordinate the flow of power between the grid and the batteries in a controlled fashion using FLC. A suitable algorithm has been designed which takes into consideration C_{rate} and SOC of the batteries. EVs batteries are not discharged beyond the owner's preferred SOC limit and C_{rate}. An algorithm for distribution of power among the CS and the batteries is also developed. The complete model is tested on a typical distribution grid of a city. MCS is capable of handling different scenario of EVs arrival and departure during peak and off peak hours. The dynamic load profile is obtained for a particular node and used to test the proposed model. It is verified that the proposed MCS can stabilize the grid by valley filling and peak shaving and the proposed controller can work at any charging/discharging efficiency.

It has been observed that proposed MCS can maintain the voltage profile of a distribution

node by valley filling and peak shaving for a complete 24 hrs duration. This is achieved by modelling the MCS based on different time slots. In the next chapter, coordination of the renewable energy sources in presence of the single CS at a particular node has been presented.

4

Integration of renewable energy sources and its interaction with the V2G system

Contents

4.1 Introduction

Distributed generation (DG) using renewable energy is going to play a vital role in the energy grids across the world [58]. However, to meet the base load and peak load demands, the renewable based DG has to be effectively coupled with energy storage systems (ESS) [59]. The ESS becomes essential due to the fact that renewable energy sources are highly intermittent [60]. If proper storage and coordination of renewable based DG with the grid is not done, then it will result in grid instabilities [61]. Hence, storage is imperative for large scale penetration of renewable based DG [62, 63]. Also, with the installation of distributed generation in a radial distribution network, higher power export to the transmission network is possible. If some storage devices are present at the distribution node level, they can store the excess energy during off peak hours and supply back to the grid during peak hours. The utilization of Electric Vehicles (EVs) as a distributed storage is becoming more popular as they can be used for commuting as well as for storage.

If a large number of EVs penetrate in the market, then their batteries can be utilised for the storage of excess energy produced by the DG. Hence, the EVs have a potential to act as distributed energy storage systems (DESS) and also provide support to the grid by injecting the excess stored energy back to the grid. In this chapter, a charging station (CS) capable of V2G interaction with the renewable energy sources is proposed and modelled. The CS is connected at a node of the distribution grid and at this node a mini Wind farm and Solar PV farm are also connected. The motivation behind choosing this configuration is to demonstrate the interaction between EVs, distribution grid and the DG. It is shown in this chapter that besides performing their main task of transporting its owner, EVs are able to store the excess energy produced by DG effectively and release it back to the grid during peak hours. The main focus is made on the utilisation of solar energy during day time and wind energy at night. In both the cases, EVs batteries can be utilised to store the excess energy produced by solar and wind farm during off peak hours and supply the power back into the grid when required.

In this thesis work, a real time smart CS for the EVs has been modelled. Real time implies

that the voltage of the test node (PCC) and energy of the batteries gets updated at every instant of time. Also, the sudden arrival and departure of EVs with different specifications and user preferences have been taken into consideration. Now, based on the total EVs present at the CS at any instant, the 'available energy' and the 'required energy' of the individual battery and the total EVs batteries energy are calculated. 'Available energy' is the excess energy of the battery and this energy can be discharged to the grid. 'Required energy' of the battery implies the amount of energy required from the grid for charging up to 100% of SOC. Based on the energy calculated, distribution of power, among the batteries, which would flow between the grid and the EV's battery, is decided. For example, batteries having high energy requirement will draw more power from the grid to charge. Also, the batteries having less available energy can discharge a lesser amount of power to the grid and vice versa.

To protect the battery from over-discharging, an algorithm has been developed which prevents operation beyond the specified end-of-discharge voltage similar as used in chapter 3. Another algorithm is designed to check the owner's preferred maximum C_{rate}. This implies that the individual EV's battery is not charged or discharged beyond the specified C_{rate}. FLC is implemented at the distribution node (PCC). FLC requires a set of three variables to decide the amount of power flow between the grid and the CS. These are namely the energy available from the CS, voltage of the distribution node and the power to be compensated. The power flow between the grid and the CS may be negative or positive. 'Negative power' implies, power has to be transferred to the grid from the batteries and 'positive power' implies, power is drawn from the grid to charge the batteries.

The entire model of the CS is simulated by modeling a practical system which is a reduced substation of Guwahati city. The ratings of solar PV plant and wind turbine used in this work are 50 kW and 60 kW respectively. Insolation and wind speed of the Guwahati city ($250^0 06'$ N, $910^0 35'$E) have been obtained for a particular day from Regional Meteorological Centre, Guwahati [64]. The average insolation of Guwahati city is found to be 4.47 kWh/m^2/day. Based on these data, a power curve has been estimated for the 50 kW solar cells and 60 kW wind turbine. Lower power ratings of the renewable energy sources have been assumed due

to their integration with the 11 kV/440 V sub feeder in the proposed 33 kV substation of Guwahati city. EVs' CS and its interaction with the renewable energy sources are shown in Figure 4.1.

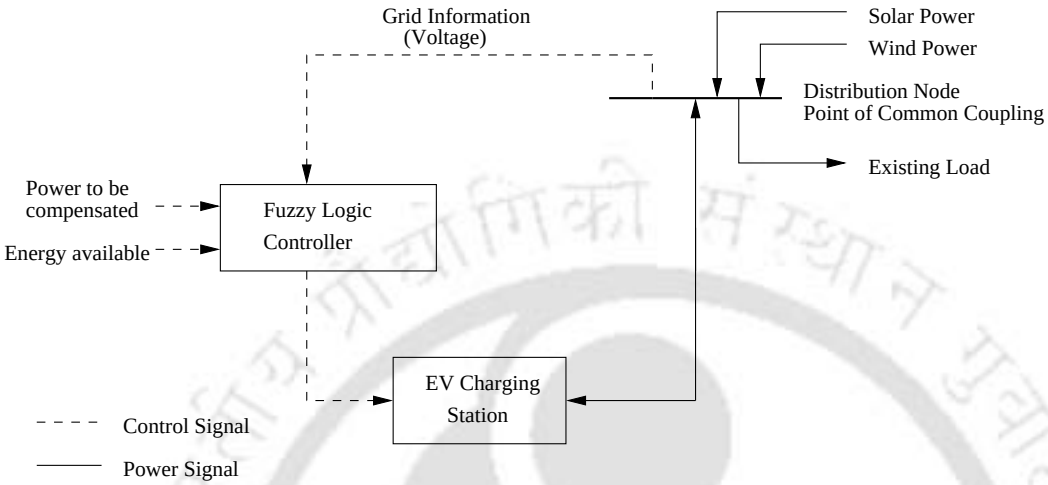

Figure 4.1: EV charging station and its interaction with renewable energy sources.

Following assumptions have been made in this work.

- CS for the EVs using FLC has been designed at system level.
- Due to large dynamics involved in the distribution system, converters connected to charge and discharge the EVs have not been modelled. Also the converters for the solar and wind energy have not been modelled.
- Efficiencies of the batteries, charging system and converters have not been considered since the aim of this work is to elaborate on the implementation of grid support at system level.
- Loss in the battery's capacity with respect to cycling is not considered.

The chapter is organised as follows: Section 4.2 discusses the modelling of the charging station, distribution grid and the battery. Section 4.3 formulates the problem in which, integration of renewable energy source, algorithm, FLC are discussed. The results and their interpretation are presented in Section 4.4. Conclusions are presented in Section 4.5.

4.2 Modelling of the V2G system

In this section, modelling of the CS which is capable of coordinating with the renewable energy sources is presented. The distribution network where the test model is validated is also discussed. EV's battery used for the modelling of the V2G is similar as used in Chapter 3, Section 3.2.

4.2.1 Modelling of the charging station

CS is a place where all the EVs of particular distribution node area will participate for grid support. The proposed CS will utilize the EVs' batteries to discharge their excess energy to the grid for meeting the peak demand and other required ancillary services. A total of 50 EVs are assumed to be present at the CS. All the EVs may have different battery conditions such as initial SOC, SOC limit and C_{rate} limit (limit set by the vehicles' owner). Assuming real conditions, EV's battery may arrive at the CS below the specified SOC limit and will always charge first to reach the SOC limit. For example, 10 kWh batteries (40% SOC) will always charge first to reach the SOC limit (say 50%) even during peak hours. The detailed technical specifications and the functioning of CS are discussed in section 4.3.

4.2.2 Distribution substation

The distribution test system presented in chapter 3, Section 3.2 has been used to validate the proposed model.

4.3 Controllers and aggregators

In this section, Fuzzy Logic based controller which is used to control the flow of energy between the grid and the CS has been discussed. The detailed explanation of the V2G system and its coordination with the renewable energy sources has been discussed along with the aggregators.

4.3.1 Integration of renewable energy sources

Power curves for the solar and wind energy sources have been obtained for a particular day of the year 2011 based on the insolation and wind speed of Guwahati city [64]. The power curve is the power obtained from the solar/wind energy v/s time (24 hours duration). Similarly, an existing load curve of the 11 kV/440 V distribution node has been obtained from the substation. From these two inputs,(i.e. total power available from the renewable energy sources and the existing load) the effective load (net load) is obtained. Another load, i.e. 'base' load which is provided by the substation has been used to find the power to be compensated. At this load, the voltage remains close to unity. Now, the difference between the effective load (net load) and the base load is the 'power to be compensated' by CS. The detailed diagram is shown in Figure 4.2. The power to be compensated can be positive or negative. Positive power implies EVs batteries at the CS have to be charged and negative power implies that the stored energy in the batteries have to be discharged to the grid.

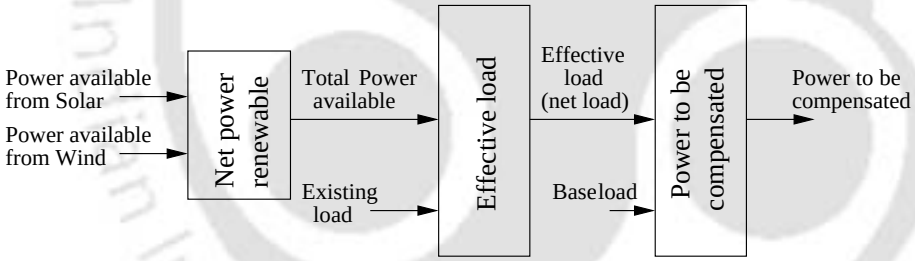

Figure 4.2: Power to be compensated by the EVs present at the CS.

The 'power to be compensated' together with the voltage of the distribution node and the available energy of the batteries are used as the inputs of the FLC. Based on these three inputs, FLC decides the amount of power to be drawn from the grid to charge the EVs batteries or the power to be injected into the grid. This power is referred as 'required power' by the CS. The block diagram of the CS and its integration with the renewable energy sources is shown in Figure 4.3.

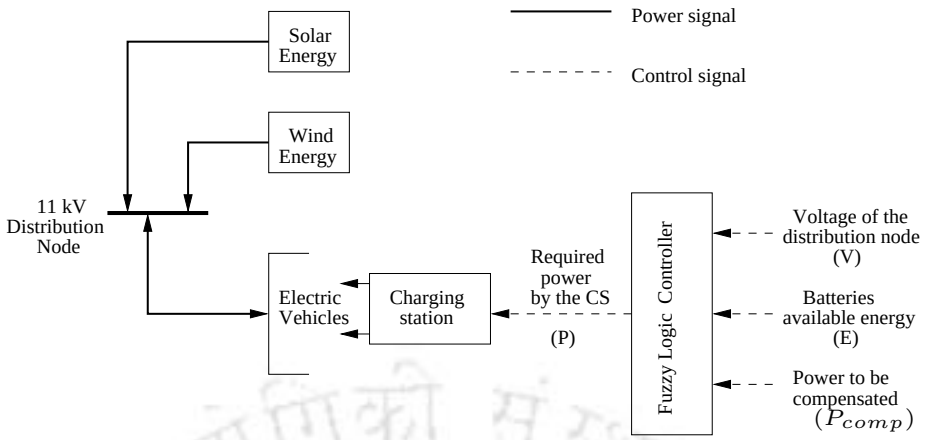

Figure 4.3: Flow chart for controlling the flow of power in individual battery.

4.3.2 Fuzzy Logic Controller

The 'required power' obtained by the CS from the FLC can be negative or positive. Negative power indicates deficiency of power (the EVs at the CS can discharge their excess energy to the grid). Positive power implies the excess power generated by the renewable energy sources which may be utilised by the EVs present at the CS. However, charging or discharging of the EVs' batteries will depend upon the requirement of energy by the CS or availability of the batteries energy at the CS. Therefore, the third input to the FLC is taken to be the energy available at the CS. The energy required will be the complement of the energy available. The FLC is shown in Figure 4.4.

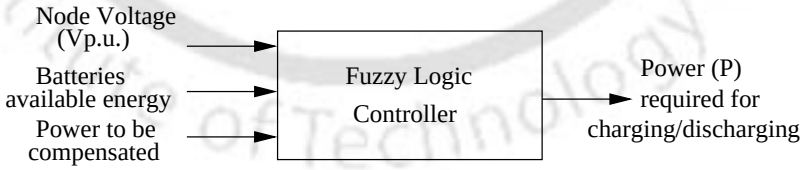

Figure 4.4: Block diagram of the FLC

Membership functions for inputs and outputs are shown in Figure 4.5. In this figure, $V(p.u.)$ is the voltage of the node in p.u., E is the energy available in the batteries, P_{comp} is the power to be compensated and P is the required power by the CS. The membership functions of the controller are as follows.

- The first input, node voltage is fuzzified into corresponding fuzzy signals with three linguistic variables; low (L), medium (M) and high (H).
- The second input, power to be compensated is fuzzified into six fuzzy regions representing the linguistic variables; negative high (NH), negative medium (NM), negative low (NL), positive low(PL), positive medium (PM) and positive high (PH).
- The third input, available energy is fuzzified with three linguistic variables similar to the first input.
- The output is fuzzified into seven fuzzy regions represented by linguistic variables; negative high (NH), negative medium (NM), negative low (NL), zero (ZR), positive low (PL), positive medium (PM) and positive high (PH).

Rule base for the FLC is mentioned in Table 4.1, where V is the node voltage in p.u., P_{comp} is the power to be compensated, E is the energy available from the CS and P is the total power which should flow between the grid and the CS.

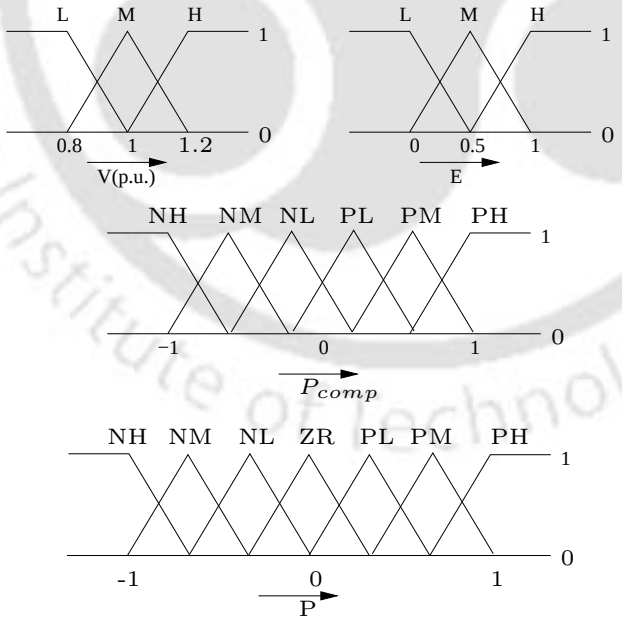

Figure 4.5: Membership functions of the FLC.

For example, let us take the first rule mentioned in Table 4.1. If node voltage V is L, P_{com} is NH and E is L, then the batteries need to deliver power to the grid. Since the batteries

Table 4.1: Rule Base for the FLC

Input			Output	Input			Output
V	P_{comp}	E	P	V	P_{comp}	E	P
L	NH	L	NL	M	PL	L	PL
L	NH	M	NM	M	PL	M	PL
L	NH	H	NH	M	PL	H	PL
L	NM	L	NL	M	PM	L	PL
L	NM	M	NM	M	PM	M	PL
L	NM	H	NM	M	PM	H	PL
L	NL	L	NL	M	PH	L	PL
L	NL	M	NL	M	PH	M	PL
L	NL	H	NL	M	PH	H	PL
L	PL	L	ZR	H	NH	L	ZR
L	PL	M	ZR	H	NH	M	NL
L	PL	H	ZR	H	NH	H	NL
L	PM	L	PL	H	NM	L	ZR
L	PM	M	ZR	H	NM	M	NL
L	PM	H	ZR	H	NM	H	NL
L	PH	L	PL	H	NL	L	ZR
L	PH	M	ZR	H	NL	M	ZR
L	PH	H	ZR	H	NL	H	ZR
M	NH	L	NL	H	PL	L	PL
M	NH	M	NL	H	PL	M	PL
M	NH	H	NL	H	PL	H	PL
M	NM	L	NL	H	PM	L	PM
M	NM	M	NL	H	PM	M	PM
M	NM	H	NL	H	PM	H	PM
M	NL	L	NL	H	PH	L	PH
M	NL	M	NL	H	PH	M	PM
M	NL	H	NL	H	PH	H	PL

themselves have low energy availability, it can deliver only low power to the grid and hence P is NL. If E were M or H, P would be NM or NH. Now, let E be the energy required instead of energy available. Energy available L implies energy required is H. Using the same input already used in the former case, power output P for the inputs (Rule 1) would be NL. This is because, at low node voltage, power cannot be drawn by the batteries, though the grid have high energy requirement.

4.3.3 Division of power among the batteries

The control flow diagram of a CS is shown in Figure 4.6. The power required by the CS to charge the batteries or discharge the batteries energy to the grid is represented by P. Here, P can be negative or positive depending on the direction of power flow. Again, P is divided

among the batteries of CS as Pb_1 (1^{st} battery of CS) to Pb_n (n^{th} battery of CS). If Pb_1 is positive, the battery will get charged and if negative, the battery will be discharged. Charging and discharging of the EV's battery can be controlled with the help of an algorithm which is explained in the next subsection. In this part, division of power among the batteries is discussed.

The amount of power flow (P) which is decided by the FLC is divided among the batteries as:

$$Pb_i = \frac{Eb_i}{E} P \tag{4.1}$$

where, Pb_i is the power required by the i^{th} battery of the CS, Eb_i is the available energy of the i^{th} battery and P is the output power as decided by the FLC. The total energy of the batteries E can be calculated as follows:

$$E = \sum_{i=1}^{i=n} Eb_i \tag{4.2}$$

where, Eb_i can be the available energy in the battery for discharging or the required energy by the battery for charging. This can be derived using the following equations.

$$E_{avail}^{com} = E_{rated}(SOC_{initial}/100) - E_{com} \tag{4.3}$$

where, E_{avail}^{com} is the energy available after commuting certain distance, E_{rated} is the rated energy of the EV's battery, $SOC_{initial}$ is the SOC at the time of starting from home/office and E_{com} is the energy used while commuting. Now, the SOC after commuting can be found as:

$$SOC_{postcom} = (\frac{E_{avail}^{com}}{E_{rated}})100 \tag{4.4}$$

where, $SOC_{postcom}$ is the SOC of the battery after commuting, E_{avail}^{com} and E_{rated} are same as defined in Eq. (4.3). Using Eq. (4.3) and Eq. (4.4), the 'energy available' and 'energy required' for the i^{th} battery can be found as:

$$Eb_i(avail) = ((SOC_{postcom} - SOC_{lt})/100)E_{rated} \tag{4.5}$$

$$Eb_i(required) = ((100 - SOC_{postcom})/100)E_{rated} \tag{4.6}$$

where $Eb_i(avail)$ and $Eb_i(required)$ are the energy availability and the energy required for the i^{th} battery.

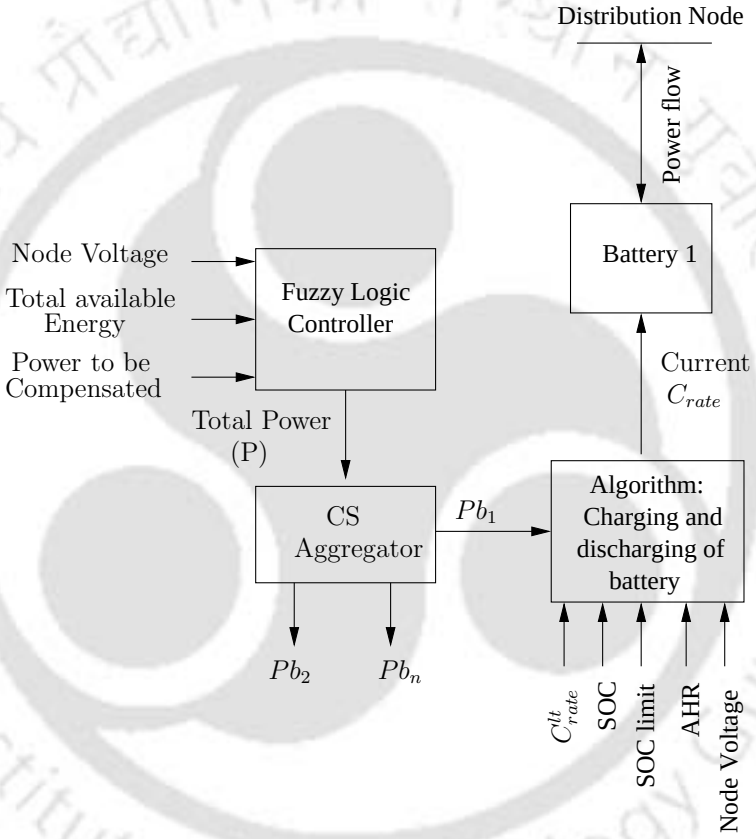

Figure 4.6: Control flow from the charging station to individual battery.

4.3.4 Individual battery control

Individual battery control discussed in this part is similar as discussed in the chapter 3. However, to maintain the continuity few equations are repeated in this subsection.

To control the flow of energy between the grid and an individual battery, an algorithm has been developed. Charging and discharging of an EV's battery can be controlled by changing

the C_{rate}. Power required for charging/discharging the battery and 'available/required' energy of the battery are used to calculate the C_{rate} and it is given as:

$$C_{rate} = \frac{Pb_i}{V_i Ahr_i} \tag{4.7}$$

where, C_{rate} is the required charging/discharging rate of the individual batteries. Pb_i is the power required to charge/discharge the i^{th} battery of the CS. V_i is the voltage of the i^{th} battery and Ahr_i is the current Ampere Hour (AHR) of the i^{th} battery. However, the C_{rate} calculated in Eq. (4.7) should not exceed the preferred rate of the Vehicle's owner and this is taken into account as given in the flow chart of Chapter 3 (Figure 3.5).

Current Ampere Hour is calculated as:

$$Ahr_i = Ahr_{rating}(SOC_{rem}/100) \tag{4.8}$$

where, Ahr_{rating} is the rated AHR of the battery, SOC_{rem} is the difference of the current SOC (SOC_{cr}) and SOC limit (SOC_{lt}). In the case of discharging, SOC_{rem} is calculated as follows:

$$SOC_{rem} = SOC_{cr} - SOC_{lt} \tag{4.9}$$

In the case of charging, SOC_{rem} is calculated as below.

$$SOC_{rem} = 100 - SOC_{cr} \tag{4.10}$$

Finally, the current of the battery is controlled based on the required C_{rate} and Ahr_i of the battery. Using Eq. (4.7) and Eq. (4.8), the battery current is calculated as given in Eq. (4.11). Ahr_{bi} is the current which flows between the battery and the grid. Ahr_{bi} is positive, if power is flowing to the battery during charging and negative if power is flowing to the grid from the battery during discharging.

$$Ahr_{bi} = Ahr_i C_{rate} \tag{4.11}$$

The detailed flow chart for charging and discharging of a battery is similar as shown in

Figure 3.5 of chapter 3. In the Figure 3.5, C_{rate}^{limit} is the preferred maximum C_{rate} set by the vehicle's owner(refer Table 4.2) and V_{bat} is the voltage of the battery. All the other symbols have same description as mentioned in Eq. (4.8) to Eq. (4.10).

For example, if AHR_{rating}, V_{bat}, SOC_{cr} and SOC_{lt} of a battery (1^{st} battery of CS) is 32 AHR, 250 V, 90 and 25 respectively then SOC_{rem} can be found from Eq. (4.9) to be 65 and Ahr_i can be found from Eq. (4.8) to be 20.8 AHR. If Pb_1= 1.16 kW (power required for discharging to the grid by the EV's battery), as decided by Eq. (4.1) (say during peak hours) then the C_{rate} at 90% of SOC can be calculated using Eq. (4.7) as 0.223.

4.3.5 Assumptions and background

As mentioned in Section 4.3, there will be a maximum of 50 EVs at the CS. However, for the sake of better representation all these EVs are divided into 5 categories. Table 4.2 shows the type of batteries along with their energy ratings in kWh, commuting energy in kWh (energy consumed by EV while commuting), initial SOC, SOC after commuting, SOC limit and C_{rate} limit. The energy available to discharge to the grid and energy required by the batteries for charging are also shown in the table. Eq. (4.3)- Eq. (4.6) have been used to find the available and required energy of the batteries as mentioned in Table 4.2.

The following assumptions are made to validate the proposed model.

- The initial SOC of the EVs' batteries at the time of leaving from their home or office is taken to be 90%.
- EVs will travel an average distance of 20 Km to reach the CS and the energy consumed in travel is assumed to be 6 kWh per 20 km [65, 66].
- EVs' arrival at the CS is assumed to be Gaussian because in real situations, EVs may arrive and depart CS at different times as per the owners' need . The cumulative number of EVs are assumed to vary at every hour(Figure 4.7 and Figure 4.8).

Accordingly, the energy curve is estimated for two different time slots. Two types of time slots have been considered assuming two scenarios:

Table 4.2: Battery specifications

Energy rating (kWh)	Commuting energy (kWh)	Initial SOC (%)	SOC after commuting (%)	SOC limit (%)	C_{rate} limit	energy available (kWh)	energy required (kWh)
10	6	90	33	20	2	1	7
12	6	90	45	25	2.5	1.8	7.2
16	6	90	58	30	1.5	3.6	7.6
20	6	90	67	35	2	5	8
24	6	90	72	40	3	6	8.4
Total energy of 5 EVs(kWh)						17.4	38.2

- First scenario is that EVs will travel to office or working place from their residential area in the morning hours and they will return in the evening hours.
- Second scenario is considered during night hours. In this case EVs starts arriving at the residential area in evening hours and stay during night in the same area. However, they start leaving for the office or working place in the morning hours.

The two time slots are as follows:

- First slot is taken during day time (0800 hrs-1800 hrs)
- The second slot is during night time (1800 hrs- 0800 hrs).

Two types of energy curves (energy availability and energy required) are shown in the (Figure 4.7 and Figure 4.8) and these curves are used in the simulation work. The energy availability and energy required curves are based on the assumed gaussian curves for arrival of EVs at the CS.

However, the energy utilization curve of the batteries available at the CS will be different because, the energy required/available will be updated at every instant of time. This is because, the power is changing at every instant of time and therefore the energy required/available will change depending on the FLC output. The energy utilization curve is shown in the result section (Figure 4.20). The two type of energy curves are as follows:

Type A: EVs arrive during day time at the CS directly from their residence will have energy curve similar to Figure 4.7. The duration of the EVs' availability at the CS during the day time is assumed to be from 0800 hrs to 1800 hrs. This curve shows the energy available for peak shaving and energy required for charging the EVs. In other words, this energy curve is the cumulative energy (available and required) due to arrival of EVs in a particular hour. Numbers mentioned in the figure are the cumulative number of EVs at that time. The energy (available/required) is calculated using Eq. (4.3)- Eq. (4.6) and also mentioned in Table 4.2.

For example, at 1000 hours, 30 EVs have arrived. Using Table 4.2, the available energy of 30 EVs will be 104.4 kWh and the required energy for charging is 229.3 kWh. It implies that EVs can charge as well as discharge depending on the grid condition. Similarly at 1800 hrs, 5 EVs are present and therefore, the available and required energy will be 17.4 kWh and 38.2 kWh respectively.

It can also be observed from Figure 4.7 that the energy available in the batteries is low when compared to energy required by the batteries. This is due to the assumption regarding the batteries SOC limit and their commuting energy.

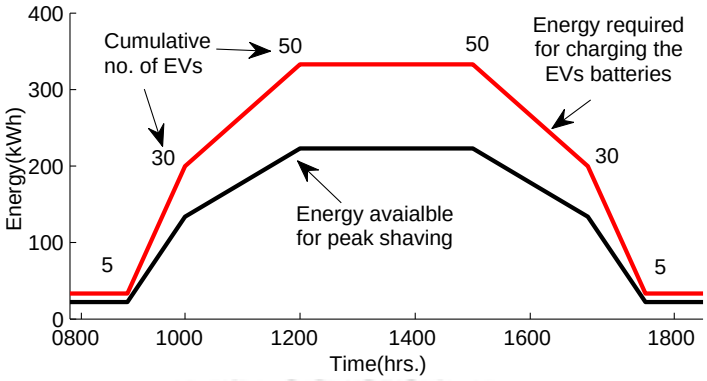

Figure 4.7: Energy curve during day time as per the arrival of EVs at the CS

Type B: EVs which arrive at the CS in other times such as in the evening hours will have the energy curve as shown in Figure 4.8. The duration for this type of energy curve is longer as compared to **Type A**, because during this period, (1800 hrs. to 0800 hrs.) most of the EVs will be in residential area. Numbers mentioned in the figure are the cumulative number of EVs at the respective hours. It is observed that between 2300 hrs and 0300 hrs, movement of

EVs to & from the CS will reduce to zero. Hence, cumulative numbers of EVs at the CS will become constant(50 EVs) and so will be the available and required energy.

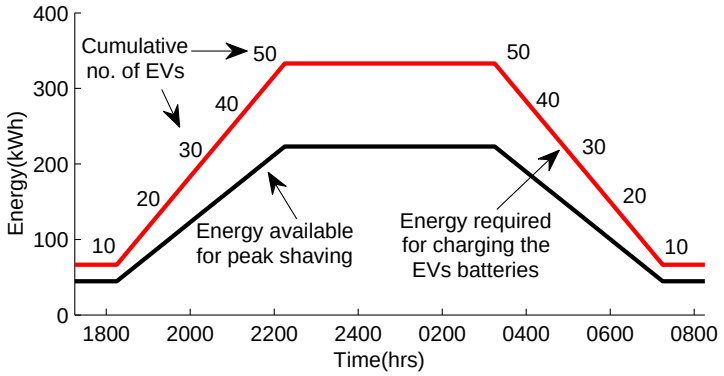

Figure 4.8: Energy curve during evening and night time as per the EVs arrival at the CS

The proposed CS is validated for two distribution nodes each having a different load pattern but similar solar & wind power profile. At a time, only one node has a dynamic load profile and other nodes are assumed to have constant load as mentioned in Table 3.1. Base load for the two test nodes is found to be 150 kW. The peak and off peak load is compared with base load. The load above the base load is called the peak load (peak shaving area) and below it is called off-peak load (valley filling area). The load profile mentioned in CASE I and CASE II are without the integration of renewable energy sources. Two case studies are described below.

CASE I: The load curve of the first test node(**Node 3.3**) is shown in Figure 4.9 and this is obtained from the substation on a particular day of the year 2011. This node has a commercial as well as residential load. The peak load starts exceeding the base load from the day time and reaches its peak during evening hrs due to lightening in the commercial as well as residential area. During 0800 hrs-1800 hrs, the energy of EVs arriving at the CS will be utilised as per the **Type A** energy curve and during 1800 hrs-0800 hrs, the same will be utilised as per **Type B** energy curve, as shown in Figure 4.9.

CASE II: The load curve of the second test node (**Node 2.3**) is shown in Figure 4.10, which is obtained from the substation. This node consists of only industrial load. Therefore peak load is found in the day time as shown in the figure. As the peak load is during the day time, hence, energy of EVs arriving in the office hours will be utilized at the CS (**Type A**).

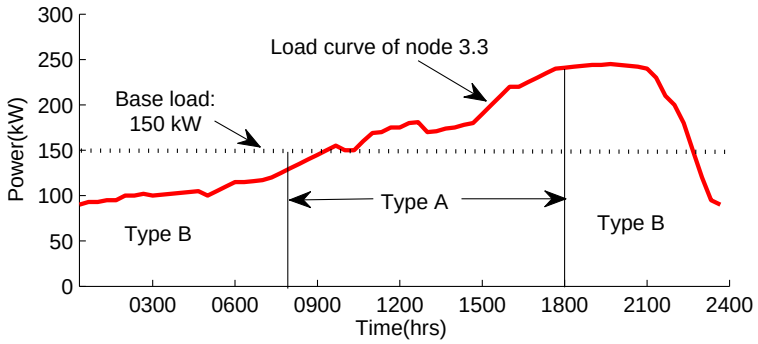

Figure 4.9: : Load curve of node 3.3, without integration of renewable energy sources

The simulation is carried out between 0800 hrs to 1800 hrs.

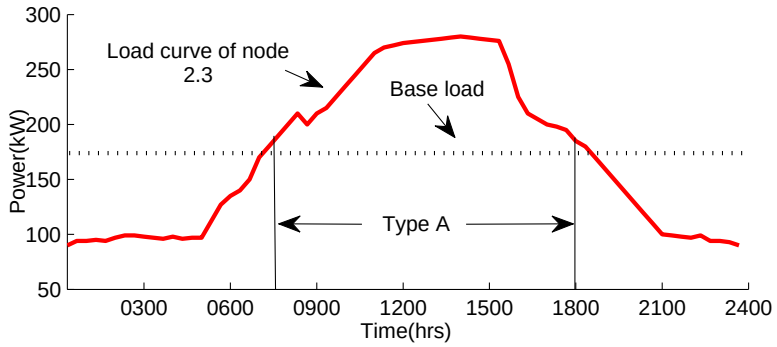

Figure 4.10: Load curve of node 2.3, without integration of renewable energy sources.

4.4 Results and discussion

4.4.1 Case I: Commercial and residential load at node 3.3

Load curve of node 3.3 which is shown in Figure 4.9, has been utilised for the real time implementation of the proposed model. In Figure 4.11, the solar power and the wind power curves along with the total power obtained from these two power curves (solar and wind) have been shown. With the inclusion of renewable energy sources at the node, some part of the existing load is met by the renewable energy sources. Therefore, with the inclusion of renewable energy source, the effective load demand reduces. The load profile without the renewable sources and the effective load with integration of renewable energy sources are also shown in the figure. It is seen that the load above the base load will lead to drop in the

voltage level and load lower than the base load will lead to rise in the voltage level. In other words, valley filling area is increased and the peak shaving area is reduced with the inclusion of renewable energy sources. If the utilisation of EVs in peak and off-peak hours is achieved then the load curve is flattened and the voltage becomes closer to unity.

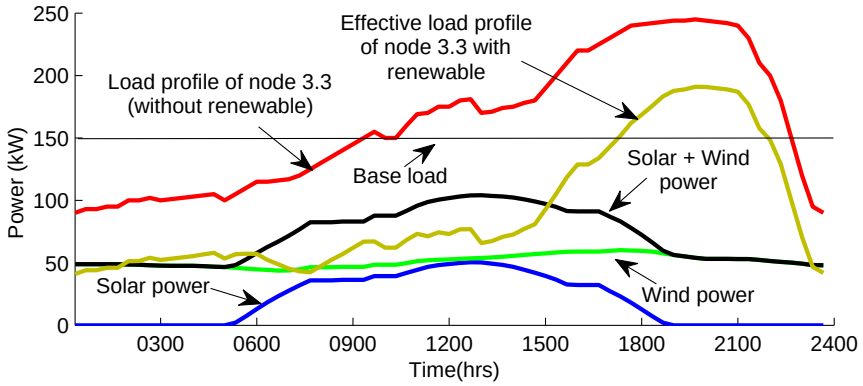

Figure 4.11: CASE I: Load curve of node 3.3 with integration of renewable energy sources

Considering the base load to be 150 kW, 'power to be compensated' is shown in Figure 4.12. **X** and **Y** marked regions in the figure represents the amount of power to be compensated (P_{comp}). Negative area (**Y**) is for discharging excess energy to the grid and the positive area (**X**) is for charging the EVs batteries at the CS. **Type A** and **Type B** energy curve is used between 0800 hrs - 1800 hrs and 1800 hrs - 0800 hrs respectively. With the utilization of EVs as a storage, X and Y area can be reduced resulting in the flattening of the node voltage. The voltages of the node with and without integration of the solar and wind energy sources are shown in Figure 4.13. It is observed that voltage of the node diverges from 1 p.u to a higher value with the integration of renewable energy sources.

Now, based on the energy availability at the CS, node voltage and power to be compensated (Figure 4.12), FLC decides the flow of the amount of power between the grid and the CS and it is shown in Figure 4.14. It is observed from this figure that at 0800 hrs, there is a large gap between the FLC output and the power to be compensated. This is due to low energy availability of battery during this time, which is a consequence of the assumption of Gaussian arrival of the EVs at the CS. But after this duration, the difference is very small. Similar scenario is observed at 1800 hrs. The node voltage after the inclusion of the FLC based CS has

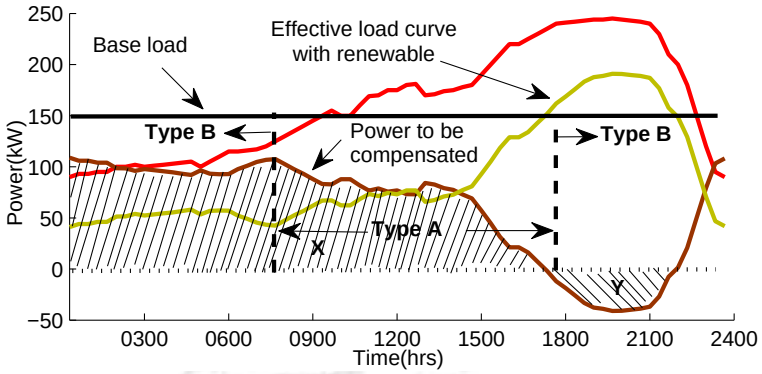

Figure 4.12: CASE I: Power to be compensated at node 3.3 with the integration of solar and wind energy

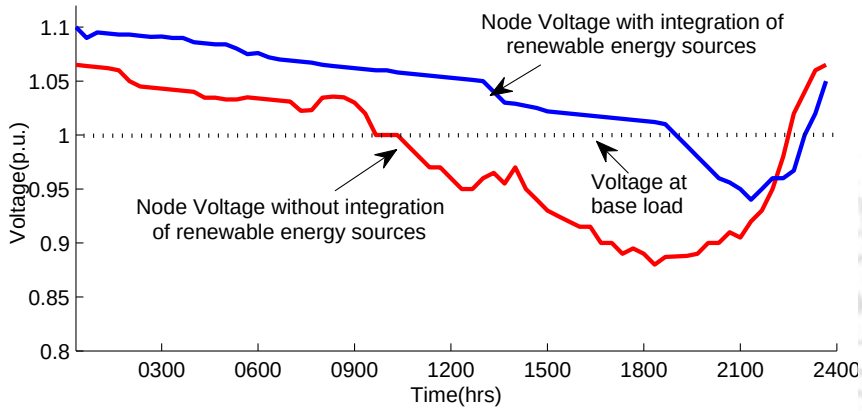

Figure 4.13: CASE I: Voltage of node 3.3 with and without integration of renewable energy sources.

been maintained near to unity due to flattening of the load profile and it is shown in Figure 4.15.

4.4.2 Case II: Industrial load at node 2.3

In this case, the load curve as shown in Figure 4.10 is used to study the interaction of renewable energy sources in the presence of FLC based CS. The analysis will be done only between 0800 hrs and 1800 hrs since, only industrial load is connected at this node and therefore, people working in this area will park their EVs at the CS only during day time. Load curve of node 2.3 with integration of solar and wind power is shown in Figure 4.16. With the integration of renewable energy sources, the effective load has been reduced. Therefore, the valley filling area is increased and the peak shaving area is reduced as shown in the figure.

The 'power to be compensated' has been shown in Figure 4.17. **'X'** and **'Y'** marked region

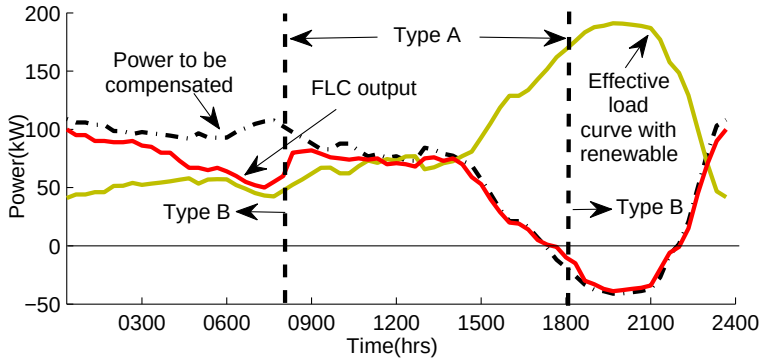

Figure 4.14: CASE I: FLC power output and the power to be compensated

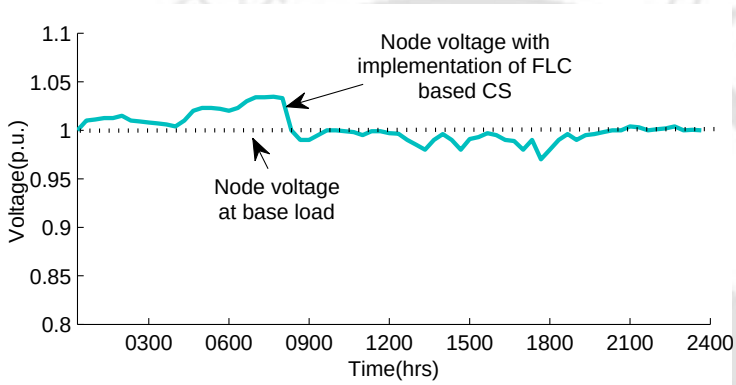

Figure 4.15: CASE I: Node voltage with implementation of FLC based CS

in the figure represents the amount of power to be compensated. Negative area (**Y**) is for discharging the excess energy to the grid and positive area (**X**) is for the charging of EVs batteries at the CS.

The voltage of the node 2.3 (with and without renewable energy sources) is shown in Figure 4.18.

The FLC output is shown in Figure 4.19. In this figure, FLC output is only shown for 0800 hrs to 1800 hrs. It is observed that the proposed controller maintains almost similar curve as that of 'power to be compensated'. Similarly, the voltage of the node can be shown to be near to unity after the inclusion of FLC based CS.

The energy utilization for the CASE I and CASE II have been shown in Figure 4.20. The positive energy shown in this figure is the required energy and the negative energy is the available energy. These energy curves are different from the curves shown in Figure 4.7 and

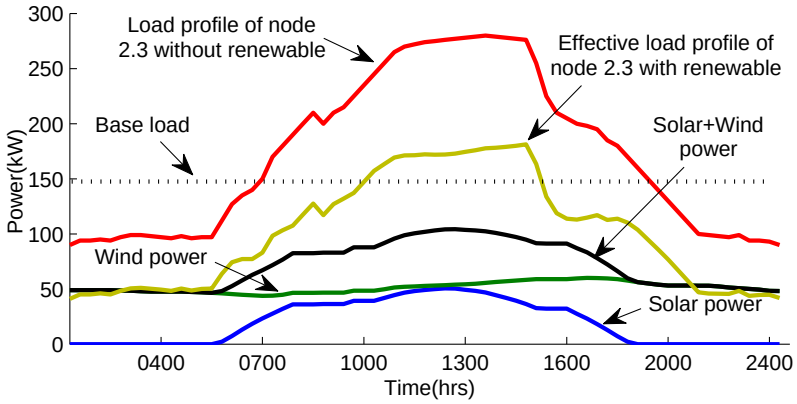

Figure 4.16: CASE II: Load curve of node 2.3 with integration of renewable energy sources.

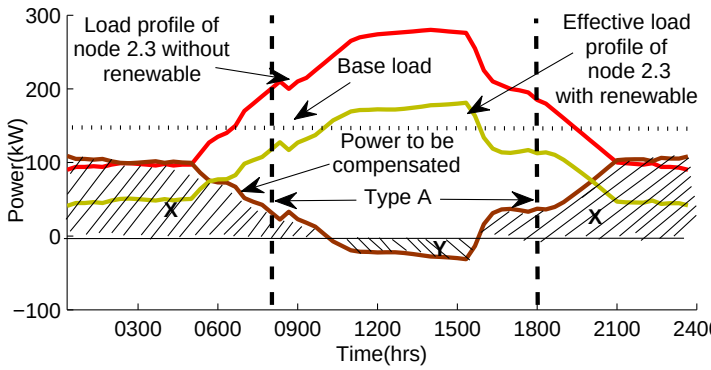

Figure 4.17: CASE II: Power to be compensated at node 2.3 with the integration of solar and wind energy

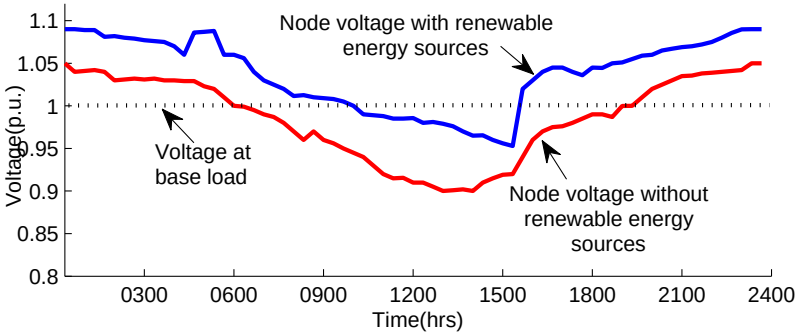

Figure 4.18: CASE II: Voltage of node 2.3, with and without renewable energy sources

Figure 4.8. It is observed that the energy curve is changing very steeply at certain value of time. This is because EVs arrive/depart every hour. Due to sudden arrival of EVs, the energy level of the CS increases. But, during a certain period, the energy reduces as it is utilised by the grid or by the EVs' batteries at the CS.

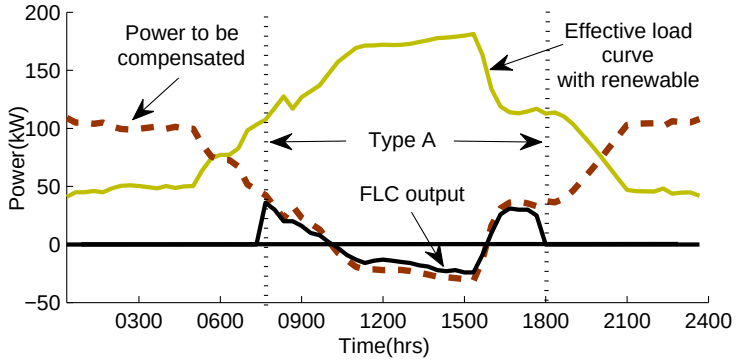

Figure 4.19: CASE II: FLC power output along with 'power to be compensated'

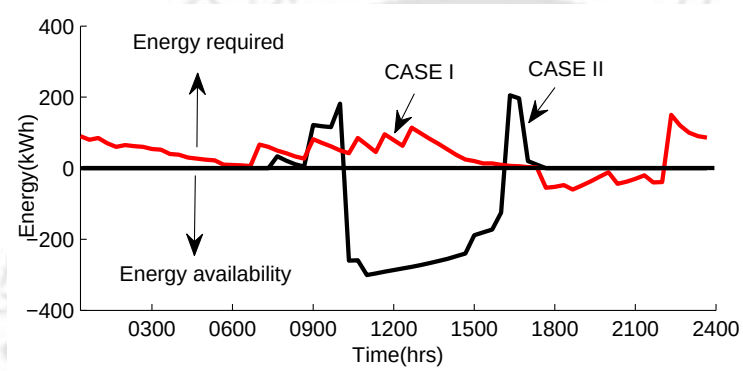

Figure 4.20: Energy utilization of the CS batteries for the CASE I and CASE II

4.5 Summary

In this chapter, the charging station has been modelled for the Electric Vehicles and its interaction with the renewable energy sources has been presented. Individual EV's battery participates in the valley filling and peak shaving. A fuzzy logic controller has been designed which controls the flow of power based on the node voltage and the available energy of the batteries. To protect the battery from over-discharging, an algorithm has been developed which prevents operation beyond the specified end-of-discharge voltage. The batteries are not charged/discharged beyond the owner's preferred maximum C_{rate}. A practical distribution system has been simulated to test the proposed model. It has been analysed that the proposed charging station can handle the inclusion of renewable energy sources and stabilise the grid in real time scenario.

In the next chapter, various CSs connected to different nodes of a radial subfeeder and their

coordination with the distribution substation (DS) have been presented.

5

Real time coordination of Electric Vehicles in V2G scenario at the Distribution substation level

Contents

5.1 Introduction

Fuel based power plants can be more efficiently operated if the production levels are constant [67]. However, as the loads keep fluctuating, electricity production are drastically scaled up and down to meet momentary power demands [68]. Also, the use of renewable energy sources such as solar farms and wind farms can cause mismatch between the load and generation due to its intermittent nature [69]. Therefore, to increase the efficiency of the generating plants, and to match the load with generation, it is necessary to store electrical power when production exceeds consumption. When the power demand exceeds the generation, the stored energy can be returned back to the grid [70]. With induction of energy storage systems in the grid, the large scale penetration of renewable energy sources can be facilitated as discussed in chapter 4. Among various storage technologies, utilization of the Electric Vehicles (EVs) batteries can become the potential storage for the grid (Chapter 2 and Chapter 3). In the previous chapters, V2G architecture was developed for a particular node. However, in practical scenario, need of coordination among the different CSs connected to different nodes of a distribution substation may arise.

In this chapter, real time coordination of EVs at the Distribution Substation (DS) level has been modeled. Six CSs have been modeled and each CS is connected to a node of the radial subfeeder (11kV/440 V). A node of a subfeeder covers residential, commercial, office or industrial area of a particular region. Each CS has charging bays where EVs can charge their batteries or discharge the excess energy to the grid. The presence of EVs at the CSs is more likely because 90% of the time EVs will be idle [41]. Therefore, with large penetration of EVs, CSs will be one of the best viable options to charge the EV's battery. Batteries of the EVs are modeled which can calculate the capacity loss at different C_{rate}. Batteries are not charged or discharged beyond the maximum allowable C_{rate} and also not discharged beyond the user's preferred minimum energy limit. Block diagram representation of V2G system at the substation level is shown in Figure 5.1.

As shown in the above figure, two levels of control has been used. The first controller is at

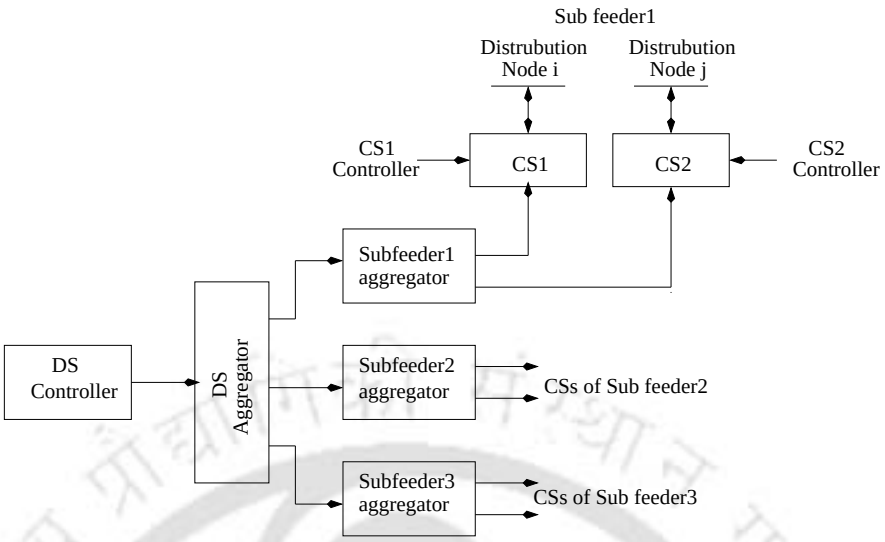

Figure 5.1: Block diagram of V2G system at the substation level.

the Distribution Substation (DS) and the second one is at the CS level. The two controllers designed are FLC based, as they provide a means of converting a linguistic control strategy based on expert knowledge into an automatic control strategy. Fuzzy control is based on a logical system which is much closer to human thinking and natural language than traditional logical systems [71]. The first controller is named as 'Distribution Substation Controller' (**DSC**) which decides the magnitude and direction of the power that should flow between the CSs and the grid. The direction of the power flow can be negative or positive. The negative power implies that the CSs have to support the grid by discharging the excess energy stored in the EVs' batteries whereas, positive power implies that CSs will charge the EVs batteries. The second FLC is termed as 'Charging Station Controller' (**CSC**). It decides the amount and direction of power flow between the individual CS and the node to which it is connected. Again, this power can be negative or positive depending on the power flow directions. The aggregator at the DS (DS aggregator) distributes the power among the subfeeder. The subfeeder aggregators allocate the power among the CSs of their respective subfeeder. Finally, the CS aggregator distributes the power among the EVs batteries present at the CS.

Following assumptions have been made in this work.

- Multi node CSs have been modeled at the system level.

- Converters connected to charge and discharge the EVs has not been modeled since the aim of this work is to show V2G implementation at the system level.

- Efficiencies of the charging system and converters have not been considered. This assumption does not affect the proposed algorithm because the capacity loss of the batteries has been considered which is the main cause of decreasing the efficiencies of the charging system.

The chapter is organized as follows: Description of the test system is presented in Section 5.2. The modeling of the V2G system at the DS and CS level along with modelling of the battery is presented in Section 5.3. Algorithms are developed for the entire V2G system in Section 5.4. The FLC controllers and aggregators are also discussed in this Section. The background and possible assumptions for this work are presented in Section 5.5. Results are analysed in Section 5.6. Finally, the summary of this chapter is presented in Section 5.7.

5.2 Description of the test system

The test system is a reduced substation network of the distribution system of Guwahati city (the state capital of Assam) and is shown in Figure 5.2. This radial test system consists of one main feeder and four subfeeders. The main feeder has a transformer of rating, 5 MVA, 33kV/11 kV and each subfeeder has a 500 kVA, 11kV/440 V transformer. CSs are connected to the nodes of three subfeeders (**1.1**, **1.3**, **2.2**, **2.3**, **3.1** and **3.2**). Peak hour substation load of a typical distribution system of Guwahati city for 2012 is given in Table 5.1. In this table, P and Q represent active and reactive power respectively. Off peak hour load is approximated to be 60% of the peak hour load as per the data provided by the Assam State Electricity Board (ASEB) [43] . The impedance of the entire section is assumed to be constant with a resistance of 0.0027 p.u and reactance of 0.0023 p.u. The system is assumed to be a balanced three phase system. The base values used for the apparent power and the voltage are 500 kVA and 0.44 kV respectively and the feeder voltage is taken to be 1.0605 p.u.

Table 5.1: Existing load of substation

Nodes	P(p.u.)	Q(p.u.)	Nodes	P(p.u.)	Q(p.u.)
1.1	0.50	0.22	**3.1**	0.43	0.29
1.2	0.47	0.23	**3.2**	0.23	0.13
1.3	1.13	0.64	**3.3**	00	00
2.1	0.27	0.15	**4.1**	0.63	0.33
2.2	0.42	0.29	**4.2**	0.67	0.23
2.3	0.94	0.43	**4.3**	0.53	0.37

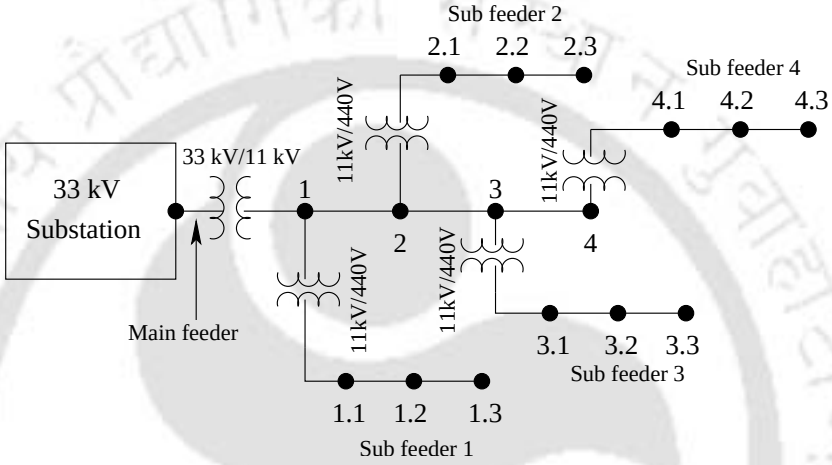

Figure 5.2: Radial distribution system of a substation of Guwahati city.

5.3 Modelling of the system

In this Section, detailed models of the V2G at the DS, subfeeder and the CS level have been presented.

5.3.1 Modeling of the V2G at the substation level

The DS can be used to coordinate among the EV's, present at the CS, for charging their batteries or discharging their excess energy to the grid. This control can be accomplished by designing a suitable controller which will collect the information of the grid and the net available energy at the CSs (E^{net}_{avail}). Information of the grid includes surplus power ($P_{surplus}$) at the DS and the duration of grid support ($D_{gridsprt}$). Based on these three information, **DSC** decides 'power to be compensated' by the CSs (P_{grid}) as shown in Figure 5.3. The P_{grid} is the power which is to be supplied/drawn to/from the CSs. Now, P_{grid} is distributed among the three

subfeeders as P_{sf1}, P_{sf2} and P_{sf3}. This distribution is based on the energy available with the CSs of that subfeeder and they are namely E_1, E_2 and E_3. The detailed algorithm is presented in Section 5.4.

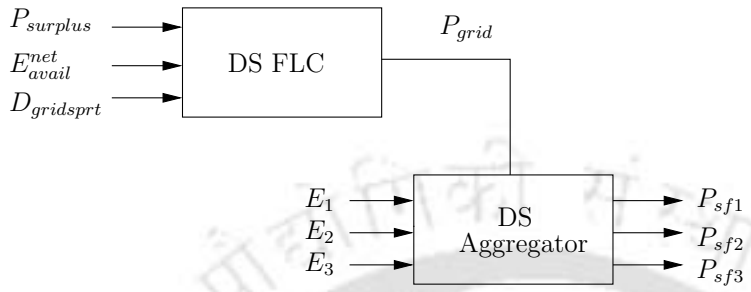

Figure 5.3: Block diagram of controller and aggregator at the substation level.

5.3.2 Aggregator at the subfeeder level

Figure 5.4. shows the block diagram of the subfeeder aggregator. The power which is obtained from the DS aggregator (P_{sf1}) is divided among the two CSs present at the subfeeder 1 and they are denoted as P_{11} and P_{12} (Power supplied/drawn to/from CS_{11} and CS_{12} respectively). CS_{11} and CS_{12} are the 1^{st} and 2^{nd} CS of the subfeeder 1 connected at **node 1.1** and **1.3** respectively. The division of the powers among the CS is based on the net energy available at the CSs of subfeeder 1 and the individual CS energy of the same subfeeder. Similarly, the division of power among the CSs of other subfeeders is done. In this figure, V_{11} is the voltage of node (1.1) and E_{11} and E_{12} are the energy available at the CS_{11} and CS_{12}. E_1 is same as mentioned in Figure 5.3.

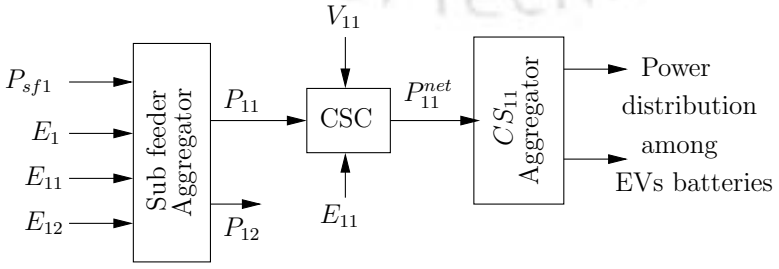

Figure 5.4: Block diagram representation of subfeeder aggregator.

5.3.3 Modeling of the CS

Each CS consists of 200 charging bays. This implies that a maximum of 200 EVs can be charged at a particular charging station at a time. CS has a **CSC** which decides the amount and direction of the power flow between the CS and the grid. This decision is carried out on the basis of three inputs namely the total energy available at the CS ($E_{avail}^{CS_1}$), voltage of the node in p.u. (V_{11}) and the power required (P_{11}) as decided by the subfeeder aggregator. The output of the FLC is the power (P_{11}^{net}) which has to be distributed among the different EVs present at the CS_{11} by the CS_{11} aggregator. The detailed block diagram of the CS FLC and its aggregator along with individual battery control at the CS is shown in Figure 5.5. The power to be supplied/drawn (P_{11}^{net}) by CS_{11} is divided among the batteries of CS_{11} as Pb_{111} (power flow in 1^{st} battery of CS_{11} of subfeeder 1) to Pb_{11n} (power flow in n^{th} battery of CS_{11} of subfeeder 1).

In the Figure 5.5, V_{bat} is the battery voltage. C_{rate}^{lt} is the maximum limit of charging/discharging rate(C_{rate}) of the battery respectively. SOC is the initial state of charge and SOC limit is the maximum allowable state of charge for discharging. Q is the current capacity of the battery in Ampere Hour(Ah). These sets of values are required to calculate the current C_{rate} of the batteries, which in turn will decide the amount of power that will flow between the battery and the grid. The detail algorithm at the battery level and FLC have been presented in Section 5.4.

5.3.4 Battery

A simple electric equivalent circuit (EEC) of Li-ion battery is shown in Figure 5.6. The EEC model has three parameters: an open circuit voltage (V_0), an internal resistance having two parameters R_1 and R_2 and the effective capacitance (C). This model is used to extract the circuit parameters for different charge/discharge rate. The mathematical representations for R_1, R_2, C and V_0 under constant current charging conditions are given in [72]. The battery parameters are represented as polynomial equations as a function of (C_{rate}) and SOC/DOD(depth of discharge) [73]. Under the constant current, the battery terminal voltage for charging scenario

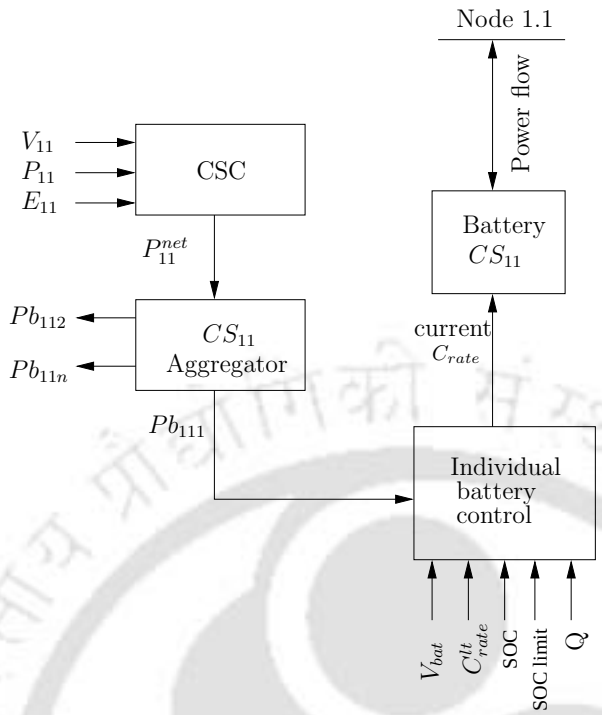

Figure 5.5: Block diagram representation of the CS and the individual battery control.

with respect to time is given as below.

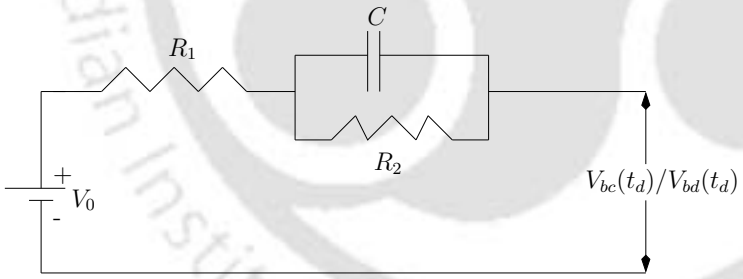

Figure 5.6: Electric equivalent circuit (EEC) for Li-ion battery.

$$V_{bc}(t_c) = \left(\left(\frac{Q}{C} + I_c \times R_2\right) \times \exp\left(-\frac{t_c}{R_2 \times C}\right)\right) + V_0 - (I_c \times (R_1 + R_2)) \tag{5.1}$$

where Q is capacity of the battery, I_c is charging current, t_c is charging time and $V_{bc}(t_c)$ is battery charging voltage with respect to time. Similarly, the battery terminal voltage for discharging scenario is given below.

$$V_{bd}(t_d) = \left(\left(\frac{Q}{C} + I_d \times R_2\right) \times \exp\left(-\frac{t_d}{R_2 \times C}\right)\right) + V_0 - (I_d \times (R_1 + R_2)) \tag{5.2}$$

where I_d is discharging current, t_d is discharging time and $V_{bd}(t_d)$ is battery discharging voltage with respect to time. Figure 5.7 represents the block diagram of the battery with capacity model. It calculates total processed energy, available energy for charging/discharging and capacity losses. The processed energy for charging scenario (PE_c) and discharging scenario (PE_d) are given below.

$$PE_c = \sum_{n=1}^{z} V_{bc}(t_c) \times I_c \times (t_n - t_{n-1}) \tag{5.3}$$

$$PE_d = \sum_{m=1}^{z} V_{bd}(t_d) \times I_d \times (t_m - t_{m-1}) \tag{5.4}$$

where, t_n and t_m are the simulation time for the charging and discharging respectively. The required energy for charging scenario and the available energy for discharging scenario under constant current condition is given by Eq. (5.5) and Eq. (5.6) and these equations are used to find the required energy for charging(AE_c) and the available energy for discharging(AE_d) and this is explained in Section 5.4.

$$AE_c = V_{bc}(t_c)Q(SOC_{fc} - SOC_{cr}) \tag{5.5}$$

$$AE_d = V_{bd}(t_d)Q(SOC_{cr} - SOC_{fd}) \tag{5.6}$$

where SOC_{fc}, SOC_{cr} and SOC_{fd} are the final SOC (100%) for charging, current SOC of the battery and SOC limit for discharging respectively.

The battery capacity represents the maximum amount of energy that can be extracted from the battery under certain specified conditions such as C_{rate}, SOC and temperature [74]. The capacity loss of Li-ion batteries can be related to the unwanted side reactions that occur during the overcharge and high charge/discharge conditions, which reduces the battery's lifetime time [75, 76]. Thus, capacity loss is directly proportional to the C_{rate} of the battery.

The mathematical model for capacity loss is developed based on the Arrhenius equation [75]. This equation is used for calculating capacity loss under fixed C_{rate}. The mathematical modeling techniques are comparatively simple and are sufficient to calculate battery capacity loss at

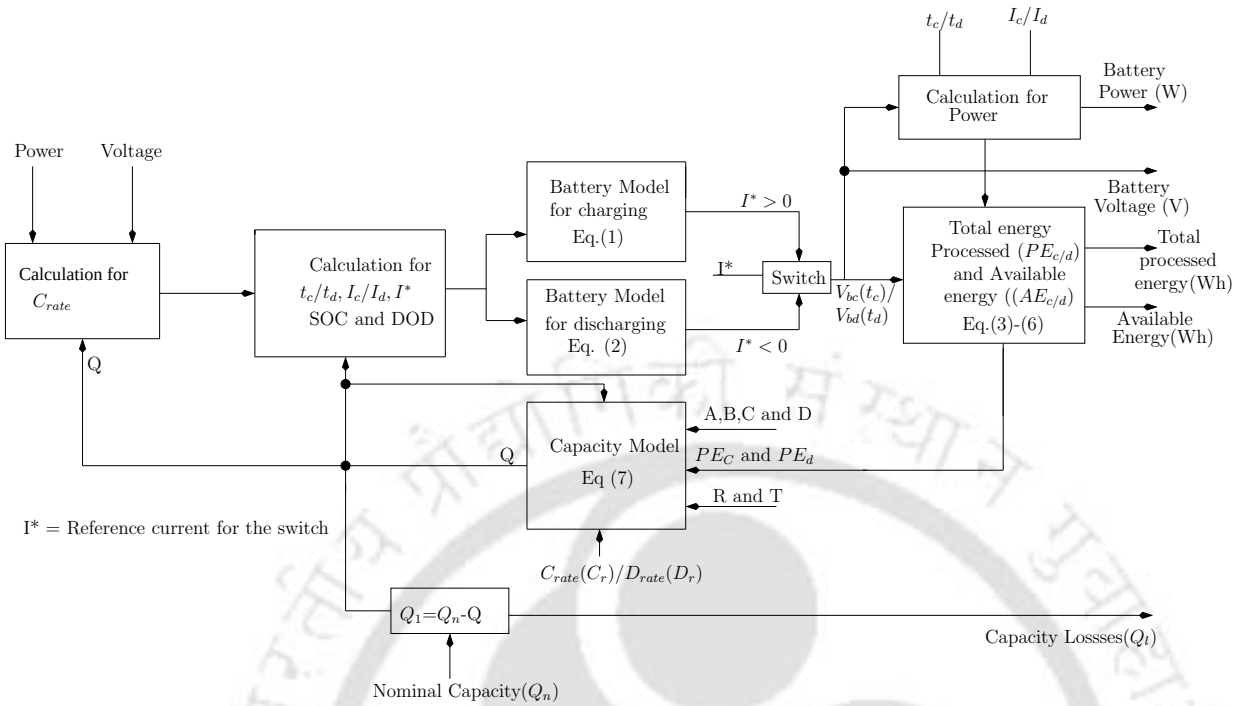

Figure 5.7: Detailed modeling of battery with processed energy and capacity loss model.

different C_{rate}. The mathematical model for capacity loss (Q_l) at different C_{rate} is given below.

$$Q_l = \left(A \times \exp\left(-\frac{C \times PE_c \times Q \times C_r}{R \times T}\right)\right) + \left(B \times \exp\left(-\frac{D \times PE_d \times Q \times D_r}{R \times T}\right)\right) \quad (5.7)$$

where, A and B are pre-exponential factors, C and D are adjustable factors, PE_c and PE_d is similar as defined in Eq. (5.3) and Eq. (5.4). C_r and D_r is charging and discharging rate(C_{rate}), Q is the current capacity of the battery (Ah), R is gas constant (J/mol K) and T is temperature (K). The advantage of this model is that it is capable of determining the capacity loss of the battery when it is subjected to different C_{rate}. The detailed block diagram of the battery model based on the capacity loss is shown in Figure 5.7. Q which is the current capacity (Ah) of the battery is evaluated at every instant of time and it is given in Eq. (5.8). Q_n is the rated capacity of the battery in Ah. The energy of the battery is updated based on the processed energy and at different C_{rate}.

$$Q = Q_n - Q_l \quad (5.8)$$

5.4 Design of controller and aggregators of the multi node CSs

In this section, the two controllers first at the DS level and second controller at the CS level is presented. Finally the algorithm is developed for the aggregators at the DS, subfeeders and CS level.

5.4.1 Controller and aggregator at the DS

The fuzzification is largely determined by the shape of the membership functions [51,77]. In order to facilitate computations, triangular membership functions are utilized in this study for both the input and output membership functions. The membership functions used in this work are having equal distribution for each input and output similar as used in Chapter 3 and Chapter 4. The inputs or output notations used for the membership functions have meaning such as L means low, H means high, M stands for meduim, NL means negaitve low, PL means positive low, Z stands for zero and so on. The Mamdani type inference (also known as the max-min inference method), utilizes the minimum function for the implication of the rules. Defuzzification is performed using the center of gravity method [49, 50]. It performs defuzzification by finding the center of the area encompassed by all the rules, and is mathematically described by

$$u(t) = \frac{\sum_{i=1}^{n} u_i \mu_v(u_i)}{\sum_{i=1}^{n} \mu_v(u_i)} \tag{5.9}$$

where $u(t)$ refers to the defuzzified overall control output, while u_i refers to the output variable and μ_v represents the aggregated membership function. The rule base for the **DSC** is given in Table 5.2.

DSC as mentioned in Figure 5.3, decides the total amount of power to be transferred (P_{grid}) to/from the CSs. This decision is taken based on three inputs namely $P_{surplus}$, E^{net}_{avail} and $D_{gridsprt}$.

$$P_{surplus} = P^{grid}_{surplus} \pm \sum_{i,j} P^{net}_{ij} \tag{5.10}$$

where $P_{surplus}$ is the net power which is to be supplied/drawn to/from the CSs. $P^{grid}_{surplus}$ is the power required/available for the grid support as decided by the substation. P^{net}_{ij} is the net power of the i^{th} CS of n^{th} subfeeder as decided by the **CSC** and whose direction is different than the $P_{surplus}$. This power is to be accounted because some CSs may be charging due to high node voltage but at the same time the grid requires power from the CSs. Hence, the $P_{surplus}$ will be the addition of the net power discharge by the CS to the grid during off peak time and the power required/available for the grid support($P^{grid}_{surplus}$).

For example, let us consider $P^{grid}_{surplus}$ is the excess power available (say 1500 kW) at the DS apart from meeting its regular loads and this power should be utilized by the CSs during off-peak hours. At the same time, say CS_{22} has low node voltage. Since, the node voltage is low, P^{net}_{22} will be negative and **CSC** present at the CS_{22} decides the power to discharge to the grid which is 120 kW (say). It implies that during off-peak time, discharge of power at a node will increase the amount of available power to 1620 kW. This power is the net power which should be compensated by the CS and is named as $P_{surplus}$.

The P_{grid} obtained from the substation FLC is to be divided among the subfeeders. The distribution of power among the subfeeders is done by the DS aggregator. The net energy available of the CSs and the net energy available by the CSs of each subfeeder are used to distribute the power among the subfeeders.

To calculate the net energy, direction of the power flow between the CS and the node is also taken in to account. Since, there may be cases where P_{grid} is positive (charging power) but the node voltage is very low at a particular node. Since, the node voltage is very low, **CSC** of this CS decides to discharge the batteries energy to the grid. Therefore, the energy available of this CS cannot be utilized (E^{net}_{avail}) in the decision making of the **DSC**. This is explained through following equation.

Table 5.2: Rule Base for **DSC**

E^{net}_{avail}	$D_{gridsprt}$	$P_{surplus}$	P_{grid}	E^{net}_{avail}	$D_{gridsprt}$	$P_{surplus}$	P_{grid}
L	L	NH	NM	M	M	PL	PL
L	L	NM	NM	M	M	PM	PM
L	L	NL	NL	M	M	PH	PM
L	L	Z	Z	M	H	NH	NM
L	L	PL	PM	M	H	NM	NL
L	L	PM	PH	M	H	NL	NL
L	L	PH	PH	M	H	Z	Z
L	M	NH	NM	M	H	PL	PL
L	M	NM	NL	M	H	PM	PL
L	M	NL	NL	M	H	PH	PM
L	M	Z	Z	H	L	NH	NH
L	M	PL	PL	H	L	NM	NH
L	M	PM	PM	H	L	NL	NM
L	M	PH	PH	H	L	Z	Z
L	H	NH	NL	H	L	PL	PL
L	H	NM	NL	H	L	PM	PL
L	H	NL	NL	H	L	PH	PL
L	H	Z	Z	H	M	NH	NM
L	H	PL	PL	H	M	NM	NM
L	H	PM	PL	H	M	NL	NL
L	H	PH	PM	H	M	Z	Z
M	L	NH	NH	H	M	PL	PL
M	L	NM	NM	H	M	PM	PL
M	L	NL	NL	H	M	PH	PL
M	L	Z	Z	H	H	NH	N
M	L	PL	PL	H	H	NM	N
M	L	PM	PM	H	H	NL	N
M	L	PH	PH	H	H	Z	Z
M	M	NH	NM	H	H	PL	PL
M	M	NM	NM	H	H	PM	PL
M	M	NL	NL	H	H	PH	PL
M	M	Z	Z				

Table 5.3: Value of K

P_{status}	P_{11}^{net}	K_{11}
$+Ve$	$-Ve$	0
$+Ve$	$+Ve$	1
$-Ve$	$-Ve$	1
$-Ve$	$+Ve$	0

$$E_{avail}^{net} = E_1 + E_2 + E_3 \tag{5.11}$$

$$\begin{aligned} E_1 &= E_{11}K_{11} + E_{12}K_{12} \\ E_2 &= E_{21}K_{21} + E_{22}K_{22} \\ E_3 &= E_{31}K_{31} + E_{32}K_{32} \end{aligned} \tag{5.12}$$

Subscripts 1, 2 and 3 for E refer to the energy available/required by the CSs connected to three subfeeders. Subscripts such as 11 for E and K refer to the 1^{st} CS of 1^{st} subfeeder. K represents the factor which is either 0 or 1 depending on the power status (P_{status}) and the direction of power flow at the point of common coupling (PCC). The value of K is tabulated in Table 5.3. Similar relations can be derived for other K factors such as K_{12}, K_{21}, K_{22}, K_{31} and K_{32}.

Now, the P_{grid} as decided by the substation controller has to be divided between the three subfeeders. This division is made according to the equations shown below.

$$\begin{aligned} P_{sf1} &= \frac{E_1}{E_1+E_2+E_3} P_{grid} \\ P_{sf2} &= \frac{E_2}{E_1+E_2+E_3} P_{grid} \\ P_{sf3} &= \frac{E_3}{E_1+E_2+E_3} P_{grid} \end{aligned} \tag{5.13}$$

where P_{grid} is the power requirement at the substation level; P_{sf1}, P_{sf2} and P_{sf3} are the power required/available at the three subfeeders. E_1, E_2 and E_3 are the energy available at the CSs of the 1^{st}, 2^{nd} and 3^{rd} subfeeder respectively.

5.4.2 Aggregator at the subfeeder level

Once, the power (P_{sf1}) is allotted to the subfeeder 1 by the substation, it has to be divided among the various CSs connected to this subfeeder. The power to be supplied to each of the CS connected at the subfeeders are obtained as follows.

$$P_{11} = \frac{E_{11}K_{11}}{E_{11}K_{11} + E_{12}K_{12}} P_{sf1} \tag{5.14}$$

where, P_{11} is the power allocated to CS_1 of subfeeder 1. P_{sf1} is same as that defined in Eq. (5.13). E_{11}, E_{12} are the energy available/required by the CS_{11} and CS_{12} respectively. K_{11} and K_{12} are the factors which are either 0 or 1 depending on the P_{status} and the direction of the power flow at the PCC/node as defined in Table 5.3.

5.4.3 Controller at the CS level and the aggregator

The FLC at the CS level takes three inputs namely P_{11}, V_{11} and E_{11} as discussed in Section 5.3. The output of the controller is the net power (P_{11}^{net}) which should flow between the node and the CS. P_{11}^{net} may be negative or positive depending upon the direction of power flow similar as defined for the **DSC**. The rule base for the **CSC** controller is given in Table 5.4. The notations for the membership functions are similar as discussed for **DSC**.

Now P_{11}^{net} can be redistributed to every individual battery according to following equations. This task is performed by the aggregator at the CS level.

$$Pb_{ijk} = \frac{Eb_{ijk}}{\sum_{\{i,j,k\}=1}^{m,n,o} Eb_{ijk}} P_{11net} \tag{5.15}$$

where Pb_{ijk} is the power required by the k^{th} battery of j^{th} CS of i^{th} subfeeder. Eb_{ijk} is the available/required energy of the k^{th} battery of j^{th} CS of i^{th} subfeeder. In Eq. (5.16), AE_d and AE_c are same as defined in the battery modeling.

$$\begin{aligned} Eb_{ijk} &= AE_c \\ Eb_{ijk} &= AE_d \end{aligned} \tag{5.16}$$

Similarly, available energy of the i^{th} subfeeder of j^{th} CS (E_{ij}) can be calculated as follows.

$$E_{ij} = \sum_{ijk}^{m,n,o} Eb_{ijk} \tag{5.17}$$

$$E_i = \sum_{i=1,j=1}^{m,n} Eb_{ij} \tag{5.18}$$

5.4.4 Control scheme of the battery

In this part, an algorithm to control the flow of energy between the test node and an individual battery is developed. Charging and discharging of EV's battery can be controlled by changing their C_{rate}. Power required by the battery or power to be supplied by the battery to the grid and energy available/required by the batteries are used to calculate the C_{rate} and it is given as:

$$C_{rate} = \frac{Pb_{ijk}}{V_{ijk}Q_{ijk}} \tag{5.19}$$

where, C_{rate} is the required charging/discharging rate of the individual battery, Pb_{ijk} is the power required or to be supplied by the k^{th} battery of j^{th} CS of i^{th} subfeeder. V_{ijk} is the voltage of the k^{th} battery and Q_{ijk} is the current capacity of the k^{th} battery of j^{th} CS of i^{th} subfeeder. However, the C_{rate} calculated in Eq. (5.19) should not exceed the Vehicle's owner's preferred rate and this is taken into account by using the proposed algorithm and is shown in the Figure 5.8. Now, with the change of C_{rate}, the battery current (Ib_{ijk}) will change and that is given as follows.

$$Ib_{ijk} = C_{rate}Q_{ijk} \tag{5.20}$$

The detail flow chart for charging and discharging of a battery is shown in Figure 5.8. In this figure, C_{rate}^{lt} is the maximum C_{rate} as preferred by the vehicle's owner. All other symbols have same meaning as mentioned in Eq. (5.1) to Eq. (5.20).

Table 5.4: Rule Base for **CSC**

E_{11}	V_{11}	P_{11}	P_{11}^{net}	E_{11}	V_{11}	P_{11}	P_{11}^{net}
L	L	NH	Z	M	M	PL	PM
L	L	NM	Z	M	M	PM	PM
L	L	NL	Z	M	M	PH	PH
L	L	Z	Z	M	H	NH	NH
L	L	PL	PM	M	H	NM	NM
L	L	PM	PH	M	H	NL	NM
L	L	PH	PH	M	H	Z	Z
L	M	NH	NM	M	H	PL	PL
L	M	NM	NL	M	H	PM	PL
L	M	NL	NL	M	H	PH	PL
L	M	Z	Z	H	L	NH	NM
L	M	PL	PM	H	L	NM	NM
L	M	PM	PH	H	L	NL	NL
L	M	PH	PH	H	L	Z	Z
L	H	NH	NM	H	L	PL	PL
L	H	NM	NL	H	L	PM	PL
L	H	NL	NL	H	L	PH	PL
L	H	Z	Z	H	M	NH	NH
L	H	PL	PM	H	M	NM	NM
L	H	PM	PH	H	M	NL	NM
L	H	PH	PH	H	M	Z	Z
M	L	NH	NM	H	M	PL	PL
M	L	NM	NL	H	M	PM	PL
M	L	NL	NL	H	M	PH	PL
M	L	Z	Z	H	H	NH	NH
M	L	PL	PL	H	H	NM	NH
M	L	PM	PM	H	H	NL	NM
M	L	PH	PH	H	H	Z	NH
M	M	NH	NH	H	H	PL	PL
M	M	NM	NM	H	H	PM	PL
M	M	NL	NM	H	H	PH	PL
H	H	PH	PL				

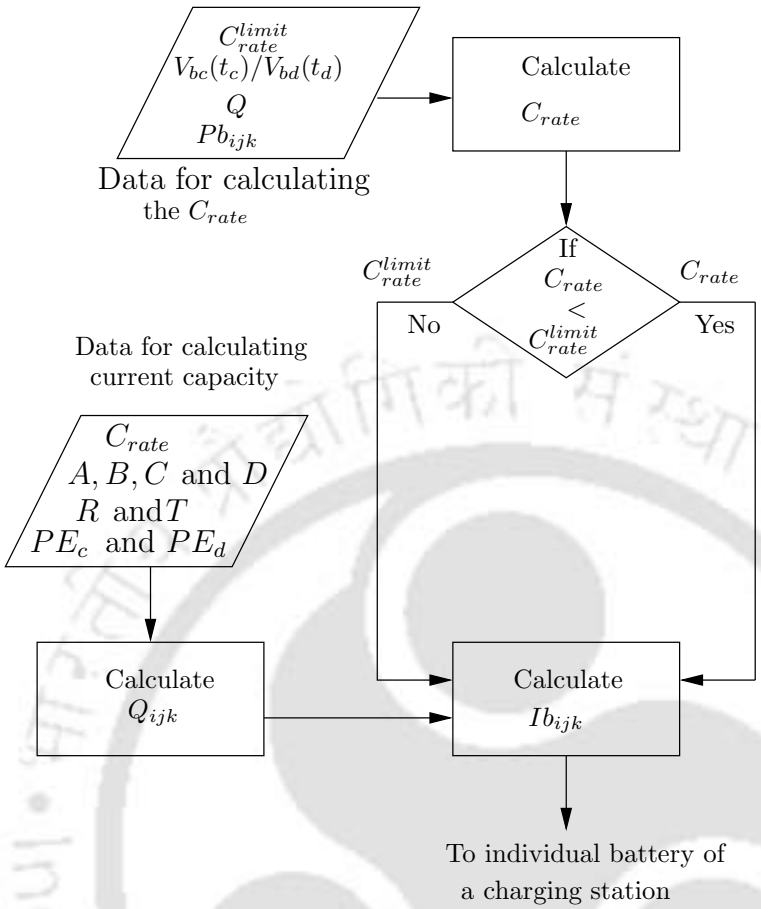

Figure 5.8: Flow chart for controlling the flow of power in individual battery.

5.5 Development of scenarios

Each of the six CSs considered for this V2G model consist of 200 EVs and all these EVs are divided into five types based on different battery specification as mentioned in Table 5.5. The driving of EVs may be inter-node but in this work it is assumed that during peak and off-peak hours each CS has 200 EVs. Since, the main focus of this work is to show the coordination of the EVs at the substation level, the driving pattern is not discussed. However, this model can work on any number of EVs present at the CS. Simulations are carried for off-peak hours and peak hours. Off-peak hours in this study are assumed to be between 2200 hrs to 0800 hrs of 10 hrs. Peak hours in this region is generally for 5 hours from 1700 hrs to 2200 hrs and hence the second study is carried for 5 hrs [43].

Each EV will have different battery conditions. But for ease of representation, all the EVs

are divided in to five categories and they are given in Table 5.5. Division of the batteries are based upon the Energy (kWh), SOC initial (SOC at which the EVs arrive at the CS), SOC limit (maximum allowable discharging limit as fixed by the vehicle's owner), Q (Ah), C_{rate} limit.

Table 5.5: Specifications of the EV's battery

Type of battery	Energy (KWH)	SOC initial (%)	SOC limit (%)	Q (Ah)	C_{rate}^{limit}
A	8	70	25	32	3
B	10	40	45	40	2.5
C	16	50	30	64	3
D	20	85	40	80	4
E	24	30	20	96	4

5.6 Results and discussion

In this section, two case studies have been carried out.

- In the first case, V2G behavior during off-peak hours is considered. During off-peak hours, the load demand is very low and therefore, the EVs will charge their batteries.
- In the second case, V2G behavior during peak hour is considered where the grid is heavily loaded and the EVs will discharge their excess energy to the grid.

The simulation results are shown for 10 hours during off-peak hours and 5 hours during peak hours. For both the cases, 200 EVs are assumed to be present at each CS and therefore the required energy for charging is same. The power factor of the entire system is assumed to be unity. The main focus of this work is to coordinate the EVs present at the CSs to achieve the grid support in terms of peak shaving, valley filling and flattening of voltage profile. Apart from these analyses, batteries capacity loss is considered for the aforementioned period (10 hrs. in off-peak hours and 5 hrs. in peak hours).

5.6.1 CASE I: Off-Peak hours (2200 hrs to 0800 hrs)

Due to light loading in this duration, the voltage of the node is generally very high (> 1 p.u.) and therefore, the DS has surplus power. This power can be utilized for charging the EVs present at the CSs. For validating our model, load of one node of the subfeeder 3 (**3.2**) has been increased by 60%. This is done to decrease the node voltage of one node during off-peak hours and to validate the proposed model in any scenario. Due to low voltage at node 3.2, **CSC** of this node will never allow the EVs batteries to charge. Instead, the EVs will discharge to the grid. Therefore, the energy of the CS connected to this node will not be included in the net energy (E^{net}_{avail}) which is the input to the **DSC** and the energy at the subfeeder as given in Eq. (5.12). Now, the distribution of power among the CSs will depend upon the surplus power, i.e. $P_{surplus}$ and this power will depend upon the $P^{grid}_{surplus}$ as defined in Eq. (5.10). Accordingly, for this case, $P^{grid}_{surplus}$ is assumed to be + 1.2 MW for 10 hrs. Based on these two inputs and the net energy available (7240 kWh of 5CSs), DSC decides the power to be compensated (P_{grid}) as 1.1 MW.

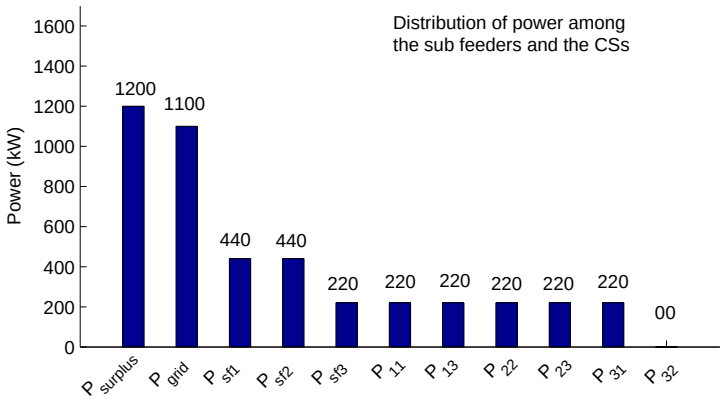

Figure 5.9: Distribution of $P^{grid}_{surplus}$ among the subfeeders and the CSs during off-peak hours.

It is observed from Figure 5.9, that the DS aggregator has divided the power among the subfeeders (P_{sf1}, P_{sf2} and P_{sf3}) to be 440 kW, 440 kW and 220 kW respectively. The last subfeeder power is less as compared to other subfeeder power because CS_{32} will not participate

in charging due to low node voltage. On the basis of subfeeder power, the subfeeder aggregator divides the power (P_{sf1}, P_{sf2} and P_{sf3}) among the CSs. Each CS has 220 kW of power distribution (P_{11}, P_{13}, P_{22}, P_{23} and P_{31}) except P_{32} whose power is zero. Since, the number of EVs are same in all the CSs, the energy requirement is similar and hence the power division is equal except for the CS_{32}.

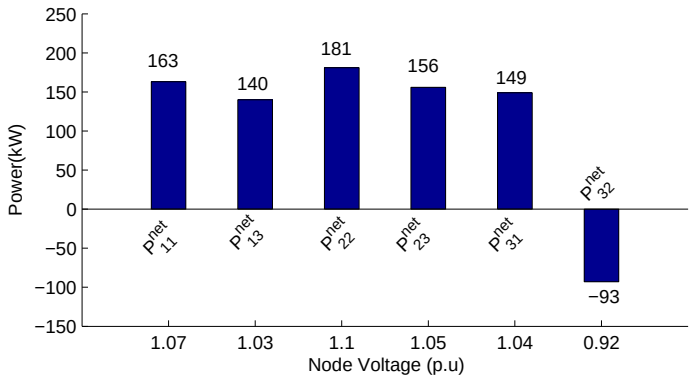

Figure 5.10: Net power flows between the CS and the grid as decided by the **CSC** during off-peak hours.

Now, based on the distribution of power among the CSs by the subfeeder aggregator, **CSC** will decide the net power flow between the CS and the node. The power distribution among the CSs as decided by the subfeeder aggregator may be different as compared to the decision by the **CSC**. The amount and direction of the net power flow between the CS and the grid is shown in Figure 5.10. It is observed from the figure that due to low voltage at node **3.2**, the CS FLC decides to inject the power to the grid which in turn increases the surplus power at the DS as given by Eq. (13).

C_{rate} of the batteries are shown in Figure 5.11. It is observed that C_{rate} of the batteries changes to maintain the magnitude of the power flow between the battery and the grid. The processed energy of each battery are mentioned for 10 hours of duration during off-peak hours and are shown in Figure 5.12.

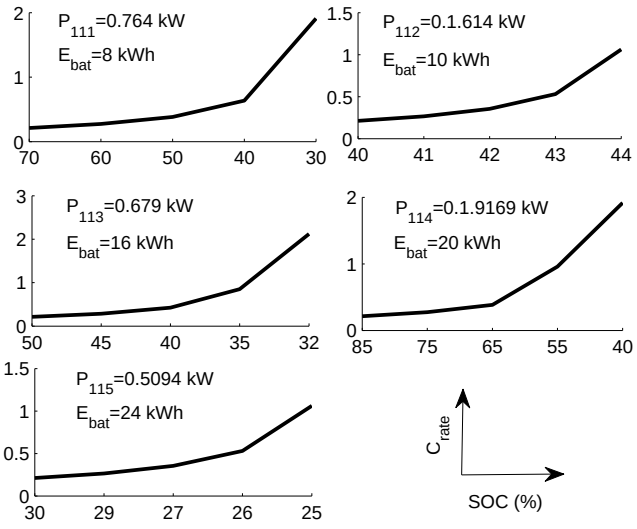

Figure 5.11: C_{rate} of the batteries at the CS_{11} based on the SOC (%) of the battery.

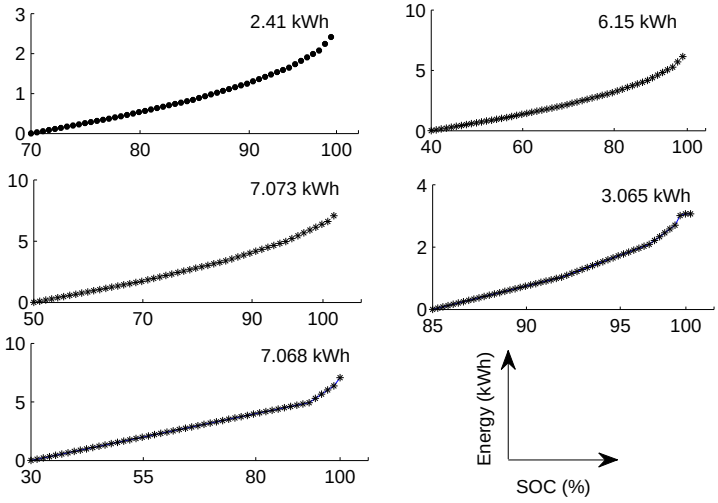

Figure 5.12: Processed Energy in kWh during off-peak hours (charging) of CS_{11} batteries.

5.6.2 CASE II: Peak hours (1700 hrs-2200 hrs)

During peak hours, grid is heavily loaded and hence there is a deficiency of power at the DS. The deficiency of power can be easily met through the excess energy of the batteries present at the CS. To validate the model, similar to case I, one of the node's (**2.3**) load has been reduced by 30%, so that during peak hours this node has high voltage and remaining other nodes have

low voltage. Accordingly, CS_{23} energy will not be included in the net available energy which is one of the inputs of DS FLC. For this case, power requirement by the grid ($P^{grid}_{surplus}$) is assumed to be -1500 kW. Now on the basis of Eq. (5.10), $P_{surplus}$ can be calculated which is one of the inputs of the **DSC**. The subfeeders and CSs power distribution are shown in Figure 5.13. On the basis of net energy availability of 3540 kWh (only 5 CS) and the $D_{gridsprt}$ for 5 hrs, **DSC** decides P_{grid} to be -1200 kW. Now the P_{grid} is to be divided among the subfeeder. It is observed from the figure that CS_{23} has the zero power allotment (P_{23} is equal to zero). This is because, during peak hours, this node is lightly loaded and therefore the node voltage is very high. Due to high node voltage, CS_{23} FLC has decided to charge the EVs batteries instead of discharging. Also mentioned in Eq. 5.13 and Eq. 5.14, there will be no power allotment to the CS_{23}. Net power as decided by the **CSC** during peak hours is shown in Figure 5.14. In this figure, it is observed that the net power of node **2.3** is positive due to high node voltage and the FLC has decided to charge the EVs and all other CSs have negative power which means they are discharging their excess energy to the grid. C_{rate} of the batteries during peak hours

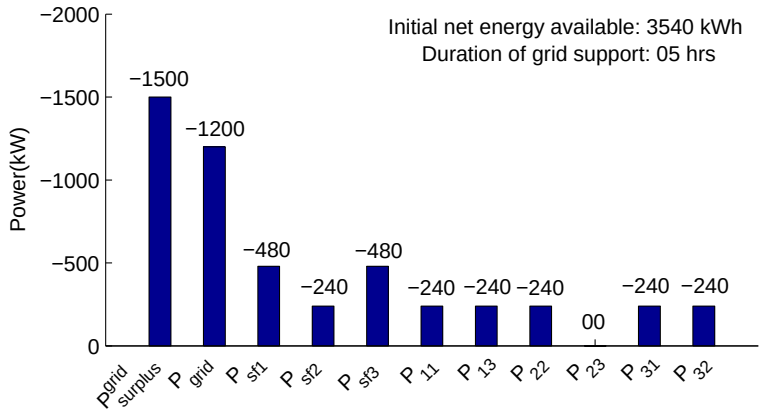

Figure 5.13: Distribution of $P^{grid}_{surplus}$ among the subfeeders and the CSs during peak hours.

is shown in Figure 5.15. It is found that even in peak hours, the battery of 10 kWh charges first to reach its SOC limit. In this figure, the C_{rate} of the 5 different types of battery at CS_{11} is shown. Similar results can be shown for other CSs. The processed energy in the case of

peak hours is shown in Figure 5.16. Node voltage with and without V2G implementation at different nodes (including the neighboring nodes) are given in Table 5.6.

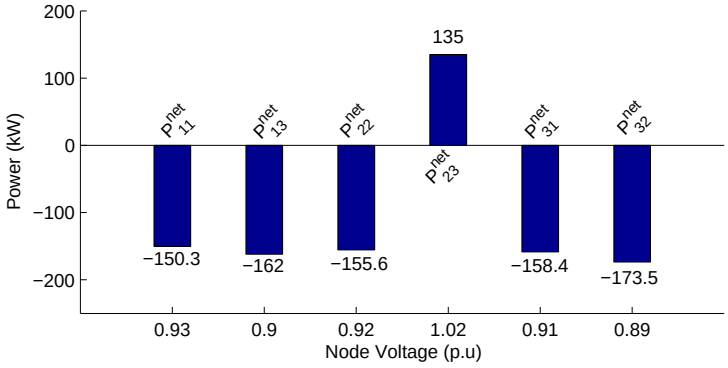

Figure 5.14: Net power which flows between the CS and the grid as decided by the CS FLC during peak hours..

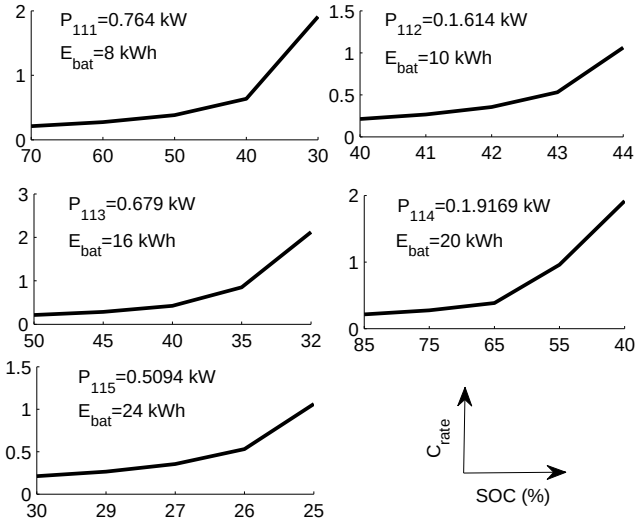

Figure 5.15: C_{rate} of the batteries at the CS_{11} at different SOC (%) of the battery.

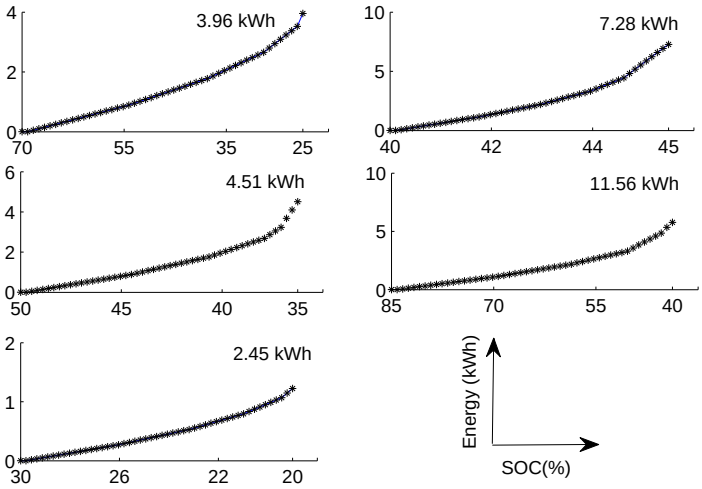

Figure 5.16: Processed energy in kWh during peak hours (discharging) of CS_{11} batteries.

Table 5.6: Node voltage with/without V2G

Node	Case I		Case II	
	Without V2G	With V2G	Without V2G	With V2G
1.1	1.07	1.01	0.93	0.97
1.2	1.07	1.04	0.94	0.96
1.3	1.03	1.02	0.90	0.98
2.1	1.04	1.01	0.95	0.97
2.2	1.1	1.02	0.92	0.98
2.3	1.05	0.99	1.02	0.97
3.1	1.04	1.00	0.91	0.96
3.2	0.92	0.99	0.89	0.97
4.1	1.07	1.05	0.94	0.97
4.2	1.08	1.06	0.95	0.97
4.3	1.04	1.03	0.93	0.95

5.7 Summary

In this chapter, EVs coordination with the DS is modeled. Six CSs are modeled and connected to different nodes of a radial subfeeder of a DS. A typical DS system of Guwahati city is modeled to validate the proposed multi node CS. Two FLCs have been designed; first one at the DS level and second one at the CS level, along with the aggregators. The controllers

decide the power flow between the EVs and the grid and the aggregators distributes the power among the subfeeders, CSs and EVs. A battery model, which is capable of calculating the capacity loss at different C_{rate}, is incorporated. Through this work, it is validated that the proposed model for V2G operation can be used for valley filling, peak shaving and flattening of load profile while updating the battery capacity loss.

In the next chapter, conclusions and possible future works are presented.

6

Summary and Conclusions

Contents

6.1 Summary of the present Work

The objective of the work presented in this thesis is to explore the different Fuzzy Logic Controller (FLC) based Vehicle to Grid (V2G) architecture. The proposed V2G architecture helps to mitigate the voltage imbalance as well as is found suitable for supporting the grid in terms of peak shaving and valley filling.

For V2G architecture developed in chapter 2, aggregated Electric Vehicles (EVs) energy at a CS is controlled with the help of two FLCs. The First controller is at the distribution node level and second one is at the charging station level. Distribution node level controller named V2G controller controls the flow of energy between the charging station and the node. Charging station controller (CSC) decides about individual EVs participation for charging or discharging, based on SOC of the battery. Hence, CSC will give the information regarding the availability of total energy or energy required to charge EVs' batteries. Both the controllers do have the information of the node voltage. Similarly, based on grid condition, energy can be drawn to charge the EVs. Availability of energy will be based on number of EVs at the charging station, their battery rating and their present state of charge (SOC). Two scenarios, each for charging and discharging have been developed. It has been found that the proposed FLC based V2G architecture is capable of peak shaving and valley filling.

In Chapter 3, instead of control mechanism for the aggregated energy of EVs at the CS, individual control of each EV's battery is developed. Three CSs are separately modelled and connected to a single node and termed as Multi Charging Station (MCS). MCS has been modelled to achieve the continuous grid support throughout a day by considering the realistic scenario of EVs movement at the CSs. A dynamic load at a particular node is incorporated to validate the controller. It has been found that the proposed MCS can maintain the voltage profile of a node, even the loads are fluctuating at every instant of time. This is achieved by designing a suitable aggregators at the MCS level and CS level. Aggregator at the MCS level distributes the power among the CSs and the aggregator at the CS, distributes the power among the EVs batteries present at the CS. A single FLC used at the node level controls the

power flow between the MCS and the point of common coupling (PCC). Algorithms, developed for the battery, ensures that batteries are not charged/discharged beyond the owner's preferred C_{rate} limit. EVs' batteries which arrive below the SOC limit, charge first to reach the SOC limit even during peak hours. Also, the batteries will never discharge beyond the SOC limit set by the users. The intra-node driving scheme for the EVs has been developed to provide continuous support to the test node. Inter node driving has not been considered because the aim is to design an MCS which can stabilize the test node throughout a day. However, this scheme can be extended to multi node system with a single charging station at every node and in such case EVs may be considered for inter node driving.

It has been proved that the proposed FLC based CSs/MCS developed for the V2G can stabilize the grid and can be used to support the grid in terms of valley filling and peak shaving. In chapter 4, integration of renewable energy sources such as solar and wind in the existing model of the Guwahati city network has been implemented at the system level. The impact of the integration of renewable energy due to its intermittent nature on the distribution grid can be easily overcome by the FLC based V2G architecture developed in this work. It has been proved that during day time, excess energy of the solar can be stored in the EVs batteries and during peak hours the stored energy of the batteries can be given back to the grid. Also, wind speed is generally high during night time and during this duration, off-peak periods coincides and therefore, the node voltage will increase. Utilization of EVs' batteries for the storage of excess energy in this case will prove a vital for the grid support. This issue is handled in this part of the thesis by coordinating the renewable energy sources with the proposed V2G model.

In the last part of this thesis work, coordination among the CSs connected to different nodes of the distribution subfeeders is presented. Thus, a large pool of energy can be stored in the batteries and supplied back to the grid when the utility demands. Two levels of control have been used. The first controller is named as 'Distribution Substation Controller' (**DSC**) which decides the magnitude and direction of the power that should flow between the CSs and the grid. The direction of the power flow can be negative or positive. Negative power implies that the CSs have to support the grid by discharging the excess energy stored in the EVs' batteries,

whereas, positive power implies that CSs will charge the EVs batteries. The second FLC is termed as 'Charging Station Controller' (**CSC**). It decides the amount and direction of power flow between the individual CS and the node to which it is connected. Again, this power can be negative or positive depending on the power flow directions. The aggregator at the DS (DS aggregator) distributes the power among the subfeeder. The subfeeder aggregators allocate the power among the CSs of their respective subfeeder. Finally, the CS aggregator distributes the power among the EVs batteries present at the CS. Different algorithms have been proposed, which can handle the scenario such as some CSs are charging their batteries and at the same time remaining CSs are discharging their excess energy to the grid. Peak shaving and valley filling are the main achievements of the proposed V2G architecture presented in this chapter. The battery has been modelled to calculate the capacity loss and thus updates its energy at every instant of time.

In all the works presented in this thesis, it is found that the FLC based V2G architecture can be implemented in real time scenarios to achieve the valley filling and peak shaving along with maintaining the node voltage within specified limit.

6.2 Development of a complete system

In this thesis, Chapter 2 discusses about the aggregated EVs' energy at the CS and the control mechanism to control the power flow between the CS and the grid. This chapter lacks discussion about the coordination among different EVs present at the CS. However, the coordination among different EVs has been achieved at the CS in Chapter 3. In this chapter, coordination among different CSs connected to a single node is achieved. Moreover, the dynamic load model is implemented at the test node to validate the proposed controller.

In chapter 4, integration of renewable energy sources has been accomplished and the excess or shortage of renewable energy at the distribution node is balanced by coordinated EVs present at the CS. In this chapter, EVs store excess energy produced by the renewable energy sources and supply when there is a deficiency of power at the PCC. In chapter 5, multi node CSs has been modelled where CSs are connected to majority of the distribution nodes (11kV/440V) and

coordination among CSs is achieved. It is validated that CSs connected to different nodes of a substation can coordinate among themselves to achieve the desired peak shaving and valley filling to mitigate the voltage imbalance.

It has been observed that, each chapter of this thesis presented a real time coordination of the EVs at the CS either at single node or at a multi node to achieve the desired power flow between the CS and the grid. If, all the works of V2G presented in this thesis is combined together, the complete system can handle renewable energy sources at the distribution node as well as maintain the voltage profile of the grid throughout a day. The complete system is shown in Figure 6.1. In this figure, CS_{11}, CS_{12} and CS_{13} are the CS connected to node 1,2 and 3 of subfeeder 1 of the 33 kV substation. Subfeeder voltage level is 11kV/440 V. Two controllers haven been shown where first controller is the substation controller and the second one at the CS level. Three aggregators namely substation, subfeeder and CS, distribute the power among different subfeeder, CSs and EVs' batteries respectively.

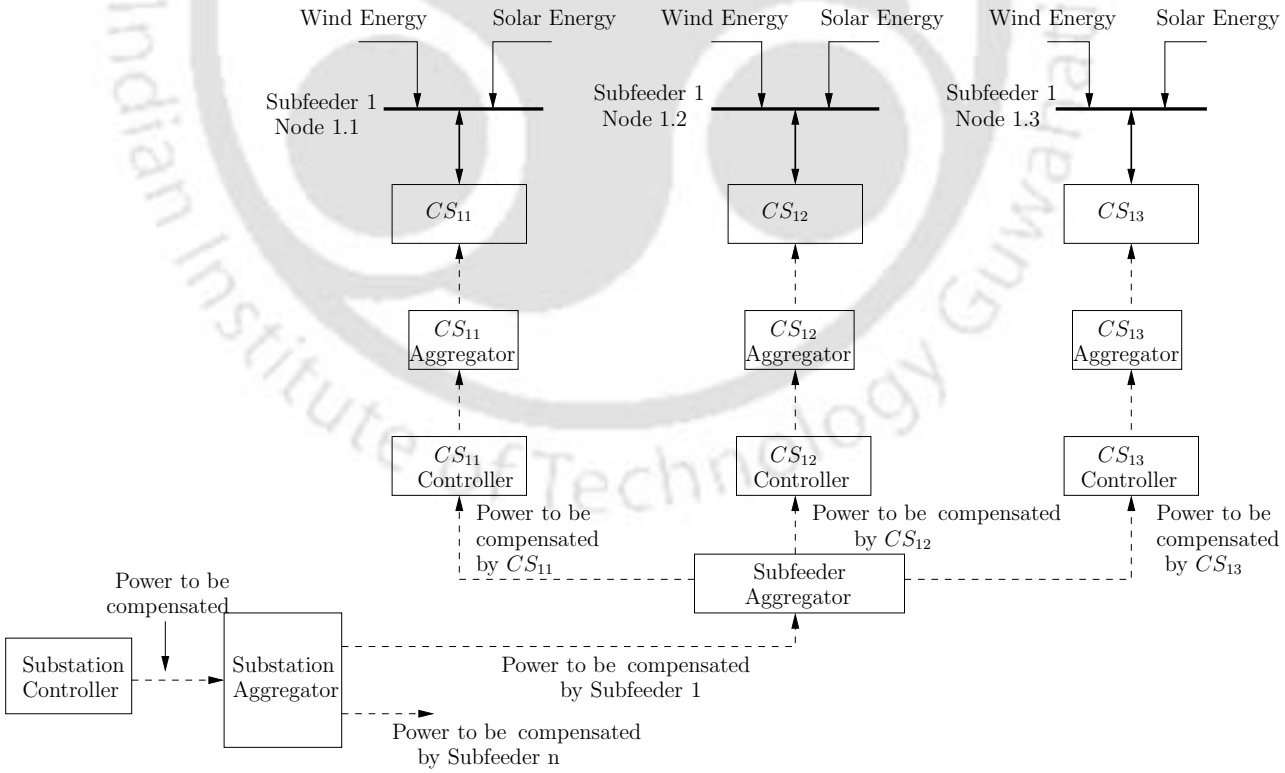

Figure 6.1: Complete V2G system along with the control architecture

6.3 Contributions of the present Work

The important contribution of the research work reported in this thesis is the development of different FLC based V2G architectures. These include,

(i) FLC based V2G architecture for aggregated EVs present at the CS.

(ii) FLC based V2G architecture by controlling the individual battery for the desired power flow between the grid and the battery.

(iii) Modelling of the MCS to achieve the continuous grid support.

(iv) Integration of renewable energy sources and its coordination with the proposed V2G system.

(v) Developing the multi-node CSs to realize the V2G system in real time scenario.

While developing these methods the other contributions of the thesis are as follows:

(i) Different aggregators are developed to distribute the power among the EVs and CSs.

(ii) A new control scheme of the battery has been developed which can change the C_{rate} of the battery on the basis of power requirement at the grid.

(iii) Batteries are not charged/discharged beyond the user's preferred C_{rate} limit.

(iv) Also, the batteries are not discharged beyond the SOC limit.

(v) Sudden arrival and departure of EVs at the CSs and their impacts on the grid have been studied.

6.4 Suggestions for future research

In this section we provide some suggestions for further research.

(i) The integration of the renewable energy sources can be implemented at multi node system along with multi node CSs. Thus the impact on the distribution substation can be studied.

(ii) The component level modelling can be developed for all the chapters discussed in this thesis. Moreover, the synchronization of the CSs with the grid will be one of the important issues which can be handled at the component level.

(iii) Proper battery model has to be included which can calculate the capacity fading at different C_{rate} and update the battery as per the catalogue of the battery.

(iv) The frequency regulation can be achieved with the V2G in real time situation. The proposed model can be validated by changing the algorithm for real time frequency regulation which is one of the burning topic of research in the area of V2G.

(v) The economic aspect of the frequency regulation in real time simulation can be analysed if the batteries with capacity fading is modelled.

(vi) The voltage management between the CSs of the MCS connected at single node can also be investigated. However, this can be achieved, if detailed modeling of the MCS is performed and the AC-DC converters are taken into account.

(vii) Issue of battery degradation which is very important for peak shaving and valley filling has to be investigated. In this thesis, importance of developing an algorithm for managing the EVs charging/discharging to support the grid has been discussed and all the issues related to real time implementation of the MCS at the system level have been handled. Battery degradation is a very important issue, since it depends upon capacity fading, loss of charge acceptance, elevated self-discharge and premature voltage cut-off. All these issues can be handled if more attention is paid to the detailed battery modelling.

A

Fuzzy Logic Controller

Contents

A.1 Introduction

This part of appendix explains a fuzzification and defuzzification process by taking an example of FLC designed in Chapter 2. However, similar way of explanation can be presented for different FLC used in other chapters.

A.2 Fuzzy Logic Controller

Fuzzy Logic (FL) is a many valued logic derived from fuzzy set theory which can deal with uncertainties in systems. Unlike "crisp logic", fuzzy logic variables may have a truth value that ranges in different degrees between 0 and 1. This is popularly known as membership grade. FL incorporates a simple, IF-THEN rule based approach to solve a control problem rather than attempting to mathematically model a system. FL does not require precise inputs and can process any reasonable number of inputs, but system complexity increases rapidly with more inputs and outputs. The first step in implementing FL is to decide exactly what is to be controlled and what are the input variables. Mamdani type FLC [51, 77], which uses linguistic variables to represent a fuzzy system's operating parameters, is used in this thesis and is explained hereby.

Each fuzzy set is defined by a particular membership function, which may be triangular, trapezoidal, exponential or Gaussian in shape depending on the kind of application. In order to facilitate computations, triangular membership functions are utilized in this thesis for both the input and output membership functions [78]. A fuzzy controller has fuzzy sets which are characterized by a membership function to map a parameter to a membership grade between the scaled intervals. To model the objectives and the constraints in fuzzy environment, the initial step is the fuzzification process, which is constructed over the fuzzy membership functions. Each fuzzy set can be defined by one particular membership function. Fuzzy sets representing the objectives and constraints may vary considerably. The triangular membership function is selected for representing fuzzy sets. Other most common shapes are Trapezoidal, Exponential and Gaussian which can also be used for representing the fuzzy sets depending on

the applications.

The Mamdani type inference (also known as the maxmin inference method), utilizes the minimum function for the implication of the rules. Defuzzification is performed using the center of gravity method. It performs defuzzification by finding the center of the area encompassed by all the rules, and is mathematically described by

$$u(t) = \frac{\sum_{i=1}^{n} u_i \mu_v(u_i)}{\sum_{i=1}^{n} \mu_v(u_i)} \tag{A.1}$$

where $u(t)$ refers to the defuzzified overall control output, while u_i refers to the output variable and μ_v represents the aggregated membership function [49, 79].

A.3 Fuzzification and Defuzzification

This part presents the fuzzification and defuzzification in the V2G controller for a practical example of chapter 2 and is shown in Figure A.1. The range of the voltage level is between 0.8 to 1.1 p.u. The range of the energy signal is between -1 which corresponds to maximum energy required during charging of EVs and 1 which corresponds to maximum energy available by the charging station for the grid support. Similarly, the range of output power is between -1 which corresponds to maximum power supplied to the grid and 1 which corresponds to maximum power drawn by the charging station.

The rule base which represents the control law has 50 rules for the V2G controller and is shown in Table A.1.

Let us suppose that the actual value of the energy available is 0.227 and the actual voltage is 0.95 p.u. The two rules that are given by the membership functions are as follows and are taken from Table A.1. This table is similar as discussed in Chapter 2, Section 2.4.

- Rule 1- If Voltage is Medium (M) and Energy is Very Positive Low (VPL), then Power is Negative Low (NL).

- Rule 2- If Voltage is Medium (M) and Energy is Positive Low (PL), then Power is Negative

Table A.1: Rules for V2G Controller

$E \backslash V \rightarrow$ $\downarrow$	VL	L	M	H	VH
VNH	VPL	PL	PM	VPM	PH
NH	VPL	PL	VPM	PH	VPH
NM	VPL	PL	PM	VPM	PH
NL	VPL	PL	PM	PH	VPH
VNL	VPL	PL	VNL	NL	NM
VPL	VNL	VNL	NL	PL	VPL
PL	VNL	NL	NM	NM	VNM
PM	NH	VNH	NM	NL	VNL
PH	VNH	NH	NM	NL	VNL
VPH	VNH	NH	VNM	NL	VNL

Medium (NM).

This rule base restricts the actual power output to the node based on energy availability and voltage at the node. If the energy is less and voltage is low, a very low power can be injected to the grid. The first step in this process is fuzzification. Energy value of 0.227 is a member of both membership function's representing Very Positive Low (VPL) and Positive Low (PL), yet the degree of membership is different. Energy value of 0.227 is considered to be 65% VPL and 35% PL. Voltage of 0.95 is a member of only one membership "Medium" and is considered to be 100% Medium.

The next step is the inference process. Each rule is checked for the degrees of membership for the participating inputs. Here, rule 1 says that if voltage is M (of which one is 100% certain) and Energy is VPL (of which one is 65% certain), the output power is NL. In order to determine the degree of certainty with which Power is a member of the NL, the minimum method is applied. That means the minimum of the degree of membership (μ) values of the inputs is going to be the μ values for the output. This is defined mathematically as

$$\mu_0(Power) = \min(\mu_0(Voltage), \mu_0(Energy)) \tag{A.2}$$

where $\mu_0(Power)$, $\mu_0(Voltage)$ and $\mu_0(Energy)$ are membership functions of power, voltage and energy respectively. Using Eq. (A.2), the values for the output can be found as given below.

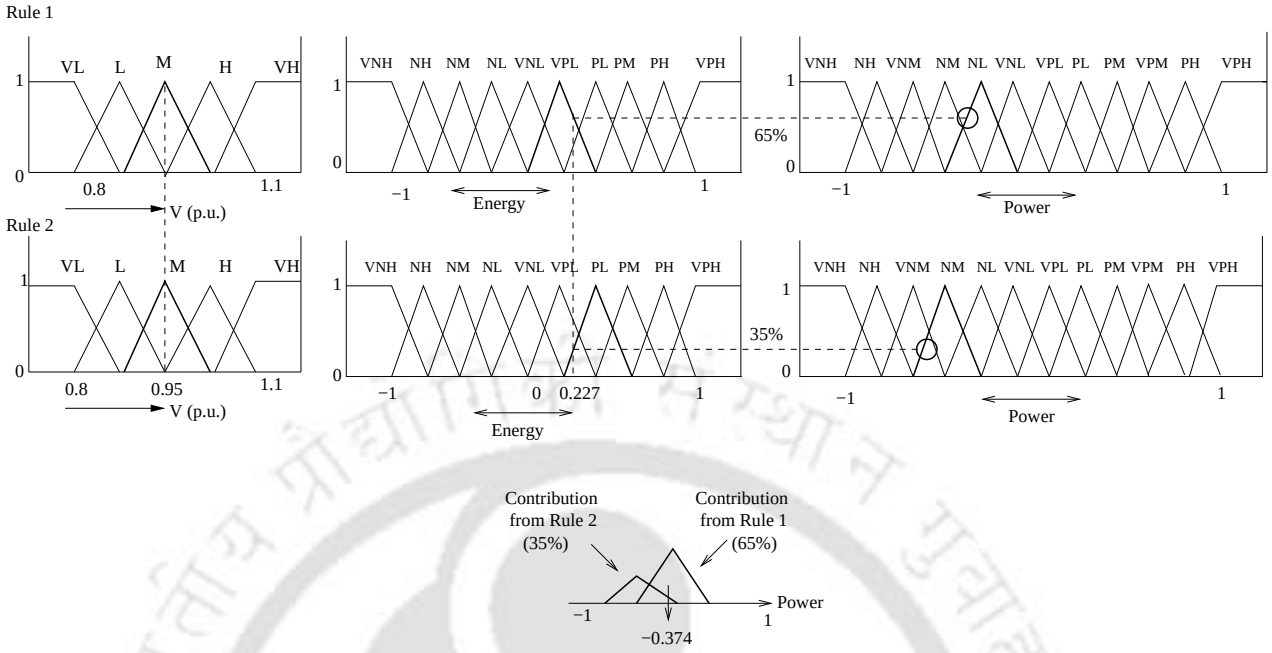

Figure A.1: Fuzzification, inference and defuzzification procedures for the presented example.

- Rule 1 min(1, 0.65) is 0.65
- Rule 2 min(1, 0.35) is 0.35

This implies that for rule 1, there is 65% certainty that the output will be part of the NL and for rule 2 there is a 35% certainty that the output will be a part of the NM. Once the certainty for each promise or rule has been determined, the consequent for each rule can be found. It is found by taking the membership function of the premise (Power is NL) and multiplying the certainty to quantify the "then" operation. This is called the product function [80]. This results in two triangles at the bottom of Figure A.1. Note that the consequent triangle on the left has same x value as its corresponding Power (NM). The only difference is that its height has been reduced to 0.35. The larger triangle on the right has the same values as its corresponding Power (NL), but its height has been reduced to 0.65.

Now based on Eq. (A.1), defined in Section A.2, the crisp value of the output power can be calculated from the two output triangles of Figure A.1. In this case the output power is -0.374. This implies that to make node voltage near 1 p.u. the controller has sensed the energy from the charging station and based on this, it has directed the flow of power to the node. Here

negative power indicates that the charging station has supplied its energy to the grid.

B

EV's battery

Contents

B.1 EV's battery

A simple electric equivalent circuit (EEC) of Li-ion battery is shown in Figure. B.1. The EEC model has three parameters: an open circuit voltage (V_0), an internal resistance having two parameters R_1 and R_2 and the effective capacitance (C). This model is used to extract the circuit parameters for different charge/discharge rate. The mathematical representations for R_1, R_2, C and V_0 under constant current charging conditions are given in [72]. The battery parameters are represented as polynomial equations as a function of (C_{rate}) and SOC/DOD(depth of discharge) [73]. Under the constant current, the battery terminal voltage for charging scenario with respect to time is given as below.

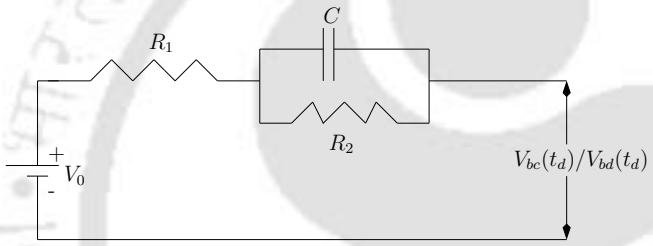

Figure B.1: Electric equivalent circuit (EEC) for Li-ion battery.

$$V_{bc}(t_c) = \left(\left(\frac{Q}{C} + I_c \times R_2\right) \times \exp\left(-\frac{t_c}{R_2 \times C}\right)\right) + V_0 - (I_c \times (R_1 + R_2)) \tag{B.1}$$

where Q is capacity of the battery, I_c is charging current, t_c is charging time and $V_{bc}(t_c)$ is battery charging voltage with respect to time. Similarly, the battery terminal voltage for discharging scenario is given below.

$$V_{bd}(t_d) = \left(\left(\frac{Q}{C} + I_d \times R_2\right) \times \exp\left(-\frac{t_d}{R_2 \times C}\right)\right) + V_0 - (I_d \times (R_1 + R_2)) \tag{B.2}$$

where I_d is discharging current, t_d is discharging time and $V_{bd}(t_d)$ is battery discharging voltage with respect to time. Fig. B.2 represents the block diagram of the battery with capacity model. It calculates total processed energy, available energy for charging/discharging and capacity losses. The processed energy for charging scenario (PE_c) and discharging scenario (PE_d) are given below.

$$PE_c = \sum_{n=1}^{z} V_{bc}(t_c) \times I_c \times (t_n - t_{n-1}) \tag{B.3}$$

$$PE_d = \sum_{m=1}^{z} V_{bd}(t_d) \times I_d \times (t_m - t_{m-1}) \tag{B.4}$$

where, t_n and t_m are the simulation time for the charging and discharging respectively. The required energy for charging scenario and the available energy for discharging scenario under constant current condition is given by Eq. (B.5) and Eq. (B.6) and these equations are used to find the required energy for charging(AE_c) and the available energy for discharging(AE_d) and this is explained in Chapter 5, Section 5.4.

$$AE_c = V_{bc}(t_c)Q(SOC_{fc} - SOC_{cr}) \tag{B.5}$$

$$AE_d = V_{bd}(t_d)Q(SOC_{cr} - SOC_{fd}) \tag{B.6}$$

where SOC_{fc}, SOC_{cr} and SOC_{fd} are the final SOC (100%) for charging, current SOC of the battery and SOC limit for discharging respectively.

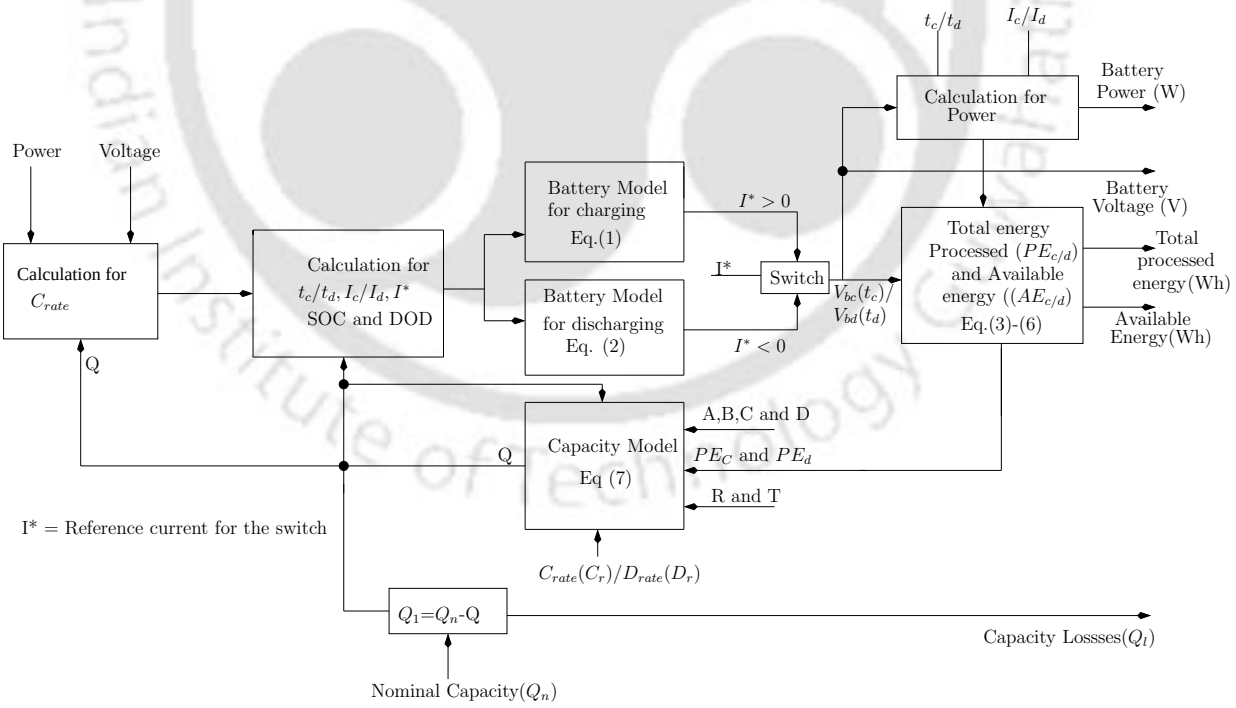

Figure B.2: Detailed modeling of battery with processed energy and capacity loss model.

The battery capacity represents the maximum amount of energy that can be extracted from the battery under certain specified conditions such as C_{rate}, SOC and temperature [74].

The capacity loss of Li-Ion batteries can be related to the unwanted side reactions that occur during the overcharge and high charge/discharge conditions, which reduces the battery's lifetime time [75, 76]. Thus, capacity loss is directly proportional to the C_{rate} of the battery.

The mathematical model for capacity loss is developed based on the Arrhenius equation [75]. This equation is used for calculating capacity loss under fixed C_{rate}. The mathematical modeling techniques are comparatively simple and are sufficient to calculate battery capacity loss at different C_{rate}. The mathematical model for capacity loss (Q_l) at different C_{rate} is given below.

$$Q_l = \left(A \times \exp\left(-\frac{C \times PE_c \times Q \times C_r}{R \times T}\right)\right) + \left(B \times \exp\left(-\frac{D \times PE_d \times Q \times D_r}{R \times T}\right)\right) \tag{B.7}$$

where, A and B are pre-exponential factors, C and D are adjustable factors, PE_c and PE_d is similar as defined in Eq. (B.3) and Eq. (B.4). C_r and D_r is charging and discharging rate(C_{rate}), Q is the current capacity of the battery (Ah), R is gas constant (J/mol K) and T is temperature (K). The advantage of this model is that it is capable of determining the capacity loss of the battery when it is subjected to different C_{rate}. The detailed block diagram of the battery model based on the capacity loss is shown in Figure. B.2. Q which is the current capacity (Ah) of the battery is evaluated at every instant of time and it is given in Eq. (B.8). The energy of the battery is updated based on the processed energy and at different C_{rate}.

$$Q = Q_n - Q_l \tag{B.8}$$

C

Charging/discharging rate (C_{rate})

Contents

C.1 Charging/discharging rate

In this appendix, variation of C_{rate} with the change in SOC during charging/discharging has been shown. The example of Chapter 3 is taken for the analysis.

Charging and discharging of an EV's battery can be controlled by changing the C_{rate}. The required C_{rate} of the individual batteries can be calculated as follows.

$$C_{rate} = \frac{Pb_{ij}}{V_j Ahr_j} \tag{C.1}$$

where, Pb_{ij} is the power required/available to charge/discharge the j^{th} battery of i^{th} CS. V_j and Ahr_j are the voltage and current Ampere Hour (AHR) of the j^{th} battery of i^{th} CS.

Current Ampere Hour is calculated as:

$$Ahr_j = Ahr_{rating}(SOC_{rem}/100) \tag{C.2}$$

where, Ahr_{rating} is the rated AHR of the battery. In the case of discharging, SOC_{rem} is the difference of the current SOC (SOC_{cr}) and SOC limit (SOC_{lt}) and it is calculated as below.

$$SOC_{rem} = SOC_{cr} - SOC_{lt} \tag{C.3}$$

In the case of charging, SOC_{rem} is calculated as below.

$$SOC_{rem} = 100 - SOC_{cr} \tag{C.4}$$

Using Eq. (C.1) and Eq. (C.2), the current of the battery is calculated based on the required C_{rate} and Ahr_j of the battery and is given below.

$$Ahr_{bj} = Ahr_j C_{rate} \tag{C.5}$$

where, Ahr_{bj} is the current which flows between the battery and the grid. Ahr_{bj} is positive, if power is flowing to the battery during charging and negative if power is flowing to the grid from the battery during discharging.

For example, if AHR_{rating}, V_{bat}, SOC_{cr} and SOC_{lt} of a battery (1^{st} battery of CS_1) is 32

AHR, 250 V, 90 and 25 respectively then SOC_{rem} can be found from Eq. (C.3) to be 65 and Ahr_j can be found from Eq. (C.2) to be 20.8 AHR. If Pb_{11}= 1.16 kW, which is the power required for discharging to the grid by the EV's battery as decided by Eq. (3.12) during peak hours, C_{rate} at 90% of SOC can be calculated using Eq. (C.1) as 0.223. Similarly C_{rate} at 60% and 30% of SOC can be 0.414 and 2.90 respectively. Based on this example, Table C.1 shows the C_{rate} at different SOC of all the batteries considered in Chapter 3.

C.2 C_{rate} calculation

This part presents the C_{rate} of the individual battery of each CS and for three different time slots described in Chapter 3. Distribution of battery power and number of EVs are mentioned in Table C.1. C_{rate} mentioned in the table is calculated for three different SOC. For example C_{70}: 0.112, C_{80}: 0.17, C_{95}: 0.69 are the C_{rate} of the battery at 70%, 80% and 90% of SOC respectively at CS_1 during off-peak hours (0900 hrs-1700 hrs). The number given in the bracket (Table C.1) shows the number of EVs. It is observed that during each time slot, different CS (CS_1, CS_2 and CS_3) may have similar C_{rate}. It means that power flow is divided equally among the similar batteries. The types of batteries are represented by A,B,C,D and E which are same as mentioned in Table 3.4.

Table C.1: C_{rate} of the batteries during three time slots and the power drawn or supplied by each battery

A,B,C,D and E are the type of batteries which travel from the CSs and A',B',C',D' and E' have arrived from the Transit

A/A'= 8kWh, B/B'=10kWh, C/C'=16 kWh, D/D'=20 kWh and E/E'=24 kWh

[**Pb** means Power flow in kW between the battery and the grid]

	0900 hrs-1700 hrs			1700 hrs-2200 hrs			2200 hrs-0900 hrs		
	CS_1 (10)	CS_2 (40)	CS_3 (100)	CS_1 (40)	CS_2 (90)	CS_3 (20)	CS_1 (130)	CS_2 (10)	CS_3(10)
A	C_{70}: 0.116 C_{80}: 0.174 C_{95}: 0.69 Pb: 0.279 (2)	C_{70}: 0.116 C_{80}: 0.174 C_{95}: 0.69 Pb: 0.279 (8)	C_{70}: 0.116 C_{80}: 0.174 C_{95}: 0.69 Pb: 0.279 (20)	C_{90}: 0.223 C_{60}: 0.414 C_{30}: 2.90 Pb: 1.160 (4)	C_{90}: 0.223 C_{60}: 0.414 C_{30}: 2.90 Pb: 1.160 (12)	C_{90}: 0.223 C_{60}: 0.414 C_{30}: 2.90 Pb: 1.160 (4)	C_{15}: 0.095 C_{55}: 0.180 C_{95}: 1.620 Pb: 0.648 (18)	C_{15}: 0.095 C_{55}: 0.180 C_{95}: 1.620 Pb: 0.648 (2)	C_{15}: 0.095 C_{55}: 0.180 C_{95}: 1.620 Pb: 0.648 (2)
A'	(0)	(0)	(0)	C_{70}: 0.22 C_{50}: 0.4 C_{30}: 2.00 Pb: 0.801 (4)	C_{70}: 0.22 C_{50}: 0.4 C_{30}: 2.00 Pb: 0.801 (6)	(0)	C_{70}: 0.095 C_{80}: 0.142 C_{95}: 0.57 Pb: 0.228 (8)	(0)	(0)
B	C_{40}: 0.116 C_{70}: 0.23 C_{95}: 1.396 Pb: 0.698 (2)	C_{40}: 0.116 C_{70}: 0.23 C_{95}: 1.396 Pb: 0.698 (8)	C_{40}: 0.116 C_{70}: 0.23 C_{95}: 1.396 Pb: 0.698 (20)	C_{90}: 0.224 C_{70}: 0.404 C_{50}: 2.02 Pb: 1.010 (4)	C_{90}: 0.224 C_{70}: 0.404 C_{50}: 2.02 Pb: 1.010 (12)	C_{90}: 0.224 C_{70}: 0.404 C_{50}: 2.02 Pb: 1.010 (4)	C_{35}: 0.095 C_{65}: 0.177 C_{95}: 0.238 Pb: 0.619 (18)	C_{35}: 0.095 C_{65}: 0.177 C_{95}: 0.238 Pb: 0.619 (2)	C_{35}: 0.095 C_{65}: 0.177 C_{95}: 0.238 Pb: 0.619 (2)
B'	(0)	(0)	(0)	C_{40}: 0.220 C_{42}: 0.36 C_{44}: 1.10 Pb: 0.110 (4)	C_{40}: 0.220 C_{42}: 0.36 C_{44}: 1.10 Pb: 0.110 (6)	(0)	C_{40}: 0.095 C_{80}: 0.191 C_{95}: 1.144 Pb: 0.572 (8)	(0)	(0)
C	C_{50}: 0.116 C_{75}: 0.23 C_{95}: 1.16 Pb: 0.930 (2)	C_{50}: 0.116 C_{75}: 0.23 C_{95}: 1.16 Pb: 0.930 (8)	C_{50}: 0.116 C_{75}: 0.23 C_{95}: 1.16 Pb: 0.930 (20)	C_{90}: 0.223 C_{65}: 0.384 C_{35}: 2.69 Pb: 2.150 (4)	C_{90}: 0.223 C_{65}: 0.384 C_{35}: 2.69 Pb: 2.150 (12)	C_{90}: 0.223 C_{65}: 0.384 C_{35}: 2.69 Pb: 2.150 (4)	C_{20}: 0.095 C_{55}: 0.169 C_{95}: 1.525 Pb: 1.220 (18)	C_{20}: 0.095 C_{55}: 0.169 C_{95}: 1.525 Pb: 1.220 (2)	C_{20}: 0.095 C_{55}: 0.169 C_{95}: 1.525 Pb: 1.220 (2)
C'	(0)	(0)	(0)	C_{50}: 0.225 C_{40}: 0.45 C_{35}: 0.90 Pb: 0.720 (4)	C_{50}: 0.225 C_{40}: 0.45 C_{35}: 0.90 Pb: 0.720 (6)	(0)	C_{50}: 0.095 C_{75}: 0.191 C_{95}: 0.954 Pb: 0.763 (8)	(0)	(0)
D	C_{85}: 0.116 C_{90}: 0.174 C_{95}: 0.349 Pb: 0.349 (2)	C_{85}: 0.116 C_{90}: 0.174 C_{95}: 0.349 Pb: 0.349 (8)	C_{85}: 0.116 C_{90}: 0.174 C_{95}: 0.349 Pb: 0.349 (20)	C_{90}: 0.22 C_{70}: 0.367 C_{45}: 2.20 Pb: 2.20 (4)	C_{90}: 0.22 C_{70}: 0.367 C_{45}: 2.20 Pb: 2.20 (12)	C_{90}: 0.22 C_{70}: 0.367 C_{45}: 2.20 Pb: 2.20 (4)	C_{30}: 0.096 C_{65}: 0.191 C_{95}: 1.34 Pb: 1.340 (18)	C_{30}: 0.096 C_{65}: 0.191 C_{95}: 1.34 Pb: 1.340 (2)	C_{30}: 0.096 C_{65}: 0.191 C_{95}: 1.34 Pb: 1.340 (2)
D'	(0)	(0)	(0)	C_{85}: 0.223 C_{70}: 0.335 C_{45}: 2.01 Pb: 2.010 (4)	C_{85}: 0.223 C_{70}: 0.335 C_{45}: 2.01 Pb: 2.010 (6)	(0)	C_{70}: 0.047 C_{80}: 0.035 C_{95}: 0.026 Pb: 0.286 (8)	(0)	(0)
E	C_{30}: 0.116 C_{60}: 0.203 C_{95}: 1.63 Pb: 1.956 (2)	C_{30}: 0.116 C_{60}: 0.203 C_{95}: 1.63 Pb: 1.956 (8)	C_{30}: 0.116 C_{60}: 0.203 C_{95}: 1.63 Pb: 1.956 (20)	C_{90}: 0.224 C_{60}: 0.392 C_{25}: 3.13 Pb: 3.760 (4)	C_{90}: 0.224 C_{60}: 0.392 C_{25}: 3.13 Pb: 3.760 (12)	C_{90}: 0.224 C_{60}: 0.392 C_{25}: 3.13 Pb: 3.760 (4)	C_{10}: 0.095 C_{50}: 0.172 C_{95}: 1.717 Pb: 2.060 (18)	C_{10}: 0.095 C_{50}: 0.172 C_{95}: 1.717 Pb: 2.060 (2)	C_{10}: 0.095 C_{50}: 0.172 C_{95}: 1.717 Pb: 2.060 (2)
E'	(0)	(0)	(0)	C_{30}: 0.225 C_{25}: 0.45 C_{21}: 2.25 Pb: 0.540 (4)	C_{30}: 0.225 C_{25}: 0.45 C_{21}: 2.25 Pb: 0.540 (6)	(0)	C_{30}: 0.095 C_{60}: 0.167 C_{95}: 1.33 Pb: 1.602 (8)	(0)	(0)

Bibliography

[1] V. Wouk, "The second century of electric and hybrid vehicles," in *34th IEEE Vehicular Technology Conference*, vol. 34, pp. 183 – 190, May, 1984.

[2] G. Maggetto and J. Van Mierlo, "Electric and electric hybrid vehicle technology: a survey," in *IEE Seminar on Electric, Hybrid and Fuel Cell Vehicles (Ref. No. 2000/050)*, 2000.

[3] R. H. Schallenberg, "Prospects for the electric vehicle: A historical perspective," *IEEE Transactions on Education*, vol. 23, no. 3, pp. 137 –143, Aug. 1980.

[4] Load Generation Balance Report, 2010, http://cea.nic.in/god/gmd/lgbr_report.pdf, Central Electricity Authority.

[5] J. Tomic and W. Kempton, "Using fleets of electric-drive vehicles for grid support," *Journal of Power Sources*, vol. 168, pp. 459–468, 2007.

[6] W. Kempton and J. Tomic, "Vehicle-to-grid power implementation: From stabilizing the grid to supporting large-scale renewable energy," *Journal of Power Sources*, vol. J144, pp. 280–294, 2005.

[7] L. Sann, "Driving the solution, the plug-in hybrid vehicle," *EPRI journal*, pp. 8–17, 2005.

[8] R. J. Bessa and M. A. Matos, "The role of an aggregator agent for EV in the electricity market," in *7th Mediterranean Conference and Exhibition on Power Generation, Transmission, Distribution and Energy Conversion (MedPower 2010)*, pp. 1 –9, Nov. 2010.

[9] C. C. Wu, W. J. Lee, C. L. Cheng, and H. W. Lan, "Role and value of pumped storage units in an ancillary services market for isolated power systems; simulation in the Taiwan power system," *IEEE Transactions on Industry Applications*, vol. 44, no. 6, pp. 1924 –1929, Nov. 2008.

[10] V. V. Thong, J. Driesen, and R. Belmans, "Using distributed generation to support and provide ancillary services for the power system," in *International Conference on Clean Electrical Power, 2007 (ICCEP '07)*, pp. 159 –163, May, 2007.

[11] M. Bolton Zammit, D. Hill, and R. Kaye, "Designing ancillary services markets for power system security," *IEEE Transactions on Power Systems*, vol. 15, no. 2, pp. 675 –680, May 2000.

[12] E. Sortomme and M. El-Sharkawi, "Optimal combined bidding of vehicle-to-grid ancillary services," *IEEE Transactions on Smart Grid*, vol. 3, no. 1, pp. 70 –79, March 2012.

[13] D. Giorgio, F. Liberati, and S. Canale, "Optimal electric vehicles to grid power control for active demand services in distribution grids," in *20th Mediterranean Conference on Control Automation (MED)*, pp. 1309 –1315, July, 2012.

[14] A. Brooks, "Integration of electric drive vehicles with the power grid-a new application for vehicle batteries," in *The Seventeenth Annual Battery Conference on Applications and Advances*, pp. 239, 2002.

[15] S. Brecker, P. Jacqmaer, K. D. Brabandere, J. Driesen, and R.Belmans, "Grid power quality improvements using grid-coupled hybrid electric vehicles," in *The 3rd IET International Conference on Power Electronics, Machines and Drives*, pp. 505–509, June, 2006.

[16] S. Han, S. Han, and K. Sezaki, "Development of an optimal vehicle-to-grid aggregator for frequency regulation," *IEEE Transactions on Smart Grid,*, vol. 1, no. 1, pp. 65–72, June 2010.

[17] J. Pillai and B. Bak-Jensen, "Vehicle-to-grid systems for frequency regulation in an islanded Danish distribution network," in *IEEE Vehicle Power and Propulsion Conference (VPPC)*, pp. 1 –6, Sept, 2010.

[18] E. Sortomme, M. A, and E. Sharkawi, "Optimal scheduling of vehicle-to-grid energy and ancillary services," *IEEE Transactions on Smart Grid*, pp. 351–359, March 2012.

[19] C. Wu, H. Mohsenian Rad, and J. Huang, "Vehicle-to-aggregator interaction game," *IEEE Transactions on Smart Grid*, vol. 3, no. 1, pp. 434 –442, March 2012.

[20] S. Han, S. Han, and K. Sezaki, "Estimation of achievable power capacity from plug-in electric vehicles for V2G frequency regulation: case studies for market participation," *IEEE Transactions on Smart Grid*, vol. 2, no. 4, pp. 632 –641, Dec. 2011.

[21] T. Masuta and A. Yokoyama, "Supplementary load frequency control by use of a number of both electric vehicles and heat pump water heaters," *IEEE Transactions on Smart Grid*, vol. 3, no. 3, pp. 1253 –1262, Sept. 2012.

[22] M. Galus, S. Koch, and G. Andersson, "Provision of load frequency control by PHEVs, controllable loads, and a cogeneration unit," *IEEE Transactions on Industrial Electronics*, vol. 58, no. 10, pp. 4568 –4582, Oct. 2011.

[23] W. Kempton, V. Udo, K. Huber, K. Komara, S. Letendre, S. Baker, D. Brunner and N. Pearre, "A test of vehicle- to - grid (V2G) for energy storage and frequency regulation in the PJM system," November 2008.

[24] K. Clement Nyns, E. Haesen, and J. Driesen, "The impact of charging plug-in hybrid electric vehicles on a residential distribution grid," *IEEE Transactions on Power Systems*, vol. 25, no. 1, pp. 371–380, February 2010.

[25] A. Masoum, S. Deilami, P. Moses, and A. Abu-Siada, "Impacts of battery charging rates of plug-in electric vehicle on smart grid distribution systems," pp. 1 –6, October 2010.

[26] J. Pillai and B. Bak-Jensen, "Integration of vehicle-to-grid in the western danish power system," vol. 2, no. 1, pp. 12 –19, January, 2011.

[27] Y. Ota, H. Taniguchi, T. Nakajima, K. M. Liyanage, J. Baba, and A. Yokoyama, "Autonomous distributed V2G (vehicle-to-grid) satisfying scheduled charging," *IEEE Transactions on Smart Grid*, vol. 3, no. 1, pp. 559 – 564, March 2012.

[28] Y. Ma, T. Houghton, A. Cruden, and D. Infield, "Modeling the benefits of vehicle-to-grid technology to a power system," *IEEE Transactions on Power Systems*, vol. 27, no. 2, pp. 1012 –1020, May 2012.

[29] K. Dyke, N. Schofield, and M. Barnes, "The impact of transport electrification on electrical networks," *IEEE Transactions on Industrial Electronics*, vol. 57, no. 12, pp. 3917 –3926, Dec. 2010.

[30] A. Masoum, S. Deilami, P. Moses, M. Masoum, and A. Abu-Siada, "Smart load management of plug-in electric vehicles in distribution and residential networks with charging stations for peak shaving and loss minimisation considering voltage regulation," *IET on Generation, Transmission Distribution*, vol. 5, no. 8, pp. 877 –888, August 2011.

[31] E. Sortomme, M. Hindi, S. MacPherson, and S. Venkata, "Co-ordinated charging of plug-in hybrid electric vehicles to minimize distribution system losses," *IEEE Transactions on Smart Grid*, vol. 2, no. 1, pp. 198 –205, March 2011.

[32] C. Guille and G. Gross, "A conceptual framework for the vehicle-to-grid (V2G) implementation," *Energy Policy*, pp. 4379–4390, 2009.

[33] W. Kempton and J. Tomic, "Vehicle-to-grid power fundamentals: calculating capacity and net revenue," *Journal of Power Sources*, vol. 13, no. 144, pp. 268–279, June 2005.

[34] Y. Ma, T. Houghton, A. Cruden and D. Infield, "Modeling the benefits of vehicle-to-grid technology to a power system," *IEEE Transactions on Power Systems*, vol. 27, no. 2, pp. 1012 –1020, May 2012.

[35] L. Pieltain, G. Romandn, and R. Cossent, "Assessment of the impact of plug-in electric vehicles on distribution networks," *IEEE Transactions on Power Systems*, vol. 26, no. 1, pp. 206 –213, Feb. 2011.

[36] D. Wu, D. Aliprantis, and L. Ying, "Load scheduling and dispatch for aggregators of plug-in electric vehicles," *IEEE Transactions on Smart Grid*, vol. 3, no. 1, pp. 368 –376, March 2012.

[37] Y. He, B. Venkatesh, and L. Guan, "Optimal scheduling for charging and discharging of electric vehicles," *IEEE Transactions on Smart Grid*, vol. 3, no. 3, pp. 1095 –1105, Sept. 2012.

[38] A. Al-Awami and E. Sortomme, "Coordinating vehicle-to-grid services with energy trading," *IEEE Transactions on Smart Grid*, vol. 3, no. 1, pp. 453 –462, March 2012.

[39] D. Dallinger, D. Krampe, and M. Wietschel, "Vehicle-to-grid regulation reserves based on a dynamic simulation of mobility behavior," *IEEE Transactions on Smart Grid*, vol. 2, no. 2, pp. 302 –313, June 2011.

[40] C. Quinn, D. Zimmerle, and T. Bradley, "An evaluation of state-of-charge limitations and actuation signal energy content on plug-in hybrid electric vehicle, vehicle-to-grid reliability, and economics," *IEEE Transactions on Smart Grid*, vol. 3, no. 1, pp. 483 –491, March 2012.

[41] W. Kempton, J. Tomic, S. Letendre, A. Brooks, and T. Lipman, "Vehicle- to-grid power: Battery, hybrid, and fuel cell vehicles as resources for distributed electric power in California, Davis, CA," in *Institute for Transportation Studies Report UCD-ITS-RR-01-03*, June 2001.

[42] NERLDC, "North Eastern Load Despatch Centre Shillong, India," http://www.nerldc.org.

[43] "Assam state electricity board, guwahati, india," http://aseb.in/.

[44] M. Baran and F. Wu, "Network reconfiguration in distribution systems for loss reduction and load balancing," *IEEE Transactions on Power Delivery*, vol. 4, no. 2, pp. 1401 –1407, April 1989.

[45] ——, "Optimal sizing of capacitors placed on a radial distribution system," *IEEE Transactions on Power Delivery*, vol. 4, no. 1, pp. 735 –743, January 1989.

[46] J. Barton and D. Infield, "Energy storage and its use with intermittent renewable energy," *IEEE Transactions on Energy Conversion*, vol. 19, no. 2, pp. 441–448, June 2004.

[47] [Online]. Available: http://www.toyota.com/prius-plug-in/features.html

[48] G. J. Klir and B. Yuan, *Fuzzy sets, fuzzy logic, and fuzzy systems: selected papers by Lotfi Asker Zadeh*. World Scientific, 1996.

[49] C. Lee, "Fuzzy logic in control systems: fuzzy logic controller. II," *IEEE Transactions on Systems, Man and Cybernetics*, vol. 20, no. 2, pp. 419–435, March/April 1990.

[50] L. Behera and I. Kar, *Intelligent Systems and Control- Principles and Applications*. Oxford University Press, 2009.

[51] H. Zimmermann, *Fuzzy set theory and its applications*. Kluwer, Boston, Second Edition, 1991.

[52] "Design department of assam electricity grid corporation ltd," http://www.aegclsldc.org/1024.html.

[53] "Matlab 2010 simpower simulation." [Online]. Available: www.mathworks.com

[54] M. Chakravorty and D. Das, "Voltage stability analysis of radial distribution networks," *Electrical Power and Energy Systems*, vol. 23, pp. 129–135, 2001.

[55] Central Electricity Authority of India standards, 2010. [Online]. Available: http://www.cea.nic.in/reports/regulation/grid_standards_reg.pdf

[56] G. J. Klir and B. Yuan, *Fuzzy sets, fuzzy logic, and fuzzy systems: selected papers By Lotfi Asker Zadeh*. World Scientific, 1996.

[57] "EV Battery specification." [Online]. Available: http://www.starnovo.com/E-car_battery.htm

[58] M. Nissen, "High performance development as distributed generation," *IEEE Potentials*, vol. 28, no. 6, pp. 25 –31, Nov-Dec 2009.

[59] J. Barton and D. Infield, "Energy storage and its use with intermittent renewable energy," *IEEE Transactions on Energy Conversion*, vol. 19, no. 2, pp. 441 – 448, June 2004.

[60] Y. Kanoria, A. Montanari, D. Tse, and B. Zhang, "Distributed storage for intermittent energy sources: Control design and performance limits," in *49th Annual Allerton Conference on Communication, Control, and Computing (Allerton)*, pp. 1310 –1317, Sept., 2011.

[61] S. Teleke, M. Baran, S. Bhattacharya, and A. Huang, "Rule-based control of battery energy storage for dispatching intermittent renewable sources," *IEEE Transactions on Sustainable Energy*, vol. 1, no. 3, pp. 117 –124, Oct. 2010.

[62] P. Brown, J. Peas Lopes, and M. Matos, "Optimization of pumped storage capacity in an isolated power system with large renewable penetration," *IEEE Transactions on Power Systems*, vol. 23, no. 2, pp. 523 –531, May 2008.

[63] S. Schoenung and C. Burns, "Utility energy storage applications studies," *IEEE Transactions on Energy Conversion*, vol. 11, no. 3, pp. 658 –665, Sept. 1996.

[64] Regional Meteorlogical Centre, Guwahati, Assam, Inida. [Online]. Available: http://www.imdguwahati.gov.in/rti.html

[65] Fuel economy of coda automotive. [Online]. Available: http://www.fueleconomy.gov/feg/noframes/32277.shtml

[66] W. kempton and S. Letendre. "Electric vehicles as a new power source for electric utilities". [Online]. Available: http://www.udel.edu/V2G/docs/Kempton-Letendre-97.pdf

[67] A. Vuorinen, *Planning of Optimal Power Systems*. Ekoenergo Oy, Finland, 2007.

[68] A. K. Srivastava, A. A. Kumar, and N. N. Schulz, "Impact of distributed generations with energy storage devices on the electric grid," *IEEE Systems Journal*, vol. 6, no. 1, March 2012.

[69] Y. Kanoria, A. Montanari, D. Tse, and B. Zhang, "Distributed storage for intermittent energy sources: Control design and performance limits," November 2011, stanford University U.C.Berkeley.

[70] B. Davidson, I. Glendenning, R. Harman, A. Hart, and et al., "Large-scale electrical energy storage," *Physical Science, Measurement and Instrumentation, Management and Education - Reviews, A IEE Proceedings*, vol. 127, no. 6, pp. 345 –385, July 1980.

[71] H. T. Nguyen and E. A. Walker, *A First Course in Fuzzy Logic*. CRC Press, 2006.

[72] P. Kumar, "Parameter extraction of battery models using multiobjective optimization genetic algorithms," in *14th International conference on Power Electronics and Motion Control (EPE-PEMC)*, 2010.

[73] K. Thirugnanam, H. Saini, and P. Kumar, "Mathematical modeling of Li-Ion battery for charge/discharge rate and capacity fading characteristics using genetic algorithm approach," in *International Transportation Electrification Conference (ITEC'12)*, June 2012.

[74] G. Ning, B. Haran, and B. N. Popov, "Capacity fade study of lithium-ion batteries cycled at high discharge rates," *Journal of Power Sources*, pp. 160–169, December 2002.

[75] P. B. Ramadass, B. Haran, R. White, and B. Popov, "Mathematical modeling of the capacity fade of Li-Ion cells," *Journal of Power Sources*, pp. 230–240, March 2003.

[76] B. YannLiaw, R. G. Jungts, G. Nagasubramanian, H. L.Case, and D. H.Doughty, "Modeling capacity fade in lithium-ion cells," *Journal of Power Sources*, pp. 157–161, August 2004.

[77] G. J. Klir and B. Yuan, *Fuzzy Sets and Fuzzy Logic: Theory and Applications*. Prentice Hall PTR, 1995.

[78] T. J. Ross, *Fuzzy Logic with Engineering Applications*. John Wiley and Sons, 2010.

[79] E. A. W. Hung T. Nguyen, *A First Course in Fuzzy Logic,*. CRC Press, 2006.

[80] T. J. Ross, *Fuzzy Logic with Engineering Applications*. John Wiley and Sons Ltd., Second Edition.

List of Publications

Journal Publications

1. Mukesh Singh, Praveen Kumar, and Indrani. Kar, "Implementation of vehicle to grid infrastructure using fuzzy logic controller," *IEEE Transactions on Smart Grid*, vol. 3, no. 1, pp. 565-577, March 2012.

2. Mukesh Singh, Praveen Kumar and Indrani Kar, "A Multi Charging Station for Electric Vehicles and its Utilization for Load Management and the Grid Support". *IEEE Transactions on Smart Grid*, vol. PP, no. 99, pp. 112, 2013.

Under Review

1. Mukesh Singh, Praveen Kumar and Indrani Kar, "A Real Time Smart Charging Station for Electric Vehicles designed for Vehicle to Grid scenario and its coordination with renewable energy sources". *IEEE Transactions on Sustainable Energy.* (under review)

Manuscripts Submitted

1. Mukesh Singh, Praveen Kumar and Indrani Kar, " Real Time Coordination of Electric Vehicles to Support the Grid at the Distribution Substation Level" *IEEE Transaction on Smart Grid.*

Conference Publications

1. Mukesh Singh, Indrani Kar, and Praveen Kumar, "Influence of EV on grid power quality and optimizing the charging schedule to mitigate voltage imbalance and reduce power loss," *Power Electronics and Motion Control (EPE/PEMC), 14th International Conference*, September 2010, pp. T2- 196 -T2-203(2010).

2. Mukesh Singh, Praveen Kumar, and Indrani Kar, "Analysis of Vehicle to Grid Concept in Indian Scenario" P*Power Electronics and Motion Control (EPE/PEMC), 14th International Conference*, September 2010, pp. T6-149-T6-156 (2010).

3. Sarthak Gupta, Prateek Jain, Mukesh Singh, Praveen Kumar and Indrani Kar, "Designing an algorithm for the Charging/Discharging of Electric Vehicles' Batteries for mitigating the voltage imbalance." in *Centenary conference, EE department, IISC Bangalore, India*, 2011.

4. Mukesh Singh, Praveen Kumar, and Indrani Kar, "Designing a multi charging station for electric vehicles and its utilization for the grid support," *IEEE PES General Meeting*, pp 1-7, July 2012.

5. Mukesh Singh, Praveen Kumar, and Indrani Kar, "A Model of Electric Vehicle Charging Station Compatibles with Vehicle to Grid Scenario" in *IEEE International Electrical Vehicle Conference (IEVC) Technology, Engineering, Standards - Challenges and Opportunities* March 4-8, 2012 Greenville, South Carolina, USA, March, 2012.

6. Mukesh Singh, Praveen Kumar, and Indrani Kar, "Coordination of Multi Charging station for Electric Vehicles and its utilization for Vehicle to Grid scenario" in *IEEE Transportation Electrification Conference and Expo(ITEC'12)*- pp.1-7, June, 2012

7. Mukesh Singh, Kannan T, Surendra Swami, Praveen Kumar and Indrani Kar, " Coordination of Electric Vehicles in Charging Stations Connected at Different Nodes of a Distribution Substation" in *India Conference (INDICON), 2012 Annual IEEE*, Dec., pp. 12601265.

Curriculum Vitae

Mukesh Singh was born in Chapra, Bihar, India, on January 25, 1978.

He received his B.Sc degree in Electrical Engineering from Bihar Institute of Technology (now known as Birsa Institute of Technology), Sindri, Jharkhand, India and Master of Engineering in Power system from Walchand College of Engineering, Sangli, Maharastra, India in 2000 and 2008 respectively.

He has worked as software tranee in Convergis Infosoft, Bangalore, India for two years.

He has worked as a faculty in reputed engineering colleges for nearly 7 years.

He started working towards a PhD. degree in July 2009 at the Indian Institute of Technology Guwahati, India. His PhD research was carried out in the department of Electronics and Electrical Engineering.

His current research interests are Vehicle to Grid (V2G), Smart Grid, Distributed Generation and Renewable Energy Resources.